


2017

Study of parameters dominating electromechanical and sensing response in ionic electroactive polymer (IEAP) transducers

Abdallah Mohammad Almomani
Iowa State University

Follow this and additional works at: <https://lib.dr.iastate.edu/etd>

 Part of the [Aerospace Engineering Commons](#), [Materials Science and Engineering Commons](#), [Mechanical Engineering Commons](#), and the [Mechanics of Materials Commons](#)

Recommended Citation

Almomani, Abdallah Mohammad, "Study of parameters dominating electromechanical and sensing response in ionic electroactive polymer (IEAP) transducers" (2017). *Graduate Theses and Dissertations*. 16068.
<https://lib.dr.iastate.edu/etd/16068>

This Dissertation is brought to you for free and open access by the Iowa State University Capstones, Theses and Dissertations at Iowa State University Digital Repository. It has been accepted for inclusion in Graduate Theses and Dissertations by an authorized administrator of Iowa State University Digital Repository. For more information, please contact digirep@iastate.edu.

Study of parameters dominating electromechanical and sensing response in ionic electroactive polymer (IEAP) transducers

by

Abdallah Mohammad Almomani

A dissertation submitted to the graduate faculty
in partial fulfillment of the requirements for the degree of
DOCTOR OF PHILOSOPHY

Major: Aerospace Engineering

Program of Study Committee:
Reza Montazami, Co-Major Professor
Wei Hong, Co-Major Professor
Ashraf Bastawros
Pranav Shrotriya
Ran Dai

The student author, whose presentation of the scholarship herein was approved by the program of study committee, is solely responsible for the content of this dissertation. The Graduate College will ensure this dissertation is globally accessible and will not permit alterations after a degree is conferred.

Iowa State University

Ames, Iowa

2017

Copyright © Abdallah Mohammad Almomani, 2017. All rights reserved.

DEDICATION

I dedicate this work to my family. A special feeling of gratitude to my loving parents, Mohammad Almomani and Etaf Almomani, who instilled in me and opened my eyes to the importance of pursuing graduate studies. They always encourage me to do my best to achieve that. My brothers and sisters, who believed in me and supported me the whole time. My beloved wife Hala, who never left my side and encouraged me throughout the whole journey of the doctoral program, and for my beloved son Diyaa who was born at the beginning of this journey and should have more caring time during his early stage of his childhood.

TABLE OF CONTENTS

LIST OF FIGURES	vii
LIST OF TABLES	xii
ACKNOWLEDGMENTS	xiii
ABSTRACT	xiv
CHAPTER 1. INTRODUCTION AND BACKGROUND	1
1.1. Smart materials overview	1
1.1.1. Piezoelectric materials	3
1.1.2. Shape Memory Alloys	3
1.1.3. Electroactive polymer	5
1.2. Electroactive Polymeric (EAP) Actuators	6
1.2.1. Electronic EAP (EEAP) Actuators	7
1.2.2. Ionic EAP (IEAP) Actuators	9
1.3. Ionic Polymer-metal Composite (IPMC) Actuators	13
1.3.1. Ionomeric membrane	15
1.3.2. Electrolyte	19
1.3.3. Conductive Network Composite (CNC) Layer	20
1.3.4. Metallic Outer Electrodes	27
1.4. Document Organization	28
1.5. References	30
CHAPTER 2. EXPERIMENTAL METHODS AND PROCEDURES	36
2.1. Materials and fabrication process	36
2.1.1. Materials	36
2.1.2. Fabrication procedure:	37
2.2. Characterizations	41
2.2.1. Actuation performance characterization	41
2.2.2. Sensing performance characterization	42
2.2.3. Electrochemical characterization	44
2.2.4. Characterization of electromechanical behavior as a function of temperature	46
2.2.5. Ion exchange procedure	48

CHAPTER 3. INFLUENCE OF IONIC LIQUID CONCENTRATION ON THE ELECTROMECHANICAL PERFORMANCE OF IONIC ELECTROACTIVE POLYMER ACTUATORS	49
3.1. Introduction.....	50
3.2. Materials and Methods.....	51
3.2.1. Sample Preparation	51
3.2.2. Electrochemical characterization	52
3.2.3. Electromechanical characterization	52
3.3. Results and discussions.....	53
3.3.1. Current flow	53
3.3.2. Electromechanical Response	54
3.3.3. Electrochemical Studies.....	55
3.3.4. Discussion.....	60
3.4. Conclusion	61
3.5. References.....	62
CHAPTER 4. ELECTROCHEMICAL AND MORPHOLOGICAL STUDIES OF IONIC POLYMER METAL COMPOSITES AS STRESS SENSORS.....	64
4.1. Introduction.....	64
4.2. Experimental Section.....	66
4.2.1. Materials	66
4.2.2. Methods.....	67
4.3. Results and Discussion	70
4.3.1. Morphological characterization	70
4.3.2. Electrochemical analysis.....	72
4.3.3. Mechanoelectrical sensing performance.....	75
4.4. Conclusions.....	77
4.5. References.....	78
CHAPTER 5. SOFT IONIC ELECTROACTIVE ACTUATORS WITH TUNABLE NON-LINEAR ANGULAR DEFORMATION	83
5.1. Introduction.....	84
5.2. Experimental	86

5.2.1. Materials	86
5.2.2. Sample Fabrication	86
5.2.3. Sample nomenclature.....	88
5.2.4. Electrochemical characterizations	88
5.2.5. Electromechanical Characterizations.....	88
5.2.6. Morphological and mechanical characterizations.....	89
5.2.7. Finite element modeling	90
5.3. Results	90
5.3.1. Cyclic Voltammetry.....	90
5.3.2. Equivalent circuit modeling.....	91
5.3.3. Charging and discharging	94
5.3.4. Electromechanical response.....	95
5.4. Discussion and simulation	96
5.4.1. Discussion.....	96
5.4.2. Finite element simulation.....	98
5.5. Conclusion	102
5.6. References.....	103
5.7. Supporting information for: Soft Ionic Electroactive Actuators with Tunable Non-Linear Angular Deformation.....	108
5.7.1. Morphological and mechanical characterizations.....	108
5.7.2. Simulation of electromechanical response by FEM	109
5.7.3. Supporting Information References	113
CHAPTER 6. INFLUENCE OF TEMPERATURE ON THE ELECTROMECHANICAL PROPERTIES OF IONIC LIQUID-DOPED IONIC POLYMER-METAL COMPOSITE ACTUATORS	115
6.1. Introduction.....	116
6.2. Materials and Methods.....	120
6.2.1. Materials	120
6.2.2. Sample Preparation	120
6.2.3. Electromechanical characterization	121
6.2.4. Electrochemical characterization	122

6.3. Results	123
6.3.1. Electromechanical Response	123
6.3.2. Electrochemical characterization	128
6.4. Discussion	129
6.5. Conclusion	134
6.6. References.....	135
CHAPTER 7. ENGINEERING IONIC CONDUCTIVITY OF IONOMERIC MEMBRANES: INFLUENCE OF VAN DER WAALS VOLUME OF COUNTERIONS AND TEMPERATURE.....	139
7.1. Introduction.....	140
7.2. Materials and Methods.....	142
7.2.1. Materials	142
7.2.2. Sample Preparation	142
7.2.3. Experimental Procedure.....	143
7.3. Results and Discussion	143
7.4. Conclusion	148
7.5. References.....	148
CHAPTER 8. CONCLUSIONS AND FUTURE WORK	151
8.1. Conclusions.....	151
8.2. Future Work.....	153

LIST OF FIGURES

Figure 1-1 : Austenite and martensite phases	4
Figure 1-2 : First commercial EAP actuators in swimming fish. Produced in Japan in 2002 by Eamex.	6
Figure 1-3: Principle of actuation of dielectric polymer actuators (a) Due to Coulombic attraction between opposite charges on electrodes [18] (b) Dielectric with no applied voltage (c) After applying voltage , some dielectrics add more strain (d) and some become thicker and reduce the induced strain [26].....	8
Figure 1-4 : Actuation mechanism of liquid crystal elastomers [27].....	9
Figure 1-5 : Conjugated structure in conducting polymers[27].....	11
Figure 1-6 : Actuation mechanism in conducting polymers [27].	12
Figure 1-7 : Ionic Polymer-Metal Composite Actuator [42].	13
Figure 1-8: (a) Neutral case. (b) Accumulation of different-sized ions at oppositely-charged electrodes and bending mechanism.....	15
Figure 1-9 : Nafion chemical structure	17
Figure 1-10: Nafion spherical cluster network model[48].....	17
Figure 1-11: Water channel model of Nafion [49]	18
Figure 1-12 : Curvature dependence on IEAP actuator CNC thickness[58]	20
Figure 1-13 : Cationic and anionic strains for different gold nanoparticles concentration in CNC[42].....	22
Figure 1-14: Mechanical strain for different ratio of RuO ₂ nanoparticles and gold flakes[45].	23
Figure 1-15 : Steps for direct assembly CNC manufacturing technique[62].....	25
Figure 1-16: Layer-by-Layer CNC depositing technique using gold nanoparticles and PAH [56].....	27
Figure 1-17: Hot-pressed gold electrodes	28
Figure 2-1 Nafion's chemical structure (http://www.nafionstore.com/)	37

Figure 2-2: Glass frame used to hold the membrane during LbL ionic self-assembly process (left). Nafion membrane attached to a glass frame (right).....	38
Figure 2-3: dipping robot and beakers arrangement.....	39
Figure 2-4: StratoSmart software setup for depositing of 20 bi-layers of CNC on Nafion membranes.	39
Figure 2-5: Pure Nafion (left) and Nafion membrane with 20 bi-layers CNC (right).....	40
Figure 2-6: 25T hydraulic hot press machine (left), final hot pressed membrane (right, upper), and actuators to be tested (right, lower)	41
Figure 2-7: Actuation Process. Neutral position (A), Cationic Curvature (B), Anionic curvature (C), and the time lapse for the whole actuation process (D).....	42
Figure 2-8: Sensing process. (A) The experimental setup. (B) The generated signal.	43
Figure 2-9: VersaSTAT-4 potentiostat	44
Figure 2-10: Nafion membrane between two copper electrodes	44
Figure 2-11: Different electrochemical experiments from potentiostat software.	45
Figure 2-12: Impedance test experimental properties from potentiostat software	45
Figure 2-13: Examples of electrochemical data that can be extracted from the VersaSTAT-4 potentiostat.....	46
Figure 2-14: Actuation performance at different temperatures in air setup.....	47
Figure 2-15: Water proof samples using hot glue to seal the edges of the glass substrates (left), submerged samples in hot water at the desired temperature to be tested (right).	47
Figure 3-1: Charging and discharging currents for samples containing different	53
Figure 3-2: Actuation curvatures (primary y-axis) and strain (secondary y-axis) of IEAP actuators in response to a 4 V step potential is presented as a function of EMI-Tf ionic liquid concentration.	54
Figure 3-3: Nyquist plot of impedance magnitude of IEAP actuators containing various concentrations of ionic liquid. Solution resistance is deduced from the intersection of plots with the Zre axis.....	55

- Figure 3-4 : (a) Impedance magnitude versus frequency; and, (b) phase angle versus frequency of IEAP actuator containing different ionic liquid concentration. At higher frequencies, impedance and phase angle exhibit higher dependency on ionic liquid concentration. 57
- Figure 3-5 : Equivalent electric circuit with Warburg element. 58
- Figure 3-6: The plots of $1/(R_s - R)$ versus ω with various ILs intake and their corresponding fitting lines with $y = ax^{1.5} + bx + b^2x^{0.5}/(2a)$ 60
- Figure 4-1: a) Schematic representation of layer-by-layer direct self-assembly of AuNP and PAH; b) CNC layer formed on Nafion ionomer, the membrane is mounted on a glass frame; c) foreground: schematic representation of IPMC and sensor structure, background: SEM micrograph of AuNP/PAH CNC nanostructure..... 68
- Figure 4-2: A schematic representation of the setup and operations for the mechano-electrical characterization (dimensions are not to scale). The IPMC sensor piece was covered by electrical tape, with copper tape used as electrodes to connect to an oscilloscope to monitor the generated electric signal. A 12 kPa stress was distributed evenly by a mechanical arm whose frequency was controlled at 1 Hz by a step motor. 70
- Figure 4-3: a) UV-Vis absorbance spectra of AuNP aqueous solution (20 ppm); b) UV-Vis absorbance spectra of 2, 4, 6, 8, and 10-bilayer AuNP/PAH and AuNP/PAH-NaCl nanostructures; c) plot of the absorbance peaks of CNCs consisting of different number of bilayers and morphology..... 71
- Figure 4-4: Electrochemical studies of IPMC sensors consisting of different thickness CNCs (without NaCl) a) Nyquist plot of impedance magnitude of IPMC sensors. Solution resistance values are deduced from the intersection of plots with the axis; b) Impedance magnitude as a function of frequency; c) phase angle as a function of frequency; d) plots of $1/(R_s - R)$ versus ω , and their corresponding fitting lines based on the equivalent circuit (inset). 73
- Figure 4-5: Mechano-electric sensing in repose to cyclic 12 kPa stress at 1 Hz. Insets show the zoomed in plots at the first and last 10 seconds of the experiment..... 77
- Figure 5-1 : Angled (top row) and side (bottom row) views of patterned samples; (a) 1S, (b) 2SS, and (c) 2SA. Gold leaf electrodes are not shown in the sketch to give a better view of the patterns. Not to scale. 87
- Figure 5-2: SEM image of the cross-section of specimen Nafion/1s-PEDOT:PSS/Au, indicating well interlayer adhesion between layers. 89

Figure 5-3: Cyclic voltammograms of different specimens measured at 50 mV/s.....	90
Figure 5-4: Equivalent circuit with a constant phase element	91
Figure 5-5: Impedance magnitudes of (a) BNafion, (b) Nafion/1s-PEDOT:PSS, and (c) Nafion/2s-PEDOT:PSS; and phase of (d) BNafion, (e) Nafion/1s-PEDOT:PSS, and (f) Nafion/2s-PEDOT:PSS fitted by equivalent circuit with constant phase element shown in Figure 5-4.	93
Figure 5-6 : (a) Charging/discharging currents and (b) charge density versus time for different specimens under one cycle of a 4 V square wave.	95
Figure 5-7 : Schematic representation and experimental actuation performance for (a) 1S, (b) 2SS, (c) 2SA2, and (d) 2SA3. Left picture is the cationic response and right picture is the anionic response.....	96
Figure 5-8: Displacement distribution of actuator 1S during cationic response under different hypotheses. When the total number of the movable ions in the actuator is fixed, the volume ratios of cations in the PEDOT:PSS layer (attached to the cathode) and the Nafion sub-layer (Supporting Information) are (a) 2:1 and (b) 1:2, respectively.	99
Figure 5-9: Comparison of experimental bending displacement in response to a 4 V step input (left column) and the corresponding results produced by the static theoretical model via ABAQUS (right column). Figure (a) and (b) represent actuator 1S, (c) and (d) represent actuator 2SA2, (e) and (f) represent actuator 2SA3, and (g) and (h) represent actuator 2SS. The top electrode is the cathode and the bottom electrode is the anode.....	101
Figure 6-1: Idealistic schematic of cationic and anionic bending mechanism (top, not to scale) and overlaid sequential images of cationic (red arrow) bending followed by anionic (blue arrow) bending (bottom).....	117
Figure 6-2: The cationic curvature at different temperatures.	124
Figure 6-3. (a)The maximum cationic curvature, (b) The cationic actuation time, at different temperatures.	124
Figure 6-4. The anionic curvature at 25 °C and 70 °C, both shifted to time = zero for comparison.	125
Figure 6-5: The maximum anionic curvature at different temperatures.	126
Figure 6-6 Experimental and fitted time dependent curvature at (a) at 25 °C, and (b) 70 °C.	127

Figure 6-7. The time constant of cationic and anionic curvatures at different temperatures.	127
Figure 6-8. The current flow after applying 4 V across a 1×1 cm ² Nafion membrane with 30% EMI-TF ionic liquid at different temperatures. The leftmost gray line is the current flow at room temperature; each colored line above it shows an increase in temperature from 30 °C to 90 °C.....	128
Figure 6-9: Arrhenius conductivity fitting for temperatures from 25 °C to 70 °C.....	129
Figure 7-1: Nyquist plots for membranes with different counterions at different temperatures.....	144
Figure 7-2: Conductivity across Nafion membranes with different counterions at different temperatures.....	145
Figure 7-3: Arrhenius plots of ionic conductivity for Nafion membranes at different temperatures and for different counterions.....	147
Figure 8-1: Microgrippers fabricated with actuators with angular motion.....	153
Figure 8-2: (a) Actuators with 3D motion. (b) Complex shape (cube) formation using IEAP actuators with angular motion.....	154
Figure 8-3: Some application of IEAP sensor. (a) touch sensors, (b) keyboards, (c) artificial skin, and (d) touch screen.....	154

LIST OF TABLES

Table 1-1 : Common smart materials and their responses to stimuli.....	2
Table 3-1: Solution resistance and ionic conductivity of IPMCs containing different concentrations of ionic liquid.	56
Table 4-1: Solution resistance, ionic conductivity and electric double layer capacitance of IPMC sensors with various thicknesses of CNC layers.	73
Table 5-1: The abbreviation and its definition of each sample used in this work.	88
Table 5-2: Fitting parameters for different specimens.....	93

ACKNOWLEDGMENTS

Firstly, I would like to express my sincere appreciation to my advisors Prof. Reza Montazami and Prof. Wei Hong for their continuous support of my PhD study and related research, for their patience, and motivation. Their guidance helped me in all the time during research and writing of this dissertation. I could not have imagined having better advisors and mentors for my PhD study to push me forward and encourage me whenever I have complications.

Besides my advisors, I would like to thank the rest of my dissertation committee members: Prof. Ashraf Bastawros, Prof. Pranav Shrotriya, and Prof. Ran Dai, for their encouragement, advice, and comments to widen my research from various perspectives.

My sincere thanks also go to my fellow labmates for their support in various aspects of the research and for the fun we have had together in the last five years. In particular, I'm grateful to Dr. Wangyujue Hong for enlightening me the first glance of research and participating in most of my research projects.

I would like also to thank my parents, my brothers and sisters, my wife, and my friends for supporting me and encouraging me throughout the whole journey of the PhD study, and the department faculty and staff for making my time at Iowa State University a wonderful experience.

Last but not the least, I would like to thank my sponsors Jordan University of Science and Technology for their continuous support.

ABSTRACT

Ionic electroactive polymer (IEAP) transducers are a class of smart structures based on polymers that can be designed as soft actuators or sensors. IEAP actuators exhibit a high mechanical response to an external electrical stimulus. Conversely, they produce electrical signals when subjected to mechanical force. IEAP transducers are mainly composed of four different components: The ionomeric membrane (usually Nafion) is an ion permeable polymer that acts as the backbone of the transducer. Two conductive network composite (CNC) layer on both sides of the ionomeric membrane that enhance the surface conductivity and serve as an extra reservoir to the electrolytes. The electrolytes, (usually ionic liquids (IL)), which provides the mobile ions. And two outer electrodes on both sides of the transducer to either provide a distributed applied potential across the actuators (usually gold leaves) or to collect the generated signals from the sensors (usually copper electrodes). Any variation in any of these components or the operating conditions will directly affect the performance of the IEAP transducers. In this dissertation, we studied some of the parameters dominating the performance of the IEAP transducers by varying some of the transducers components or the transducers operating conditions in order to enhance their performance.

The first study was conducted to understand the influence of ionic liquid concentration on the electromechanical performance of IEAP actuators. The IL weight percentage (wt%) was varied from 10% to 30% and both the electromechanical (induced strain) and the electrochemical (the current flow across the actuators) were studied. The results from this study showed an enhanced electrochemical performance (current flow is higher for higher IL wt%) and a maximum electromechanical strain of approximately 1.4% at 22 wt% IL content. A lower induced strain was noticed for IL wt% lower or higher than 22%.

The second study was to investigate the effect of changing the morphology of the CNC on the sensing performance of IEAP stress sensors. In this study, small salt molecules were added to the CNC layers. Salt molecules directly affected the morphology of the CNC layers resulting in a thicker, more porous, and high conductive CNCs. As a result, the ionic conductivity increased through the CNC layers and sensing performance was enhanced significantly.

In the third study, a non-linear angular deformation (limb-like motion) was achieved by varying the CNC layers of the IEAP actuators by adding some conjugated polymers (CP) patterns during the fabrication of the actuators. It was found that the segments with the CP layers will only expand and never contract during the actuation process. Depending on the direction of motion and the location of the CP layers, different actuation shapes such as square or triangular shapes were achieved rather than the typical circular bending.

In the fourth study, the influence of temperature on the electromechanical properties of the IEAP actuators was examined. In this study, both electromechanical and electrochemical studies were conducted for actuators that were operated at temperatures ranging from 25 °C to 90 °C. The electromechanical results showed a lower cationic curvature with increasing temperature up to 70 °C. On the other hand, a maximum anionic curvature was achieved at 50 °C with a sudden decrease after 50 °C. Actuators started to lose functionality and showed unpredictable performance at temperatures higher than 70 °C. Electrochemically, an enhancement of the ionic conductivity was resulted from increasing temperature up to 80 °C. A sudden increase in current flow was recorded at 90 °C indicating a shorted circuit and actuator failure.

Finally, in the fifth study, protons in Nafion membranes were exchanged with other counterions of different Van der Waals volumes. The ionic conductivity was measured for IEAP membranes with different counterions at different temperatures. The results showed higher ionic

conductivities across membranes with larger Van der Waals volume counterions and higher temperatures. A different ionic conductivity behavior was also noticed for temperatures ranging from 30 °C to 55 °C than temperatures between 55 °C and 70 °C after fitting the data with the Arrhenius conductivity equation.

CHAPTER 1. INTRODUCTION AND BACKGROUND

1.1. Smart materials overview

In material science, preferred material properties include high quality, cost-effectiveness, durability, stability, and suitability for different applications. A new class of materials called “smart materials” was discovered and developed during the last century. Future research needs and methods for producing smart materials were discussed at a special workshop organized by the US Army Research Office in 1988 [1]. At that workshop, Ahmad defined a smart system or a smart material as “*system or material which has built-in or intrinsic sensor(s), actuator(s) and control mechanism(s) whereby it is capable of sensing a stimulus, responding to it in a predetermined manner and extent, in a short/ appropriate time, and reverting to its original state as soon as the stimulus is removed*” [2]. The stimuli could range from applied pressure or electrical potential to natural or environmental changes like temperature or humidity. Sensing or responding to such a stimulus might change the shape of the material, the mechanical or electrical response, or other material properties like viscosity. To be considered a smart material, the response should be significant, fast, reversible, and repeatable. Shape memory alloys are a well-known example of smart materials. In 1941 shape memory alloys (SMAs) were first described and, because they can return to their original shape when heated, they have been widely used in a variety of applications [3]. Another jump in SMA interest occurred when Buehler, *et al.*, [4] introduced applications of nickel-titanium (NiTi) alloys in 1962 [5]. A famous example of an SMA structure is eyeglass frames that can return to their original shape after they have been deformed when heated to a certain temperature.

Depending on their response to stimulus, smart materials can be classified as either passive or active materials. Active materials respond physically (*i.e.*, in geometry, in viscosity, etc.) to stimuli. On the other hand, passive materials only sense the stimulus and do not change their physical properties. Shape memory alloys, piezoelectric materials, and electroactive polymers are some examples of active smart materials. Optical fibers are one good example of a passive material [6]. Some common smart materials and their stimuli and response characteristics are shown in Table 1-1.

Table 1-1 : Common smart materials and their responses to stimuli

MATERIAL	STIMULUS	RESPONSE
Piezoelectric material	Mechanical deformation	Electric signal
	Electric field	Mechanical deformation
Shape memory alloy	Heat	Returns to original shape (Mechanical deformation)
Electroactive polymers	Electric field	Mechanical deformation
Electro-rheological fluid	Electric field	Change in viscosity
Optical fibers	Temperature, pressure, or mechanical strain	Change in opto-electronic signals

Three well-known smart materials that respond to stimulation by mechanical deformation are: piezoelectric materials that deform electro-mechanically, shape memory alloys that deform thermo-mechanically, and electroactive polymers that also deform electro-mechanically. A brief description of such materials and their applications is shown below.

1.1.1. Piezoelectric materials

Piezoelectric materials behave electromechanically: they physically deform when subjected to an electrical field (actuator behavior) and induce electrical signals when subjected to mechanical stress (sensor behavior) [7]. The relationship between these induced electric signals and applied stress is linear and reversible, making it easier to control the deformation and measure the applied stresses [8]. Aluminum nitride (AlN) is an example of an inorganic piezoelectric crystalline material that lacks inversion symmetry structure. After deposition, AlN films have a specific arrangement of ions with specific polarization in their crystalline structure. When a mechanical stress is applied, the internal polarization of the material crystals will change, developing an electrical field across the film's boundary. Conversely, crystals will deform slightly to seek alignment with application of a strong electric field. A large number of crystals will result in noticeable deformation [8]. Piezoelectric materials are used in many applications, *e.g.*, tactile sensors (devices that measure a physical phenomenon through contact and touch) that produce a measurable signal when pressure or force is applied [8]. Another application is energy harvesting, where the basic concept is to collect induced electrical charge resulting from force application. An example illustrating energy harvesting would be putting piezoelectric material in a person's shoes and collecting the electrical charge produced through walking [8, 9]. Other examples include wrist watches, headphones, piezoelectric igniters, and many others [7].

1.1.2. Shape Memory Alloys

SMA's are alloys that can recover an original shape when heated (one-way SMA's) or when cooled (two-way SMA's); two-way SMA's are less common because of the training requirement and lower recovery strain compared to one-way SMA's [3, 7, 10]. SMA's have two phases: austenite and martensite. The austenite phase is the high temperature phase where most

alloys have a super-lattice structure and their sub-lattices have body-centered cubic (BCC) structure (e.g. titanium-nickel [Ti-Ni] alloy) or face-centered cube (FCC) structure (e.g. copper-manganese [Mn-Cu] alloy). The martensite phase is the low temperature phase and is formed by diffusionless transformation of atoms while cooling. Atoms of the austenite structure move cooperatively or by a shear-like mechanism to form a twinned martensite structure during the cooling cycle without breaking atomic bonds [11, 12]. Austenite and martensite structures are shown in Figure 1-1.

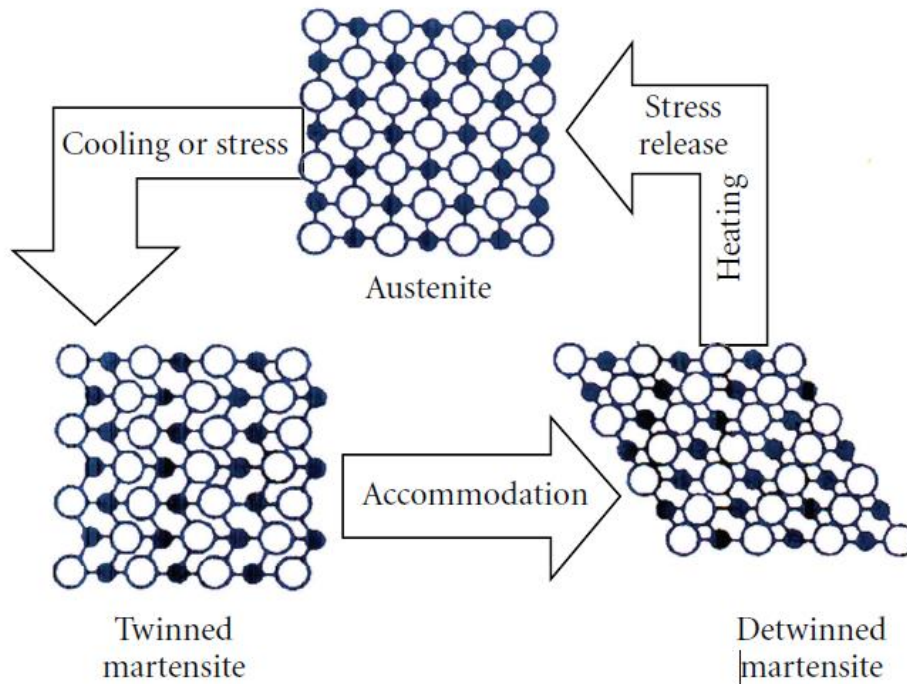


Figure 1-1 : Austenite and martensite phases

To establish an austenite shape (also known as parent shape), the alloy must be constrained to the desired shape and heated to a specific temperature. At this phase, the atoms will be arranged into the most compact pattern possible, a cubic structure (FCC or BCC). After cooling without experiencing external forces, they will retain their parent shape and transform into the martensite phase. While in this phase, they can be deformed and retain the deformation. When reheated, they

will revert to the austenite phase with the original compact cubic structure and the original shape [3, 13]. SMAs have many automotive [14] , aerospace [15] , robotics [16], and biomedical [17] applications . A simple application is their use as actuators to open or close a valve when the temperature is high, and to reverse this action in a spring-like manner when the temperature is low.

1.1.3. Electroactive polymer

Electroactive polymer (EAP) actuators, like piezoelectric materials, deform when an electrical field is applied across them. EAP actuators generally have some special characteristics usually not found in non-polymeric actuators, including flexibility, light weight, relatively inexpensive fabrication, and fracture tolerance. They also can be configured in virtually any convenient shape at any desired size while retaining their special properties [7, 18-20] . The first EAP actuators were capable of inducing only relatively small actuation, but since the 1990s many new polymers have demonstrated a relatively larger mechanical response to electric fields than electroactive ceramics. They are also faster and exhibit low density and high resilience compared to shape memory alloys [19, 21-23]. Due to their high actuation strain, high toughness, and fast response, similarity in movement of such actuators to biological muscle movement was noticed. This attractive similarity has captured the attention of engineers and scientists who may use them in artificial muscles to mimic the movements of animals and insects in robotic applications [19]. The first reported commercial product using EAP actuators was a swimming fish produced by Eamex in Japan in 2002 [18], as illustrated in Figure 1-2. These fish swam without use of batteries or motors. Their movement was produced by the simple bending of EAP actuators under the stimulation of an electrical field induced by coils at the top and bottom of the tank. The next section will present more details regarding EAP actuators.



Figure 1-2 : First commercial EAP actuators in swimming fish. Produced in Japan in 2002 by Eamex.

1.2. Electroactive Polymeric (EAP) Actuators

Based on their response mechanism, electroactive actuators can be divided it to two major groups: electronic EAP (EEAP) actuators and ionic EAP (IEAP) actuators. Both EEAP actuators and IEAP actuators are driven by electric fields. EEAP actuators respond directly to the electric field due to their crystalline or dielectric internal structure, while IEAP actuators are driven by diffusion of mobile ions inside the polymer due to attractive and repulsive forces of the electric field [19, 20, 24]. Dielectric elastomer EAPs, ferroelectric polymers, and liquid crystal elastomers (LCE) are types of EEAP actuators. Carbon nanotubes (CNT), conducting polymers (CP), ionic polymer gels (IPG), and ionic polymer-metal composites (IPMC) are types of IEAP actuators [7, 20, 24].

EEAP actuators have certain advantages over IEAP actuators. In general, they induce larger forces, actuate faster, and operate for longer times than IEAPs. They also operate without precious-metal gold or platinum electrodes. On the negative side, they require much higher operating voltage (kV-MV), and they have monopolar actuation independent of voltage polarity

because of associated electrostriction effects. The advantages of IEAP actuators over EEAP actuators are low operating voltage (1-4 volts), making IEAPs preferred in robotic battery-driven applications, and bi-directional actuation related to the polarity of the applied voltage [20].

1.2.1. Electronic EAP (EEAP) Actuators

1.2.1.1. Dielectric elastomer EAP

Dielectric elastomer EAP actuators are made from a rubber-like polymer (elastomer) sandwiched between two plate electrodes. When high electric field is applied (kV/m or MV/m) across the electrodes, the electrostatic force between the two plates will squeeze the polymer and cause actuation. This force is referred to Coulombic attraction between opposite charges on the electrodes. Electrostriction arising from strain-induced changes in dielectric properties of the materials that have some crystallinity in their structure also contributes to the actuation. Strain will change the lattice structure of the crystalline structure that in turn changes its dielectric properties. This effect is different for different elastomers and can be represented by an appropriate dielectric constant. Some dielectrics, depending on the applied voltage and particular material polarities, will result in more strain (dielectric become thinner) or oppose the induced strain from the Coulombic attraction due to electrostriction [25, 26]. Figure 1-3 shows the operating principles of this type of actuation that occurs primarily through changing the area of the actuator. Polymer thickness will decrease with a change in applied voltage (change in electrostatic force) and the area will expand accordingly to maintain constant volume [18, 27]. In general, the actuation depends on the polymer modulus, the dielectric constant, and the applied potential. Elastomers with a high dielectric constant and a low elastic modulus will generally exhibit greater strain [7]. Some advantages of these actuators are high strain (Pelrine *et al.* reported a strain of 215% for 3M VHB 4910 acrylic

elastomer [28]), the ability to be cast into different shapes, and ease of manufacturing. Their main disadvantage is the high operating voltage requirement [7, 29].

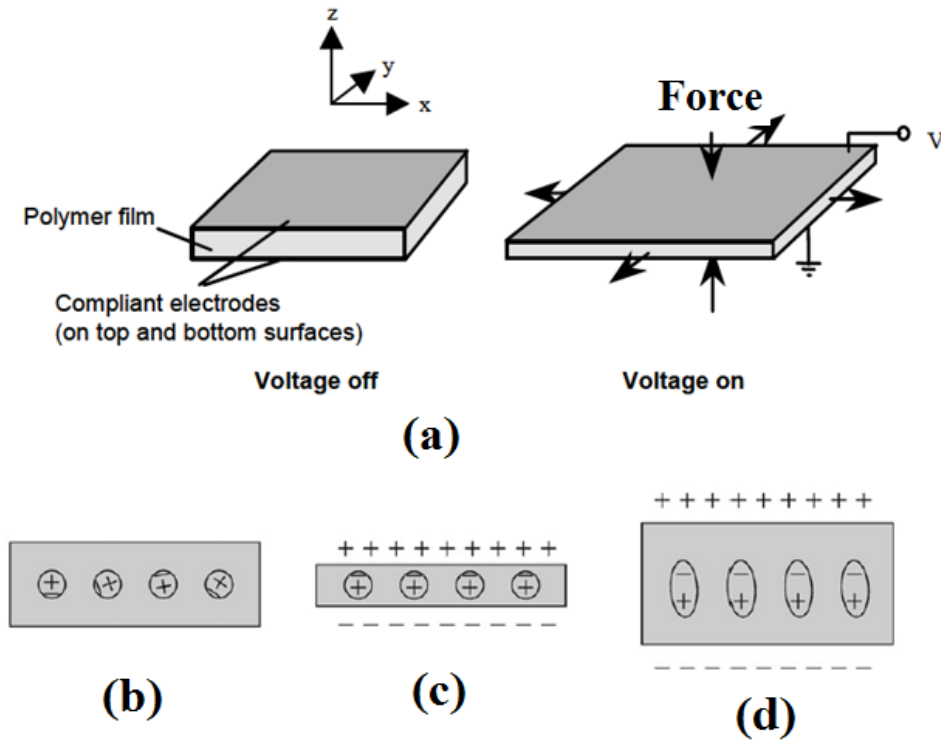


Figure 1-3: Principle of actuation of dielectric polymer actuators (a) Due to Coulombic attraction between opposite charges on electrodes [18] (b) Dielectric with no applied voltage (c) After applying voltage, some dielectrics add more strain (d) and some become thicker and reduce the induced strain [26]

1.2.1.2. Ferroelectric Polymers

Ferroelectric polymers are similar to piezoelectric materials. They have a crystalline structure with specific polarity and deformation occurs when dipoles rotate to follow the polarity of the applied electric field [7, 18, 27, 29]. Applications of ferroelectric polymers are similar to applications of piezoelectric materials. One advantage of ferroelectric materials is that they retain their polarization after removing the applied electric field [30, 31]. This property has led to use of ferroelectric materials to store data by assigning “0” and “1” values to each polarization direction after being actuated by electric field. Using arrays of microscale units of such materials,

information storage units can be fabricated. Poly vinylidene fluoride (PVDF) and its copolymers are the most common ferroelectric polymers.

1.2.1.3. *Liquid Crystal Elastomers*

Liquid crystal elastomer structures have rigid and flexible elements. The rigid parts (rod-like molecular structure, also called mesogens) tend to align their molecules in one direction more than another (anisotropic structure). At the same time, the flexible part represents the fluidity associated with liquid crystals (rubber-like elasticity) [27]. The mesogens have a specific polarity and the actuation mechanism of liquid crystal elastomers is the same as in ferroelectric polymers. When an electric field is applied, the dipoles tend to orient themselves along the direction of the field, resulting in mechanical deformation [7, 18, 27, 32]; the actuation mechanism is shown in Figure 1-4. One application of liquid crystal elastomers is their use in artificial muscles [33]

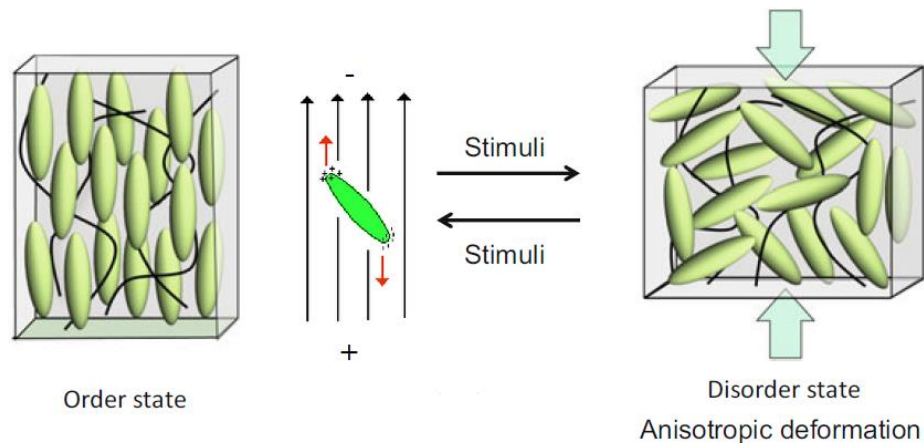


Figure 1-4 : Actuation mechanism of liquid crystal elastomers [27]

1.2.2. Ionic EAP (IEAP) Actuators

1.2.2.1. *Carbon Nanotubes (CNTs) Actuators*

Carbon nanotubes are very small tubular cylinders of carbon atoms. Previous studies have demonstrated that CNTs have attractive properties such as: high stiffness, high strength, low

density, and useful electrical and thermal properties [29, 34, 35]. Because of their electrical conductivity CNTs can be used as electrodes of ionic polymer actuators. The first reported single-wall CNT actuator was reported in 1999 by Baughman, *et al.* In that study two strips of carbon nanotubes papers were stacked using a double-sided scotch tape and soaked in an ionic liquid. The actuation occurred after applying voltage across the two strips[36, 37].

One of the actuation mechanisms for CNTs is caused by the quantum chemical effect in which the C-C bonds in CNTs expand due to injection of electrons and contract when electrons are lost. The cathode side will thus expand and be bent toward the anode. However, when a high voltage is applied, a high charge-density electrostatic force will result in equal expansion of both sides of the actuator and no bending will occur. [29, 36, 38]. Another mechanism of actuation is that deformation will occur due to the accumulation of ions on both sides of the actuator driven by the electric field. Because of anion and cation volume imbalance, swelling on one side will cause bending [34, 36]

1.2.2.2. *Conducting Polymers Actuators*

Conducting polymers are polymers with a conjugated structure. The backbone structure consists of atoms connected by alternating single and double bonds; Figure 1-5 shows an example of some conducting polymers with alternating structure. The conductivity of these polymers is due to the existence of the π -conjugated bond in the structure. [27, 39].

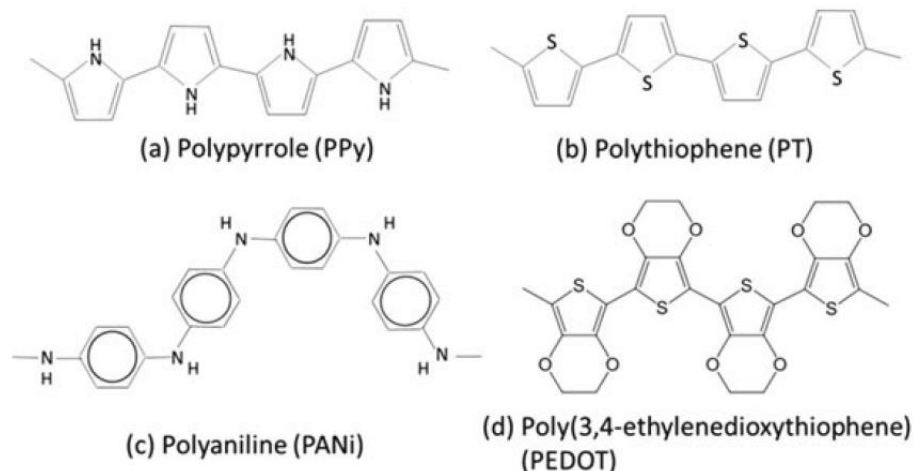


Figure 1-5 : Conjugated structure in conducting polymers[27]

With existence of ionic liquid, and exposed to an applied electric potential, oxidation and reduction will cause a deformation of the conducting polymer. Oxidation at the anode (loss of electrons) will cause insertion of anions to compensate for the charge loss, resulting in swelling and expansion of the conducting polymer. This deformation can be called electro-chemo-mechanical deformation. After oxidization, reduction (adding electrons) will cause removal of the anions and result in shrinking. This is a valid explanation if the anions are small (like ClO_4^-) and mobile within the conducting polymer; the process is called anion-driven actuation. If anions are trapped within the polymer (big [dodecylbenzenesulfonic, DBS^-] acid) or are not mobile within the polymer after oxidation, reduction will cause insertion of cations into the network instead of removing anions. In that case the polymer will expand more during the reduction state. When oxidized once again, cations will leave the network, resulting in shrinking. This process is called cation-derived actuation [27, 40]. The entire process is illustrated in Figure 1-6.

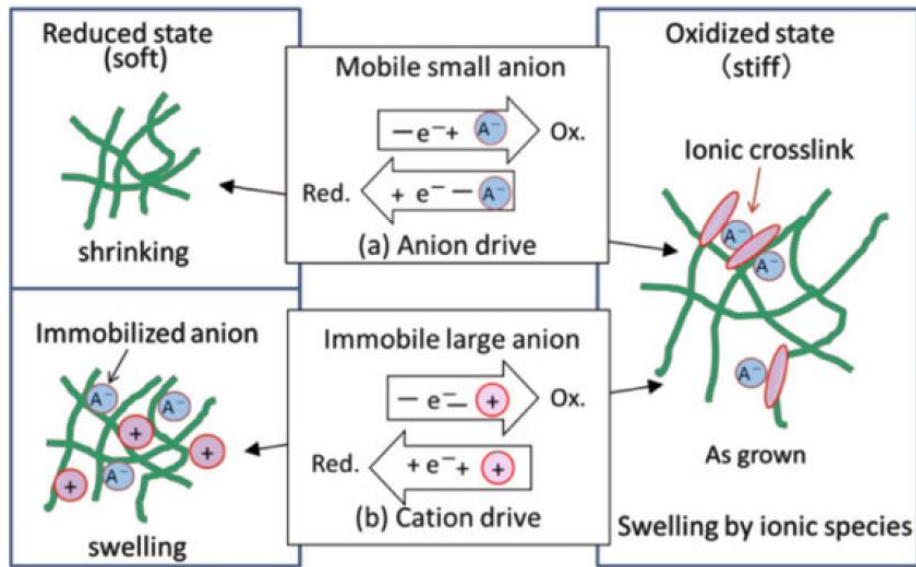


Figure 1-6 : Actuation mechanism in conducting polymers [27].

1.2.2.3. Ionic Electroactive Polymer Gels

Polymer gels can produce strong actuators that can match the force and energy of biological muscles [18]. Generally, polymer gels are composed of macromolecules cross-linked in a three-dimensional network with an interstitial spacing occupied by a fluid. These polymers are sensitive to the pH value in their aqueous environments. They will expand when alkaline solutions are added and contract when acidic solutions are added [18].

Electrically, if polymer gels contain water when a voltage of ≥ 1.2 V is applied, water electrolysis will cause the region near the cathode to become more basic as hydrogen is released from water ($H_2O = H^+ + OH^-$) and OH^- is formed in the solution. This causes a bend toward the anode [27]. In general, the actuation of polymer gel actuators is very slow (tens of minutes) and the lifetime is very short due to large deformations that damages the electrodes [7, 18]. Poly(acrylonitrile) is one example of an electroactive polymer that expands and contracts in alkaline and acidic environments, respectively.

1.2.2.4. Ionic Polymer-metal Composite (IPMC) Actuators

Ionic polymer-metal composite (IPMC) actuators contain an IPMC sandwiched between two thin metal electrodes typically composed of gold or platinum leaf. The IPMC itself consists of one polymeric ion-permeable membrane, such as Nafion, covered by two conductive network composites (CNCs) [7, 41, 42]; such a configuration is shown in Figure 1-7. The electromechanical response in ionic polymer-metal composite actuators is due to the mobility of ions through the polymer network. When an electric field is applied, ions move through attraction or repulsion to oppositely-charged electrodes. One side will swell by accumulating larger-volume ions, while accumulation of small ions on the other side will cause a contraction [7]. These actuators exhibit high deformation when small voltages (< 4 volts) are applied and will generate electrical signals when subjected to mechanical force due to the movement of charged ions. More details about these actuators will be presented in the next section.

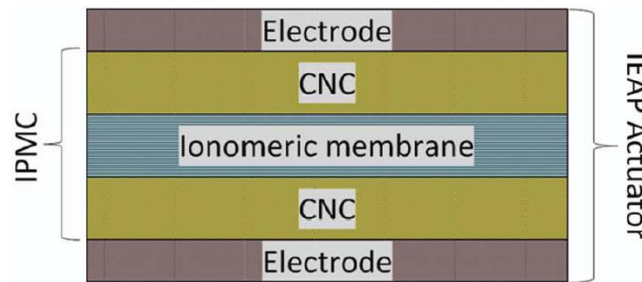


Figure 1-7 : Ionic Polymer-Metal Composite Actuator [42].

1.3. Ionic Polymer-metal Composite (IPMC) Actuators

Ionic polymer-metal composite actuators are a class of smart structures based on polymers. IPMC actuators exhibit a high mechanical response to external electrical stimulus. Conversely, they produce electrical signals when subjected to mechanical force. These actuators are shown in Figure 1-7. For simplicity this type of actuator is also called an ionic electroactive polymer (IEAP)

actuator. The backbone of the actuator is the ion permeable polymer (ionomer). The permeability of the ionomeric membrane with respect to anions and cations depends on the chemical and physical structure of the membrane. Nafion and Flemion are two popular ion-permeable polymers used in IPMC actuators.

Two CNCs are then deposited over both sides of the ionomeric polymer. The CNC layers play a significant role in actuator electromechanical behavior. They act as an extra reservoir for the electrolyte, and they provide a conductive layer that uniformly distributes electric charge across the ionomeric membrane interface. This means that they have a significant interface to and interaction with the surrounding ions. Conductivity, thickness, porosity, and pore sizes are properties that have a direct influence on the ion mobility related to the actuation magnitude and speed [42].

Ions are sourced from either an aqueous electrolyte or an ionic liquid (IL). Ionic liquids are usually preferred because their near-zero vapor pressure allows longer shelf life, operation in air, and higher operating voltages without concern with respect to ionomer hydration or electrolysis of water in aqueous electrolytes [43-45].

Upon attraction or repulsion to the oppositely charged electrodes, ions will accumulate on the sides of the actuator and generate a stress. Because of the size difference, one side will swell more than the other, resulting in bending. Figure 1-8 shows the accumulation of different-sized ions at oppositely-charged electrodes and the resulting bending mechanism. The bending direction will be reversed when the polarity of the electric field is changed.

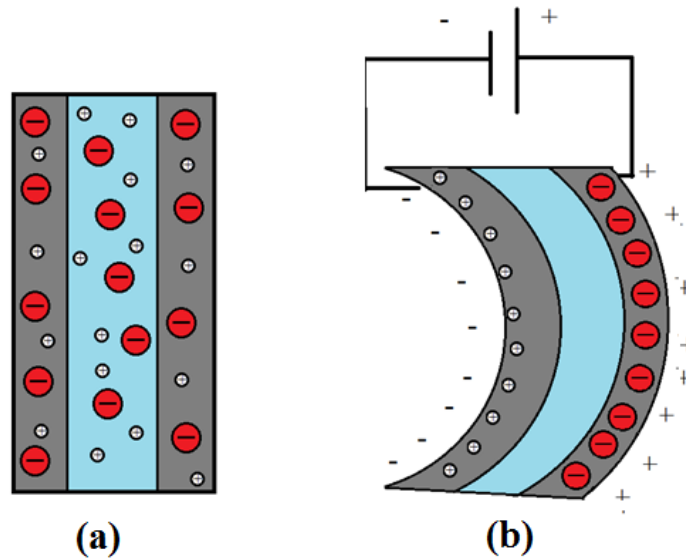


Figure 1-8: (a) Neutral case. (b) Accumulation of different-sized ions at oppositely-charged electrodes and bending mechanism

The two outer layers are the electrically-conductive electrodes. Ultra-thin metallic leaf layers (usually gold or platinum) are used as electrodes to provide extra conductivity and charge distribution, protect the actuator from the environment, and reduce electrolyte losses from the outer surfaces.

The IEAP actuator components will be discussed in detail next.

1.3.1. Ionomeric membrane

Ionomeric membranes, also known as ionomers or ion-exchange polymers, typically have nonionic repeat units and ionic groups. The ionic groups may be placed either systematically or randomly within the polymer chain as end groups or pendant groups. Some of these ionomers are called cation exchangers, in which case the ionomer will have negatively-charged ionic groups (*e.g.* SO_3^-) that can bond with and exchange cations; others are called anion exchangers, in which case the ionic groups are positively-charged groups (*e.g.* NH_3^+) that can bond with and exchange anions[46].

Ion-exchange, ionic selectivity, high elasticity, thermal stability, and water insolubility are some of the most important characteristics that make these ionomers useful for many applications. For example, proton exchange membranes are used in fuel cells and ionic electroactive actuators. Nafion and Flemion are two examples of ionomers used for electroactive actuators [7].

1.3.1.1. *Nafion*

Nafion was first developed in the 1960s by DuPont and used as electrolyte membranes in fuel cells. It is a Teflon-based polymer with short side chains terminated by ionic groups. Nafion's structure is shown in figure 1-9. It has a large tetrafluoroethylene (Teflon) backbone with short perfluorovinyl ether side chains terminated with sulfonate (SO_3^-) ionic groups. The polymer is shown in the proton (H^+) form, but this proton can be substituted by any other cation by soaking Nafion in an aqueous solution containing that cation. For this reason, Nafion is categorized as a cation-exchanger ionomer[7, 46].

Nafion has some excellent chemical, mechanical, and thermal properties. It can be cast or extruded into a very thin stable film. For example, commercial Nafion 211 has a 0.001" ($\sim 25.4 \mu\text{m}$) thickness, a weight of 50 g/m^2 , and is capable of elongation to 250% of its original length before breaking, making it very suitable for use in thin films and light-weight applications [47]. Nafion can also operate in a thermal environment of up to 190°C , making it very useful for high-temperature applications [7]. Nafion also has high chemical stability. Under normal temperature and pressure, only alkali metals can degrade Nafion. When soaked in IL or aqueous solution, Nafion can absorb up to 38 wt% of electrolytes of its dry weight. When Nafion is hydrated, cations (e.g. H^+) associated with each ionic group can move freely within the polymer matrix. On the other hand, anions are covalently fixed to the polymer backbone[27].

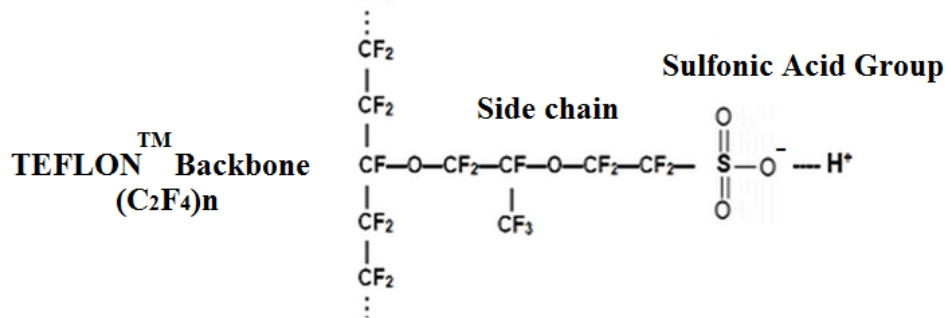


Figure 1-9 : Nafion chemical structure

The most popular model for Nafion structure was presented by Hsu and Gierke in 1982 [48]. They suggested that Nafion will have a cluster-network structure with channels that allow internal movement of ions. In their cluster-network model, they suggested that Nafion has very small hollow inverted-micelle spheres connected with nano-channels. When hydrated or soaked in ionic liquid, swelling will expand the size of these inverted micelles to have a diameter of 4 nm, separated by 5nm, and connected by 1 nm diameter channels. This configuration (shown in Figure 1-10) minimizes electrostatic repulsion between the ionic groups.

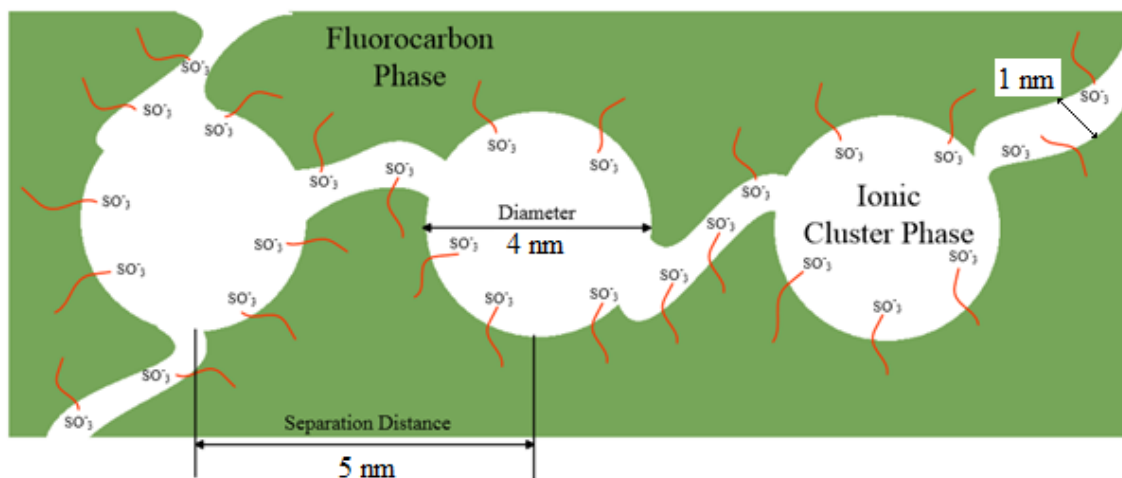


Figure 1-10: Nafion spherical cluster network model[48]

Another model was proposed by Schmidt-Rohr, *et al.*, in 2007 [49]. In that model, when Nafion is hydrated, the authors suggested that, rather than spherical micelles, the structure is made

up of 2.4 nm diameter inverted-micelle channels (cylinders) lined with hydrophilic side groups and called the water-channel model. This model is shown in Figure 1-11. This model also minimizes electrostatic repulsion between the ionic groups.

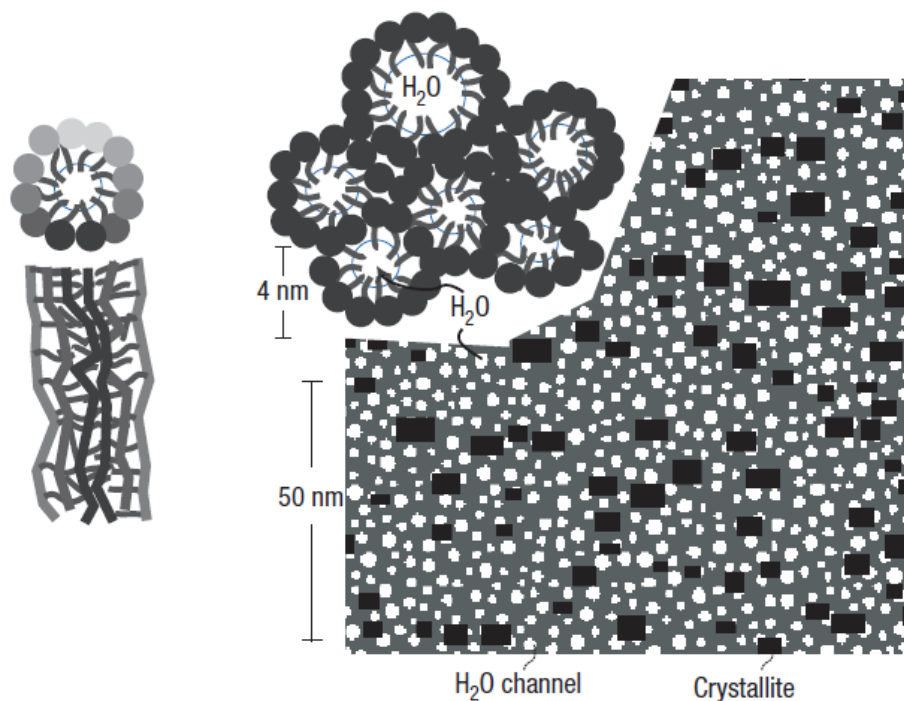


Figure 1-11: Water channel model of Nafion [49]

In both models, the existence of nano-channels will allow the transport of ions through the membrane. Nafion is known as a cation exchanger membrane (especially for protons) and used in fuel cells as a proton-permeable membrane. In case of an applied external force such as an electric field, anions can also slowly pass through the nano-channels toward the anode[7].

Flemion and Aquivion are two other examples of ionic membranes used in ionic electroactive polymer actuators. Flemion is different from Nafion in that it has carboxylate (COO^-) rather than sulfonate (SO_3^-) in its ionic group. Wang, *et al.* [50] and Nemat Nasser, *et al.* [51] have reported that actuators with Flemion instead of Nafion are preferred and perform better in ionic electroactive actuators. Aquivion is very similar to Nafion; they both have sulfonate (SO_3^-)

as their end ionic groups. The difference is that Aquivion has shorter side chains. Junhong Lin, *et al.*, found that bending actuation is higher in actuators with Aquivion rather than Nafion due to better electromechanical coupling between ions and the membrane backbone with shorter side chains [52]. Yet the actuation speed is the same as for Nafion.

1.3.2. Electrolyte

Electrolytes are liquids or solutions that contain movable ions. When an electrical field is applied, cations move toward the cathode, while anions move toward the anode. Electrolytes can be either ionic liquids or solutions containing ions. If the solvent is water, they are called aqueous solutions. Both aqueous solutions and ionic liquids are used in IEAP actuators.

Aqueous electrolytes are solutions of salts, acids, or bases in water. The main problems with aqueous solutions used in actuators are: the requirement of lower operating voltage under the water hydrolysis voltage limit (which starts at 1.2 V), the short lifespan of the actuator because of water evaporation, slow switching speed, and low ionic conductivity [41, 53, 54].

Ionic liquids are salts in their liquid form at low temperature. In general, ILs are preferred over aqueous solutions because of their superior properties. They have near-zero vapor pressure, allowing them to operate in air over a long lifespan. A large number of actuator electromechanical cycles before degradation have been reported (up to 1 million cycles at 10Hz) [54]. They can also withstand higher voltages without concern about electrolysis of water as in the case of aqueous electrolytes; this leads to higher and faster strain values [7, 44, 55]. Substantially higher ion concentration in ionic liquids, compared to that of aqueous electrolytes, and a larger Van der Waals volume difference between molecular cations and anions (compare to atomic cations and anions in aqueous electrolytes) also result in an enhanced performance of IEAP actuators doped with ionic liquids compared to those doped with aqueous electrolytes [56]. It has also been observed that

transducers with IL of 1-ethyl-3-methylimidazolium trifluoromethanesulfonate (EMI-Tf) generated the highest strain response compared with other ILs at the same temperature and applied voltage[57].

1.3.3. Conductive Network Composite (CNC) Layer

Each actuator has two conductive network composite (CNC) layers deposited on both sides of the ionomeric polymer. As mentioned before, CNC acts as an extra reservoir for the electrolyte and provides a conductive layer that uniformly distributes electric charge across the ionomeric membrane interface. Thickness, conductivity, porosity, and pore sizes are properties that directly influence ion mobility, which is related to the magnitude and speed of actuation.

Montazami, R., *et al.*, investigated the thickness dependence of curvature, strain, and response time in ionic electroactive polymer actuators fabricated via layer-by-layer assembly [58]. They showed that the curvature and net strain of IEAP actuators increase linearly with the thickness of the CNC as shown in Figure 1-12. They proposed that this increase in thickness increases the volume in which the ions can be stored and thereby leads to higher actuation curvature. The actuation time was fairly constant, suggesting that the speed is limited by motion of ions through the Nafion membrane.

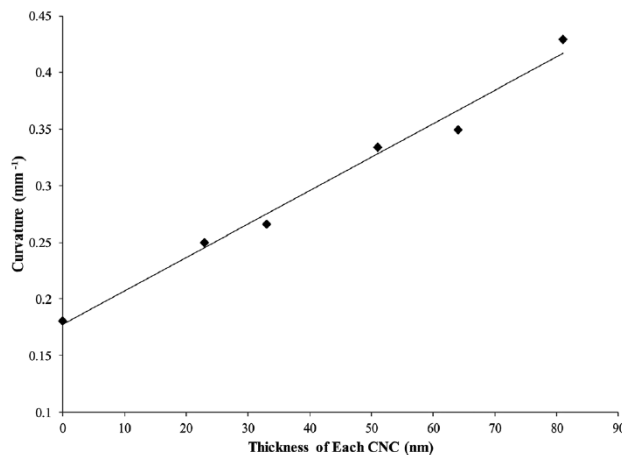


Figure 1-12 : Curvature dependence on IEAP actuator CNC thickness[58]

Montazami, R., *et al.*, conducted another study to determine the effect of CNC conductivity on actuation performance [42]. They investigated IEAP actuators with CNCs with different gold nanoparticle (AuNP) densities and found that increasing AuNP density increases CNC conductivity. The researchers used 1-ethyl-3-methylimidazolium trifluoromethanesulfonate (EMI-Tf) ionic liquid. They showed that cationic strain will increase if AuNPs concentration is increased. Cationic actuation is fast bending toward the anode caused by accumulation of cations (EMI⁺) at the cathode. As a result, cationic strain depends on how fast the cations can transit through the CNC layers. Nafion is considered to be an excellent cation-permeable polymer. Increasing the conductivity of the CNC layers results in more attraction and repulsion of the cations from the cathode and anode, producing a larger and faster strain respectively.

On the other hand, anionic strain is a slow but more effective type of strain resulting from accumulation of anionic complexes (Tf⁻-EMI⁺-Tf⁻) with higher Van der Waal volumes. As these higher-volume anionic complexes accumulate at the anode, the actuator will bend more strongly toward the cathode, canceling the cationic bending. The anionic complexes move slowly in Nafion and the overall anionic strain is controlled by their speed, so changing the conductivity of the CNC has little or no effect on anionic strain. Cationic and anionic strains for different concentrations of AuNPs in CNC are shown in Figure 1-13.

Akle, *et al.*, studied actuators with different ratios of ruthenium (IV) oxide (RuO₂) nanoparticles (3-5 nm) and gold powder (Au as gold flakes ~3μm in length) in the CNC [45]. RuO₂ has spherical nanoparticles with low conductivity but high specific area (45-60 m²/g), while gold flakes have high conductivity but lower specific area (1 m²/g). Increasing RuO₂ nanoparticles will thus increase the double-layer capacitance that depends on the interfacial area between the ionomer and the conductor. Also, with more spherical nanoparticles, the porosity of the CNC will

increase [7]. Gold flakes are more conductive but less porous. Akle, *et al*, controlled the porosity by changing the ratio of RuO₂ nanoparticles to gold flakes in the CNC. They found that actuators with 100% RuO₂ nanoparticles and 0% gold flakes exhibited highest strain due to the increase in capacitance and porosity. This indicates that the porosity of the CNC is very important even at the expense of less conductivity. Porous CNC will allow more ions to go through and generate more strain. Figure 1-14 shows the strain for different ratios of RuO₂ nanoparticles and gold flakes at the same experimental conditions.

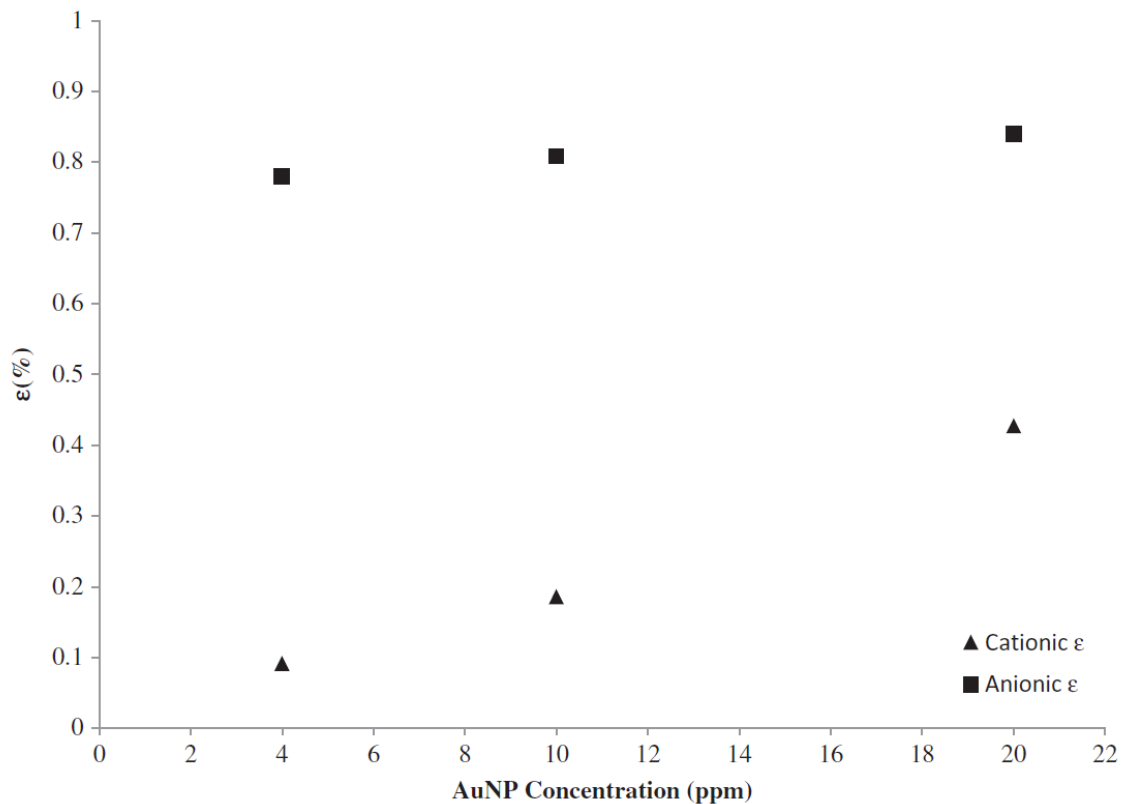


Figure 1-13 : Cationic and anionic strains for different gold nanoparticles concentration in CNC[42]

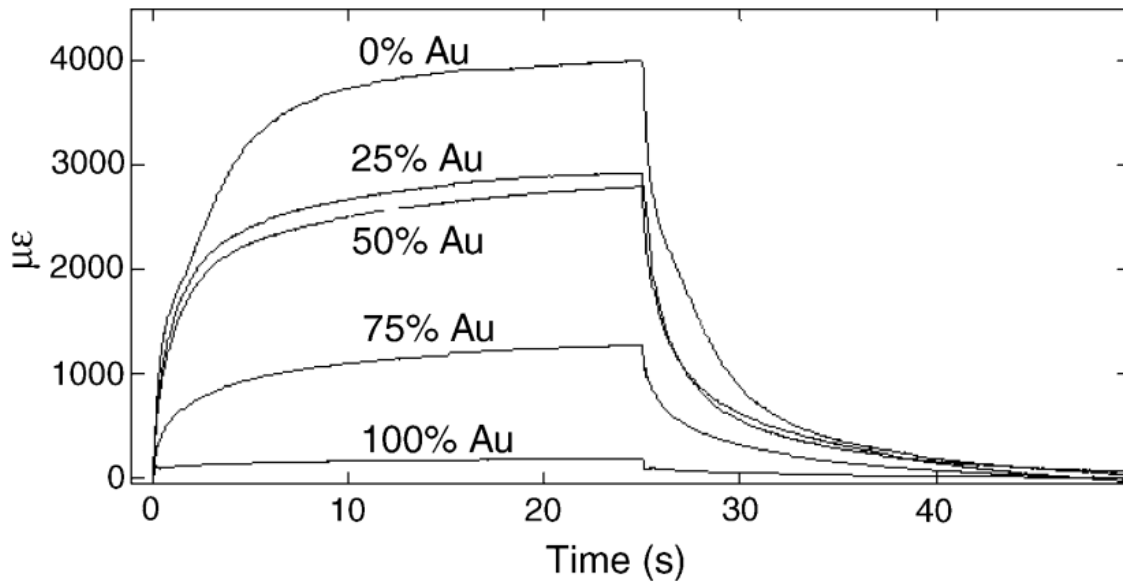


Figure 1-14: Mechanical strain for different ratio of RuO₂ nanoparticles and gold flakes[45].

1.3.3.1. Conductive Network Composite (CNC) Fabrication

As stated before, CNC layers have significant effects on actuation performance. CNCs can be fabricated using several methods, including, but not limited to: chemical plating (also called impregnation-reduction), direct-assembly plating (direct painting of the CNC on the ionomeric membrane), and the layer-by-layer self-assembly technique. The following is a brief discussion of these techniques and their advantages and disadvantages.

A) Chemical Plating

CNC fabrication has a significant effect on actuator performance, and chemical plating is one of the CNC and electrode-manufacturing techniques. In this method, the ionomer is first soaked in a solution of noble metal salt (*e.g.*, Pt(NH₃)₄Cl₂). Cations of the metal salt solution (*e.g.*, [Pt(NH₃)₄]⁺²) can then be exchanged with the cations in the membrane (*e.g.* protons in Nafion-H).

The sample is then soaked in a solution of a chemical reductant that cannot penetrate the ionomer

(sodium borohydride NaBH_4 solution). Metal ions are diffused out and reduced to form an interfacial metallic-polymer layer of nanoparticles on the surface of the membrane. The process can be repeated to produce thicker layers [59, 60]. Oguro, *et al.*, used this technique to plate gold electrodes on a Flemion-Na membrane [61]. In that case he immersed Flemion-Na in a solution of gold complex ($[\text{AuCl}_2] \text{Cl}$) to exchange Na^+ with gold cations, then reduced that with Na_2SO_3 .

Layers formed using chemical plating are very dense, reducing the ionic liquid uptake and permeability and creating slower and smaller actuation strain [7].

B) Direct Assembly Process Plating

CNC Layers can be also directly deposited over the membrane by painting or spin coating. Direct assembly-process (DAP) plating is a method proposed by Akle, *et al.*, [62-64] to manufacture the CNC and the outer electrodes. In this method, conductor nanoparticles (*e.g.* RuO_2) are mixed in an ionomer solution and directly painted over the ionic membrane to form the CNC. The membrane with the CNC layers is then sandwiched between two gold leaves and hot-pressed; the steps are shown in Figure 1-15. Akle, *et al.*, found that the interfacial area between the electrodes and the ionomer can be increased using this method, and the capacitance will also increase due the formation of an electric boundary layer on the interface between the ionomer and electrode. This increased capacitance will result in better performance. Actuators fabricated using this technique perform 2-5 times better (*e.g.*, show higher strain) than actuators fabricated by the chemical-reduction technique. The direct-assembly method is also attractive because it allows researchers to use a wide range of conductive nanoparticles, including non-metallic powder (*e.g.* carbon nanotubes[64]).

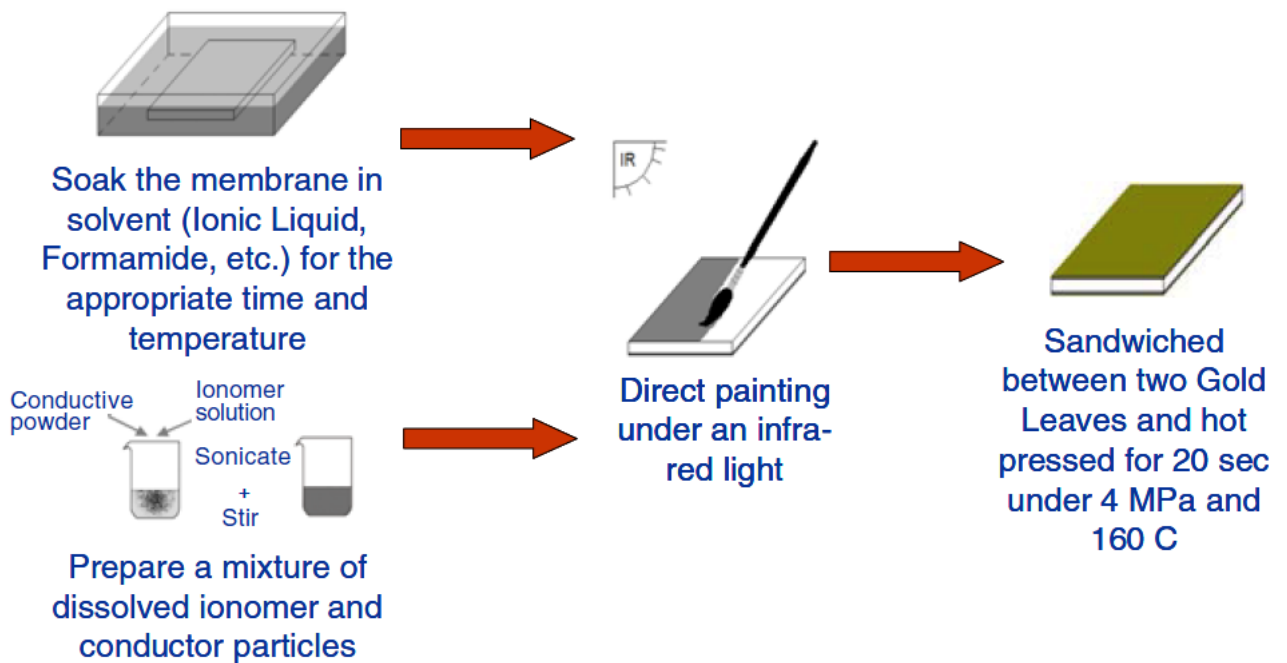


Figure 1-15 : Steps for direct assembly CNC manufacturing technique[62]

C) Layer-by-layer (LbL) self-assembly process

Although the direct-assembly process is superior to the chemical plating method, it is still difficult to obtain a homogenous thickness and to control the thickness using this method. A superior method called layer-by-layer (LbL) self-assembly can be used to manufacture a very thin homogenous CNC with precise thickness. Any species with ionic charges can be used to assemble the CNC with this technique. LbL self-assembly also provides better actuator performance than the direct-assembly method. Sheng Liu, *et al.*, [57] compared the performance of actuators with CNCs fabricated by the LbL self-assembly technique to the performance of similar actuators fabricated through the direct-assembly process. They found that the strain created by LbL actuators is about twice the strain from direct-assembly actuators. Furthermore, the LbL actuators responded in only 0.18 sec; the direct-assembly actuator took several seconds to respond instead. In our work, we mainly used the LbL technique to fabricate CNCs.

1.3.3.2. *Layer-by-Layer (LbL) self-assembly technique*

In 1966, R. K. Iler developed and introduced the layer-by-layer technique to fabricate a thin film using colloidal particles [65]. The film was developed by adding alternate layers from positively and negatively charged colloidal particles. In 1992, Decher, *et al.*, [66] used the LbL technique to fabricate a polymeric film by alternately immersing a positively-charged solid substrate in anionic and cationic polyelectrolytes, respectively. They also found that the thickness of the deposited film was linearly dependent on the number of deposited layers. The LbL technique for fabricating ultra-thin, homogenous, thickness-controlled polymeric films thus becomes attractive.

In 2009, Liu, *et al.*, [57] used the LbL technique to fabricate the conductive network composite (CNC) of ionic electroactive polymer actuators. As mentioned earlier, they were able to enhance the IEAP actuator performance by producing faster and higher strain actuators compared to actuators with CNCs fabricated by the direct-assembly method. In 2011, Montazami, *et al.*, [58] used LbL to study the effect of thickness on IEAP actuator performance. The thickness in that study was also linearly dependent on the number of deposited bi-layers.

The concept of the LbL technique is that layers are formed on a substrate as a consequence of being alternately soaked in differently-charged polyelectrolytes or solutions of charged nanoparticles. Experimental results have shown that IEAP actuators with higher porosity and conductivity perform better. Actuators that use gold nanoparticles (AuNPs) and poly(allylamine hydrochloride) (PAH) to form the CNC have excellent porosity and actuation performance [67]. In our work, we mainly adopted the LbL technique and used gold nanoparticles and PAH to form the actuator CNCs. Figure 1-16 shows the steps of CNC fabrication. A substrate with a specific electric charge is first soaked in an ionic solution with oppositely-charged molecules. Oppositely-

charged molecules are attracted to the charged substrate to form an ultra-thin layer. The substrate is then rinsed to remove the unbound and loosely-bound molecules. The substrate is next soaked in an ionic solution with oppositely-charged molecules to form a second layer, and will then be rinsed again to complete a full cycle. One full cycle will form a bi-layer with a specific, nano-scale thickness. To produce a thicker CNC, the cycle is repeated until the desired thickness is attained; this thickness is linearly dependent on the number of deposited bi-layers.

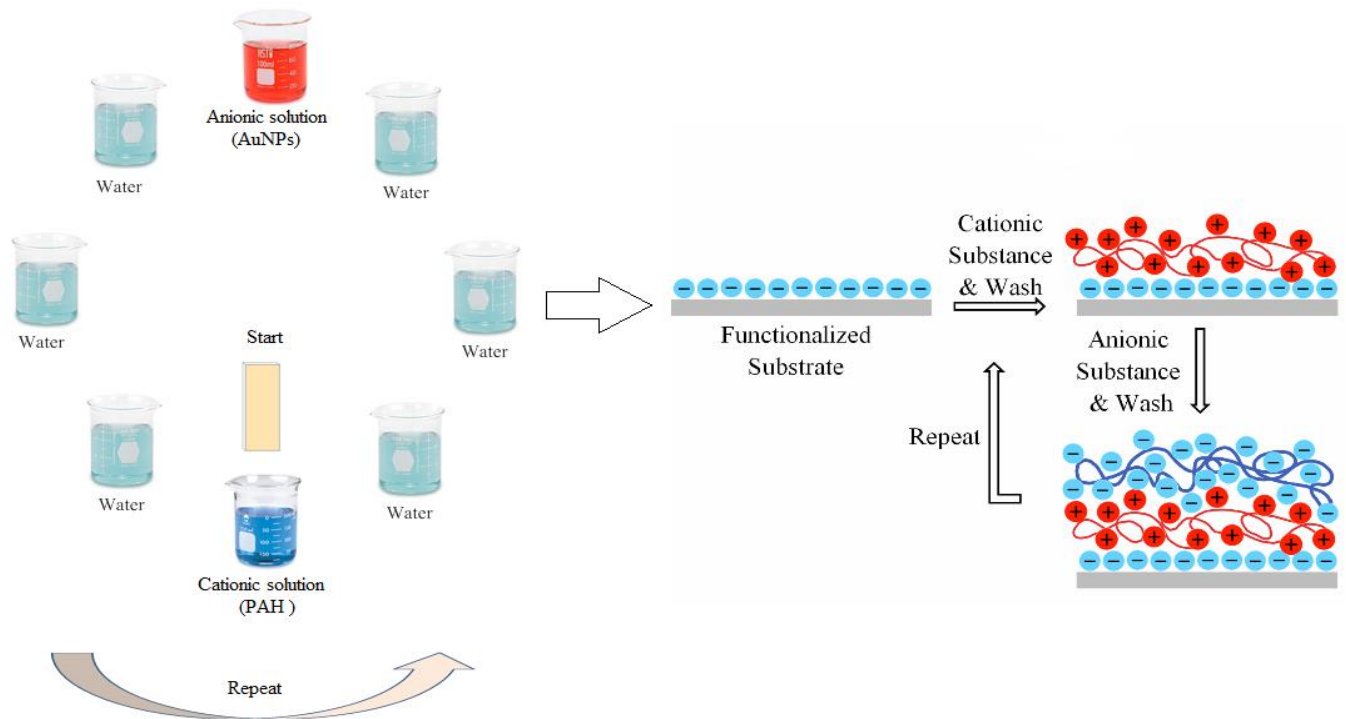


Figure 1-16: Layer-by-Layer CNC depositing technique using gold nanoparticles and PAH [56]

1.3.4. Metallic Outer Electrodes

The outer electrodes are highly electrically-conductive materials attached to both sides of the actuator. For best performance, electrodes should adhere well to the ionic polymer, be highly conductive, have high ductility and flexibility, cover a large electrochemical interfacial area, and be non-toxic [27]. The electrodes should be very thin to provide the desired actuator flexibility. Gold and platinum noble metals are usually used as electrodes. Oguro, *et al.*, first noted the bending

response of a Nafion membrane when coated with platinum [27]. In 1999, Oguro, *et al.*, [61] used gold instead of platinum electrodes for IEAP actuators. They found that gold electrodes obtained a higher strain, without gas evolution, than platinum electrodes. Other materials such as copper [68], silver [69], palladium [70], and carbon nanotubes [71] have also been used. Metallic-leaf electrodes can be hot-pressed to both sides of the actuator. Electrodes can be also chemically plated [59], electroplated [72], or sprayed [73]. Electrodes uniformly distribute the electric charge across the actuator to provide a uniform deformation and serve as a protective layer to both protect the actuator from moisture and to block the electrolyte from escaping. In our work, we hot-pressed gold leaf as electrodes on both sides of the actuator. Figure 1-17 shows an IEAP actuator with hot-pressed gold electrodes.

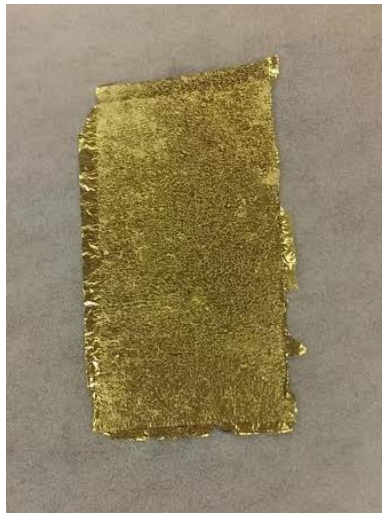


Figure 1-17: Hot-pressed gold electrodes

1.4. Document Organization

Chapter 2 describes the experimental methods and procedures that were used in conducting and analyzing the research projects that were reported in this dissertation. It describes the materials, samples fabrication process, and the experimental procedures in the research projects

in details. This includes snapshots and figures of all the equipment and materials with step by step description of sample fabrication and experimental procedures.

In **CHAPTER 3**, we investigated the influence of ionic liquid uptake percentage on the electromechanical performance of IEAP actuators. Ionic liquid uptake was increased from 10% of the membrane mass to 30%. The maximum strain was then measured and compared. We expected a higher strain by increasing the ionic liquid uptake as more accumulation of the ions at the electrodes will induce a higher stress and as a result a higher strain. The results showed a maximum peak at about 22% ionic liquid uptake and less strain at higher and lower uptakes.

CHAPTER 4 presents a study about the effect of changing the morphology of the soft composite on the sensing performance of IEAP stress sensors. Adding NaCl (salt) during the manufacturing of the CNC improved the IEAP's sensing. NaCl caused a higher thickness and higher porosity of the CNC, which improved the ions' mobility and the sensing signal of the IEAP stress sensor.

A tunable non-linear angular deformation, or limb-like motion, was achieved in the study presented in **CHAPTER 5** by adding patterns of conjugated polymers to the CNC of the IEAP actuators. The conjugated polymer patterns allowed us to control ion permeability of the soft actuator and thus the deformation shape. Actuators bent at sharp angles (90° and beyond) and exhibited limb-like deformation.

In **CHAPTER 6**, the influence of the temperature on electromechanical behavior of ionic polymer-metal composites (IPMCs) actuators was investigated. Actuators were tested at room temperature and at temperatures from 30 °C to 70 °C with increments of 10 °C. Actuators were expected to deform more and curve more as temperature increases. The results instead showed a

less cationic curvature as temperature increased and a higher anionic curvature with a peak at 50 °C followed by a sudden decrease. Both cationic and anionic deformations rates decreased with increasing temperature up to 50 °C with a sudden increase again at 60 °C. Deformation slowed at 70 °C with no practical deformation at higher temperatures.

CHAPTER 7 presents a study to explore the ionic conductivity of Nafion membranes with different exchanged counterions with different Van der Waals volume at different temperatures. The influence of Van der Waals volume of counterions and temperature on the ionic conductivity was investigated and a direct correlation between ionic conductivity and both temperature and Van der Waals volume of counterions was observed. Ionic conductivity increased by increasing the counterion size and increasing temperature.

Chapter 8 presents the overall conclusions and suggested future work.

1.5. References

- [1] C. A. Rogers and I. Ahmad, "US Army Research Office Workshop on Smart Materials, Structures and Mathematical Issues proceedings," in Workshop held in Blacksburg, VA, 15-16 Sep. 1988, vol. 1.
- [2] I. Ahmad, "Smart structures and materials," in Proceedings of US Army Research Office Workshop on Smart Materials, Structures and Mathemetacal Issues, 1988.
- [3] J. M. Jani, M. Leary, A. Subic, and M. A. Gibson, "A review of shape memory alloy research, applications and opportunities," *Materials & Design*, vol. 56, pp. 1078-1113, 2014.
- [4] G. Kauffman and I. Mayo, "The Story of Nitinol: The Serendipitous Discovery of the Memory Metal and Its Applications," *Chem. Educator*, vol. 2, no. 2, pp. 1-21, 1997.
- [5] W. J. Buehler, J. V. Gilfrich, and R. C. Wiley, "Effect of Low- Temperature Phase Changes on the Mechanical Properties of Alloys near Composition TiNi," *Journal of Applied Physics*, vol. 34, p. 1475, 1963.
- [6] S. Kamila, "Introduction, classification and applications of smart materials: An overview," *American Journal of Applied Sciences*, vol. 10, no. 8, p. 876, 2013.

- [7] R. Montazami, "Smart Polymer Electromechanical Actuators for Soft Microrobotic Applications," Virginia Polytechnic Institute and State University, 2011.
- [8] K. S. Ramadan, D. Sameoto, and S. Evoy, "A review of piezoelectric polymers as functional materials for electromechanical transducers," *Smart Materials and Structures*, vol. 23, no. 3, p. 033001, 2014.
- [9] K. I. Park et al., "Flexible nanocomposite generator made of BaTiO₃ nanoparticles and graphitic carbons," *Advanced Materials*, vol. 24, no. 22, pp. 2999-3004, 2012.
- [10] K. Otsuka, and Clarence Marvin Wayman, eds, *Shape Memory Materials*. Cambridge university press, 1999.
- [11] D. J. Fernandes, R. V. Peres, A. M. Mendes, and C. N. Elias, "Understanding the Shape-Memory Alloys Used in Orthodontics," (in en), *International Scholarly Research Notices*, Research article vol. 2011, 2011/10/03 2011.
- [12] S. Miyazaki and K. Otsuka, "Development of Shape Memory Alloys," *ISIJ International*, vol. 29, no. 5, pp. 353-377, 1989.
- [13] P. K. Gupta, P. Seena, and R. Rai, "Studies On Shape Memory Alloys—A Review," *International Journal of Advanced Engineering Technology*, vol. III, no. I, 2012.
- [14] D. Stoeckel, "Shape memory actuators for automotive applications," *Engineering Aspects of Shape Memory Alloys*, p. 283, 1990.
- [15] D. Hartl and D. C. Lagoudas, "Aerospace applications of shape memory alloys," *Proceedings of the Institution of Mechanical Engineers, Part G: Journal of Aerospace Engineering*, vol. 221, no. 4, pp. 535-552, 2007.
- [16] Savas Dilibal, R. Murat Tabanlı , Adnan Dikicioglu, "Development of shape memory actuated ITU Robot Hand and its mine clearance compatibility," vol. Volumes 155–156, pp. 1390–1394, 30 November 2004 2004.
- [17] F. El Feninat, G. Laroche, M. Fiset, and D. Mantovani, "Shape memory materials for biomedical applications," *Advanced Engineering Materials*, vol. 4, no. 3, p. 91, 2002.
- [18] T. Wallmersperger, B. Kröplin, and R. Gülch, "Electroactive Polymer (EAP) Actuators as Artificial Muscles-Reality, Potential, and Challenges; vol. PM 136, ch. Modelling and Analysis of Chemistry and Electromechanics," ed: spie Press, Bellingham, WA, UsA, 2004.
- [19] Y. Bar-Cohen, "Electroactive polymers as artificial muscles-capabilities, potentials and challenges," *Handbook on biomimetics*, vol. 8, 2000.
- [20] Y. Bar-Cohen, "Artificial muscles using electroactive polymers (EAP): capabilities, challenges and potential," 2005.

- [21] I. W. Hunter, J. M. Hollerbach, and J. Ballantyne, "A comparative analysis of actuator technologies for robotics," *Robotics Review*, vol. 2, 1991.
- [22] I. W. Hunter and S. Lafontaine, "A comparison of muscle with artificial actuators," in *Solid-State Sensor and Actuator Workshop, 1992. 5th Technical Digest.*, IEEE, 1992, pp. 178-185: IEEE.
- [23] J. Huber, N. Fleck, and M. Ashby, "The selection of mechanical actuators based on performance indices," *Proceedings of the Royal Society of London. Series A: Mathematical, physical and engineering sciences*, vol. 453, no. 1965, pp. 2185-2205, 1997.
- [24] Q. Zhang, C. Huang, F. Xia, and J. Su, "Electric eap," *Electroactive Polymer (EAP) Actuators as Artificial Muscles—Reality, Potential, and Challenges*, pp. 95-148, 2001.
- [25] A. O'Halloran, F. O'Malley, and P. McHugh, "A review on dielectric elastomer actuators, technology, applications, and challenges," *Journal of Applied Physics*, vol. 104, no. 7, p. 071101, 2008.
- [26] Z. Suo, "Theory of dielectric elastomers," *Acta Mechanica Solida Sinica*, vol. 23, no. 6, pp. 549-578, 2010.
- [27] K. Asaka and H. Okuzaki, *Soft Actuators: Materials, Modeling, Applications, and Future Perspectives*. Japan: Springer, 2014, p. 507.
- [28] R. Pelrine, R. Kornbluh, Q. Pei, and J. Joseph, "High-speed electrically actuated elastomers with strain greater than 100%," *Science*, vol. 287, no. 5454, pp. 836-839, 2000.
- [29] B. J. Akle, "Characterization and modeling of the ionomer-conductor interface in ionic polymer transducers," 2005.
- [30] Z. Lü, T. Pu, Y. Huang, X. Meng, and H. Xu, "Flexible ferroelectric polymer devices based on inkjet-printed electrodes from nanosilver ink," *Nanotechnology*, vol. 26, no. 5, p. 055202, 2015.
- [31] N. Setter et al., "Ferroelectric thin films: Review of materials, properties, and applications," *Journal of Applied Physics*, vol. 100, no. 5, p. 051606, 2006.
- [32] C. Huang, Q. Zhang, and A. Jakli, "Nematic Anisotropic Liquid-Crystal Gels—Self-Assembled Nanocomposites with High Electromechanical Response," *Advanced Functional Materials*, vol. 13, no. 7, pp. 525-529, 2003.
- [33] H. Wermter and H. Finkelmann, "Liquid crystalline elastomers as artificial muscles," *e-Polymers*, vol. 1, no. 1, pp. 111-123, 2001.
- [34] K. Asaka, K. Mukai, T. Sugino, and K. Kiyohara, "Ionic electroactive polymer actuators based on nano-carbon electrodes," *Polymer International*, vol. 62, no. 9, pp. 1263-1270, 2013.

- [35] C. Li, E. T. Thostenson, and T.-W. Chou, "Sensors and actuators based on carbon nanotubes and their composites: a review," *Composites Science and Technology*, vol. 68, no. 6, pp. 1227-1249, 2008.
- [36] L. Kong and W. Chen, "Carbon Nanotube and Graphene-based Bioinspired Electrochemical Actuators," *Advanced Materials*, vol. 26, no. 7, pp. 1025-1043, 2014.
- [37] R. H. Baughman et al., "Carbon nanotube actuators," *Science*, vol. 284, no. 5418, pp. 1340-1344, 1999.
- [38] D. Suppiger, S. Busato, and P. Ermanni, "Characterization of single-walled carbon nanotube mats and their performance as electromechanical actuators," *Carbon*, vol. 46, no. 7, pp. 1085-1090, 2008.
- [39] J. D. Madden, P. G. Madden, and I. W. Hunter, "Conducting polymer actuators as engineering materials," in *SPIE's 9th Annual International Symposium on Smart Structures and Materials*, 2002, pp. 176-190: International Society for Optics and Photonics.
- [40] E. Smela, "Conjugated polymer actuators," *MRS bulletin*, vol. 33, no. 03, pp. 197-204, 2008.
- [41] M. Shahinpoor and K. J. Kim, "Ionic polymer-metal composites: I. Fundamentals," *Smart materials and structures*, vol. 10, no. 4, p. 819, 2001.
- [42] R. Montazami, D. Wang, and J. R. Heflin, "Influence of conductive network composite structure on the electromechanical performance of ionic electroactive polymer actuators," (in en), <http://mc.manuscriptcentral.com/ijnsnm>, research-article 2012-09-18 2012.
- [43] J. Li, K. G. Wilmsmeyer, J. Hou, and L. A. Madsen, "The role of water in transport of ionic liquids in polymeric artificial muscle actuators," (in en), 2009/06/03 2009.
- [44] M. D. Bennett, and Donald J. Leo, "Ionic liquids as stable solvents for ionic polymer transducers," vol. 115, no. 1, pp. 79-90, 15 September 2004 2004.
- [45] B. J. Akle, Matthew D. Bennett, and Donald J. Leo., "High-strain ionomeric-ionic liquid electroactive actuators," vol. 126, no. 1, pp. 173-181, 26 January 2006 2006.
- [46] M. D. Bennett, "Electromechanical Transduction in Ionic Liquid-Swollen Nafion Membranes," 2005-11-11 2005.
- [47] DuPont. (2008). Nafion® Membranes - nafion-211-212-spec-sheet.pdf. Available: <http://fuelcellstore.com/spec-sheets/nafion-211-212-spec-sheet.pdf>
- [48] W. Y. Hsu and T. D. Gierke, "Ion transport and clustering in nafion perfluorinated membranes," vol. 13, no. 3, pp. 307-326, February 1983 1983.
- [49] K. Schmidt-Rohr and Q. Chen, "Parallel cylindrical water nanochannels in Nafion fuel-cell membranes," (in en), *Nature Materials*, vol. 7, no. 1, pp. 75-83, 2007-12-09 2007.

- [50] W. jin, C. Xu, M. Taya, and Y. Kuga, "A Flemion-based actuator with ionic liquid as solvent," (in en), Text 2007-04-01 2007.
- [51] Nemat-Nasser and Y. Wu, "Comparative experimental study of ionic polymer–metal composites with different backbone ionomers and in various cation forms," Text 2003/04/16 2003.
- [52] Y. L. Lin Junhong and Q. M. Zhang., "Charge dynamics and bending actuation in Aquivion membrane swelled with ionic liquids," vol. 52, no. 2, pp. 540–546, 21 January 2011 2011.
- [53] S. Mohsen, "Ionic polymer–conductor composites as biomimetic sensors, robotic actuators and artificial muscles—a review," vol. 48, no. Issues 14–16, pp. 2343–2353, 30 June 2003 2003.
- [54] W. Lu et al., "Use of Ionic Liquids for π -Conjugated Polymer Electrochemical Devices," (in en), 2002-08-09 2002.
- [55] Matthew D. Bennetta, , Donald J. Leo, G. L. Wilkes, F. L. Beyer, and T. W. Pechar, "A model of charge transport and electromechanical transduction in ionic liquid-swollen Nafion membranes," vol. 47, no. 19, pp. 6782–6796, 7 September 2006 2006.
- [56] W. Hong, A. Almomani, and R. Montazamia, "Influence of ionic liquid concentration on the electromechanical performance of ionic electroactive polymer actuators," vol. 15, no. 11, pp. 2982–2987, November 2014 2014.
- [57] S. Liu et al., "Layer-by-layer self-assembled conductor network composites in ionic polymer metal composite actuators with high strain response," Text 2009/07/16 2009.
- [58] R. Montazami, S. Liu, Y. Liu, D. Wang, Q. Zhang, and J. R. Heflin, "Thickness dependence of curvature, strain, and response time in ionic electroactive polymer actuators fabricated via layer-by-layer assembly," Text 2011/05/16 2011.
- [59] P. Millet, "Noble Metal-Membrane Composites for Electrochemical Applications," (in EN), research-article January 1, 1999 1999.
- [60] R. Tariq, U. o. N. M. (USA), M. Shahinpoor, and U. o. N. M. (USA), "Force optimization of ionic polymeric platinum composite artificial muscles by means of an orthogonal array manufacturing method," in 1999 Symposium on Smart Structures and Materials, 1999, pp. 289-298: International Society for Optics and Photonics.
- [61] K. Oguro et al., "Polymer electrolyte actuator with gold electrodes," in 1999 Symposium on Smart Structures and Materials, 1999, pp. 64-71: International Society for Optics and Photonics.
- [62] B. J. Akle, M. D. Bennett, D. J. Leo, K. B. Wiles, and J. E. McGrath, "Direct assembly process: a novel fabrication technique for large strai," 2007.

- [63] B. J. Akle, K. B. Wiles, D. J. Leo, and J. E. McGrath, "Effects of electrode morphology on the performance of BPSH and PATS ionic polymer transducers," in *Smart Structures and Materials*, 2004, pp. 413-424: International Society for Optics and Photonics.
- [64] B. J. Akle and D. J. Leo, "Single-Walled Carbon Nanotubes — Ionic Polymer Electroactive Hybrid Transducers," (in en), 2008-08-01 2008.
- [65] R. k. Iler, "Multilayers of colloidal particles," vol. 21, no. 6, pp. 569–594, June 1966 1966.
- [66] G. Decher, J. D. Hong, and J. Schmitt, "Buildup of ultrathin multilayer films by a self-assembly process: III. Consecutively alternating adsorption of anionic and cationic polyelectrolytes on charged surfaces," vol. Volumes 210–211, pp. 831–835, 30 April 1992 1992.
- [67] W. Hong and I. S. University, "Influence of conductive network composite thickness and structure on performance of ionic polymer-metal composite transducer," Iowa State University, 2013.
- [68] U. Johanson et al., "Electrode reactions in Cu–Pt coated ionic polymer actuators," vol. 131, no. 1, pp. 340–346, 14 April 2008 2008.
- [69] C.-K. Chung, P. K. Fung, Y. Z. Hong, Ming-Shaung Ju, Chou-Ching K. Lin, and T. C. Wu., "A novel fabrication of ionic polymer-metal composites (IPMC) actuator with silver nano-powders," vol. 117, no. 2, pp. 367–375, 12 October 2006 2006.
- [70] W. Aoyagi and M. Omiya, "Mechanical and electrochemical properties of an IPMC actuator with palladium electrodes in acid and alkaline solutions," (in en), Text 2013-05-01 2013.
- [71] S. Heo et al., "Multiwalled carbon nanotube/IPMC nanocomposite," in *Smart Structures and Materials*, 2005, pp. 194-202: International Society for Optics and Photonics.
- [72] J.-H. Jeon and I.-K. Oh, "Selective growth of platinum electrodes for MDOF IPMC actuators," vol. 517, no. 17, pp. 5288–5292, 1 July 2009 2009.
- [73] C. Meis, N. Hashemi, and R. Montazami, "Investigation of spray-coated silver-microparticle electrodes for ionic electroactive polymer actuators," Text 2014/04/01 2014.

CHAPTER 2. EXPERIMENTAL METHODS AND PROCEDURES

This chapter describes the materials, fabrication process, and the experimental procedures used in the research projects reported in this dissertation. Section 2.1 defines and describes all the materials, equipment, and the fabrication process. Section 2.2 describes the experimental procedures for different experiments. The procedure to characterize actuation performance is described in 2.2.1, and that for the sensing performance is described in 2.2.2, the procedure for electrochemical characterization is described in 2.2.3, testing as a function of temperatures is described in 2.2.4, and finally, the procedure for ion exchange is described in 2.2.5.

2.1. Materials and fabrication process

2.1.1. Materials

Nafion (sulfonated tetrafluoroethylene based fluoropolymer-copolymer) of 25 μm thickness (NR-211, IonPower) was used as the ionomer membrane. In most experiments, Nafion was used in its acidic form where protons (H^+) are the counter ions attached to the sulfonic acid groups. The acidic form of Nafion is shown in Figure 2.1. In some experiments, the proton counterions were substituted by other ions through an ion exchange process. 1-ethyl-3-methylimidazolium trifluoromethanesulfonate (EMI-Tf molecular formula, $\text{C}_7\text{H}_{11}\text{F}_3\text{N}_2\text{O}_3\text{S}$) (Sigma-Aldrich) ionic liquid (IL) was used as the sources of mobile ions for actuation, sensing, and electrochemical characterizations. Poly(allylamine hydrochloride) polycation (PAH^+), chemical structure $[\text{CH}_2\text{CH}(\text{CH}_2\text{NH}_2.\text{HCl})]_n$, and anionic functionalized gold nanoparticle (AuNPs) (~3 nm diameter, Purest Colloids Inc), were used to form the conductive network composites (CNCs) on both sides of the Nafion membranes using a StratoSequence 6 (NanoStarta Inc) automated thin-film fabrication robot. Gold leaves of 50 nm thickness (24K, transfer, LA Gold Leaf) were used as the outer electrodes.

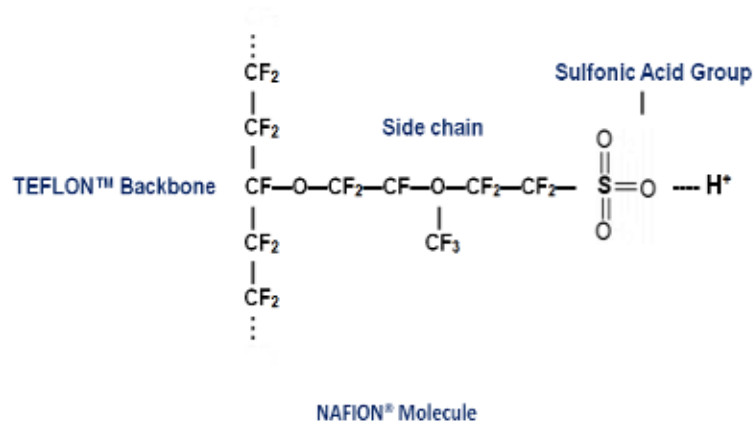


Figure 2-1 Nafion's chemical structure (<http://www.nafionstore.com/>)

2.1.2. Fabrication procedure:

Fabrication of IEAP transducer can be divided into four main steps as follows:

Step1: Preparation of materials and chemical solutions:

The 25 μm Nafion membrane, as received, is protected with two outer plastic films to protect the membrane and facilitate its storage and handling. The process starts by cutting a rectangular piece (2cm \times 5cm) of the Nafion membrane and soak it in deionized (DI) water for approximately 10 minutes to remove the protective films. After 10 minutes, the two protective films will be carefully removed and Nafion membrane will be dried by placing it between two papers to absorb the moisture. The dried Nafion membrane is then fixed by double sided adhesive tape on a glass frame that is designed to hold the sample during the deposition of the CNC on both sides of the membrane using the automated layer by layer (LBL) dipping robot. The glass frames (as shown in Figure 2.2) are made from ordinary microscope glass slides after cutting a rectangular piece from them to expose the Nafion membranes to the dipping solutions during the layering process to form the CNC. The glass frame with the Nafion will be then soaked in water while preparing the AuNPs/PAH solutions, which will make the Nafion membrane negatively charged.

The next step is to prepare a 140 ml of 10 mM concentration of PAH and adjust the pH to 4.0 (this will serve as the cationic or the positively charged polyelectrolyte) and a 140 ml AuNPs of 20 ppm concentration of functionalized gold nanoparticles (AuNPs, \sim 3 nm diameter) and adjust the pH to 9.0 (this will serve as the anionic or the negatively charged solution).



Figure 2-2: Glass frame used to hold the membrane during LbL ionic self-assembly process (left). Nafion membrane attached to a glass frame (right)

Step 2: Using the dipping robot to deposit the layers using the Layer by layer technique

In this step, an automatic dipping robot (StratoSequence 6, NanoStarta Inc.) will be used to form the CNC using the LBL technique. This robot can hold 8 (140 ml) beakers. Two of them will be used for the 10 mM concentration cationic PAH and the 20 ppm anionic AuNPs solution. The remaining 6 beakers will be filled with deionized water to rinse the membrane after each deposition with PAH and/or AuNPs.

The process starts with arranging the beakers so that the deposition will start with the positively charged PAH to form the first layer over the negatively charged Nafion, the membrane is set to rotate in PAH solution for 5 minutes. Three beakers of DI water will be placed in the consecutive spots to the PAH beaker to rinse the membrane after deposition the PAH layer, three rinsing steps for 1 min each will be required after each deposition. The negatively charged AuNPs solution beaker will be placed after the three rinsing water beakers. The membrane should also rotate in AuNPs solution for 5 minutes. Another 3 beakers of DI water will be placed in the consecutive spots the AuNPs container to rinse the membrane after deposition the AuNPs layer. The dipping robot and the beakers arrangement are shown in Figure 2.3. These steps will be repeated for more bi-layers. Each full cycle will deposit one bi-layer of PAH and AuNPs. The dipping machine is controlled by StratoSmart software that is installed on the computer connected to the machine. The setup of the StratoSmart software for depositing 20 bi-layers of the CNC is shown in Figure 2.4. Figure 2.5 shows a Nafion membrane before and after 20 bi-layers

formations. It is also important to change the solutions periodically when the concentration of the chemical solutions decrease. The DI water will be replaced automatically at each dipping cycle.

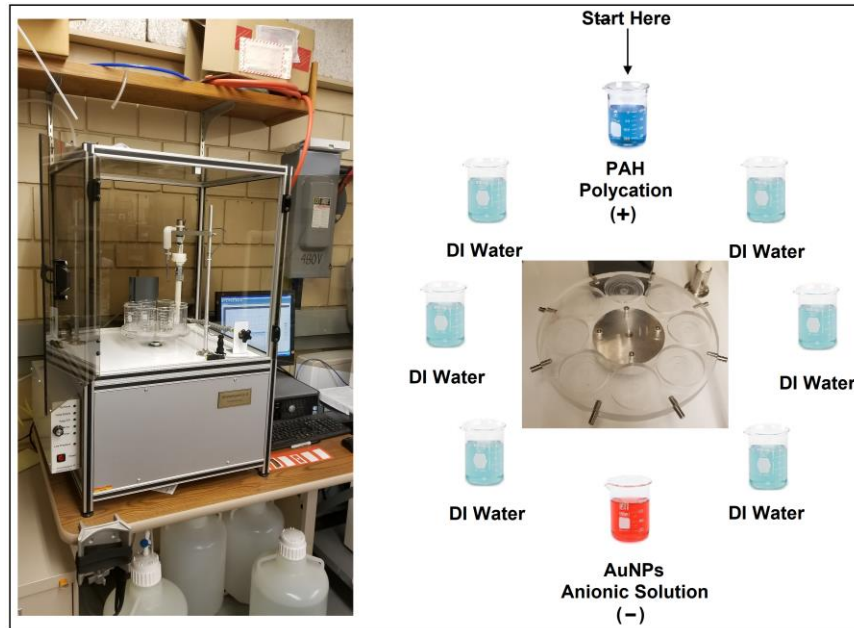


Figure 2-3: dipping robot and beakers arrangement

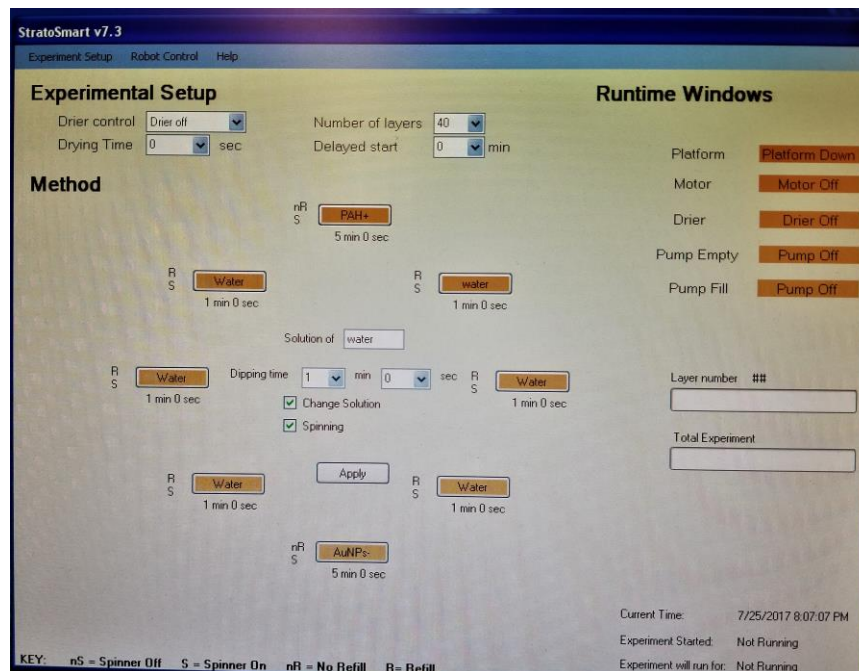


Figure 2-4: StratoSmart software setup for depositing of 20 bi-layers of CNC on Nafion membranes.

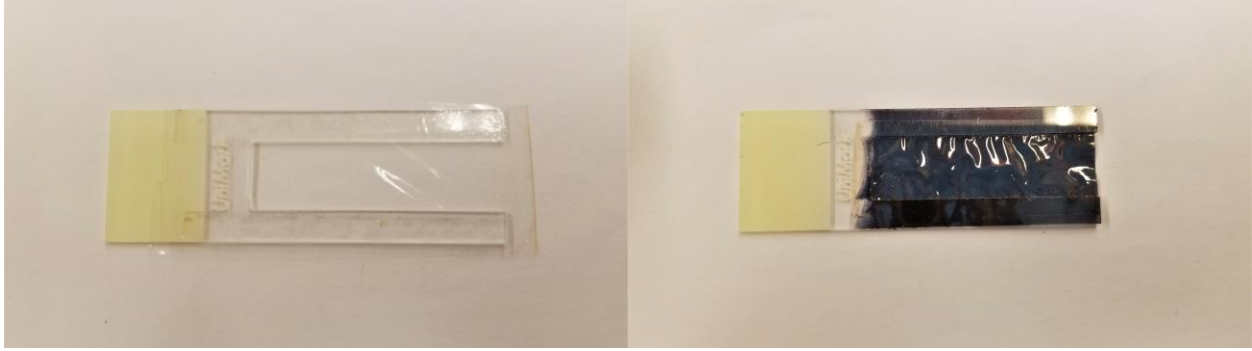


Figure 2-5: Pure Nafion (left) and Nafion membrane with 20 bi-layers CNC (right)

Step 3: Soaking the membrane in ionic liquid

The produced membrane from the previous step will be cut and weighted using a microbalance. Then, the membrane with the bi-layers will be soaked in IL for a specific time depending on the desired IL uptake. Increasing the temperature of IL bath ($\sim 80^\circ\text{C}$) expedites the intake.

After soaking, the membrane will be taken out with plastic tweezers and excess IL will be dried by placing it between papers before weighting. The weight percentage of the IL weight percentage (wt%) can be then calculated using equation 2.1.

$$\text{IL (wt\%)} = \frac{w_{\text{final}} - w_{\text{initial}}}{w_{\text{final}}} \times 100\% \quad (2.1)$$

where w_{initial} and w_{final} are the weight of the Nafion membrane in dry and IL impregnated forms, respectively.

Step 4: Hot press gold leaves on both sides of the membrane

The last step is to hot press gold leaves on both sides of the swollen membrane. Two 50 nm thick gold leaves will be cut slightly larger than the Nafion membrane. The membrane will be then placed between the two gold leaves and pressed using a 25T hydraulic hot press machine (MTI Corporation) at 95°C under ~ 100 KN of force for about 40 seconds. Gold leaves will serve as the external electrodes on the two sides of the samples. Figure 2.6 shows the 25T hydraulic hot press machine and the final fabricated actuator which will be cut later to smaller $1\text{mm} \times 1\text{cm}$ actuators for characterization and testing.



Figure 2-6: 25T hydraulic hot press machine (left), final hot pressed membrane (right, upper), and actuators to be tested (right, lower)

2.2. Characterizations

2.2.1. Actuation performance characterization

The fabricated actuators will be fixed between two titanium electrodes that are connected to a power supply. A 4V DC potential will be applied across the thickness of the actuators through the titanium electrodes. A digital oscilloscope will be used to monitor any short circuit in the system and record the applied potential. The electromechanical actuation will be then recorded by a camera and the radius of curvature as a function of time will be measured for further analysis and strain calculation. The actuation process is shown in Figure 2.7. The actuators will be first on

neutral position before applying the 4V DC potential difference (Figure 2.7 (A)) and will then start to move toward the anode (cationic bending, Figure 2.7 (B)) and go back slowly toward the cathode with a higher bending magnitude (anionic bending, Figure 2.7 (C)). The cationic bending and anionic bending are described in section 1.3.3. The entire process is shown in Figure 2.7 (D). Equation (2.2) will be then used to calculate the bending strain.

$$\varepsilon(\%) = \frac{h}{2r} \times 100 \quad (2.2)$$

where r representing the radius of curvature depending on the extent of bending and h representing the thickness of the actuators.

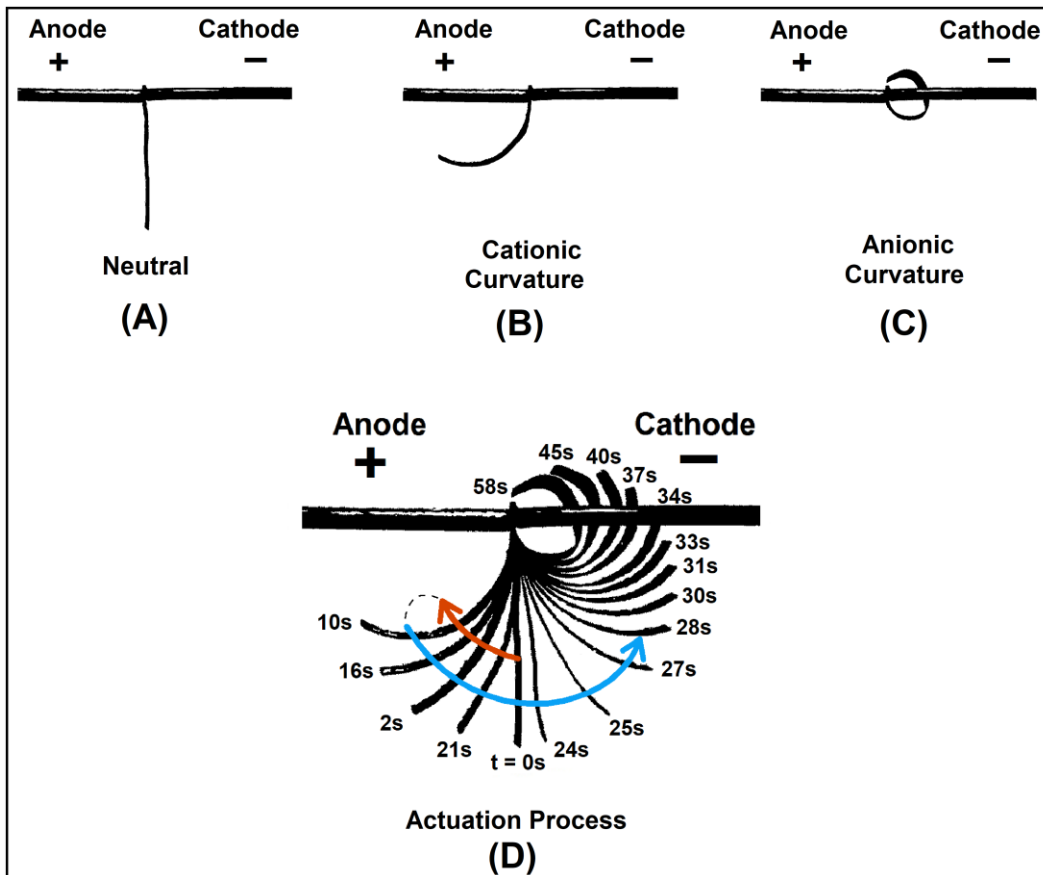


Figure 2-7: Actuation Process. Neutral position (A), Cationic Curvature (B), Anionic curvature (C), and the time lapse for the whole actuation process (D).

2.2.2. Sensing performance characterization

The fabricated sensors of about $1\text{ cm} \times 1\text{ cm}$ will be enclosed by two copper foil electrodes on both sides of the sensors. Copper electrodes were used here because they have a better physical robustness than gold leaves electrodes as sensors will be exposed to a dynamic impact during testing which will break the gold leaves electrodes. The copper electrodes will then be connected to a digital phosphor oscilloscope to record the generated voltage. To generate an electrical signal, the sensor will be disturbed by a dynamic impact generated by a motorized mechanical arm with a controllable and constant impact frequency. The sensing setup scheme and the generated signal are shown in Figure 2-8.

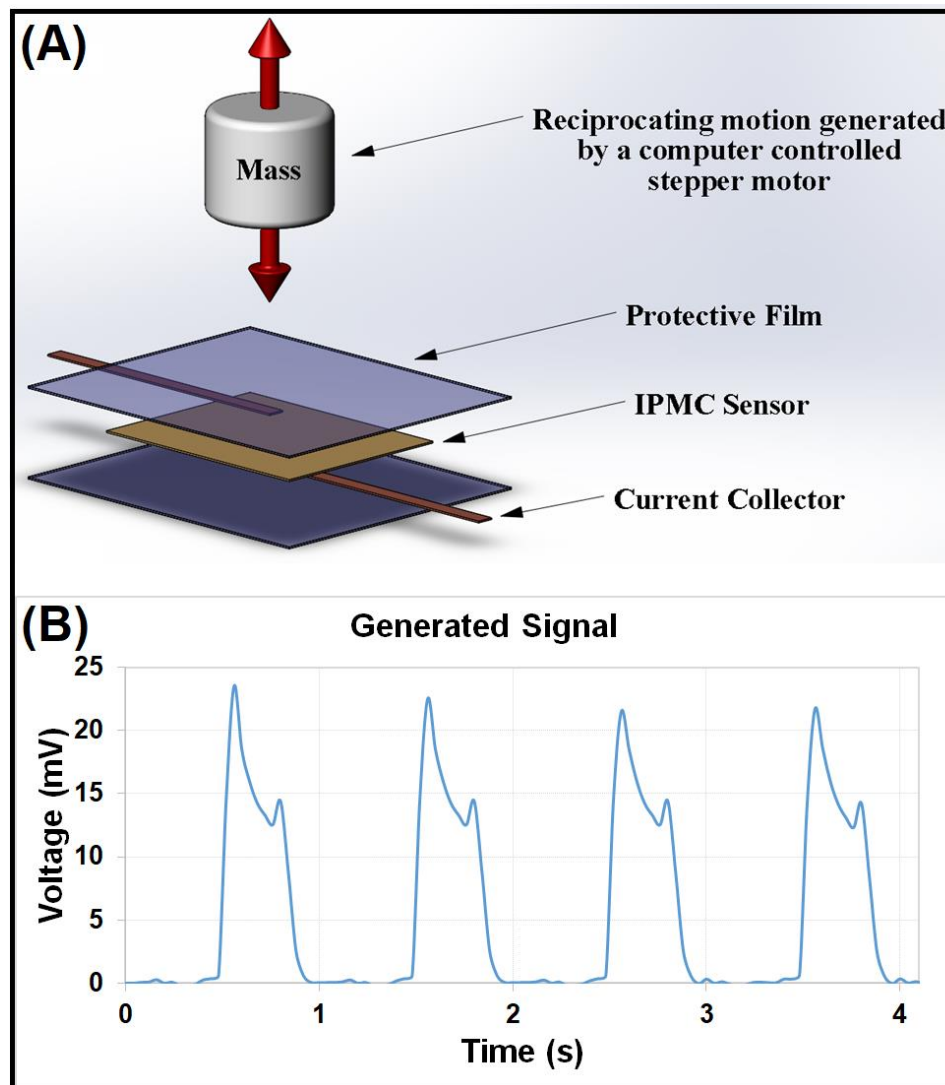


Figure 2-8: Sensing process. (A) The experimental setup. (B) The generated signal.

2.2.3. Electrochemical characterization

Electrochemical properties of the Nafion membranes, including electrical impedance, current flow, capacitance, etc., were characterized using a VersaSTAT-4 potentiostat (Princeton Applied Research) which is shown in Figure 2.9. The process starts by cutting a sample of 1.2 cm \times 1.2 cm from the membranes and place it between two 1 cm \times 1 cm copper electrodes that were glued to two separate glass substrates as shown in Figure 2.10. The copper electrodes will then be connected to the potentiostat. The potentiostat software contains several experiment options (actions) to choose from as shown in Figure 2.11.



Figure 2-9: VersaSTAT-4 potentiostat

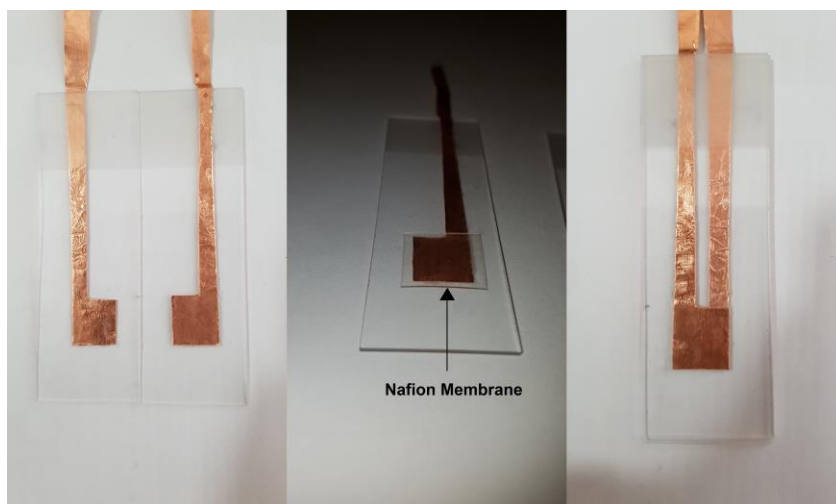


Figure 2-10: Nafion membrane between two copper electrodes

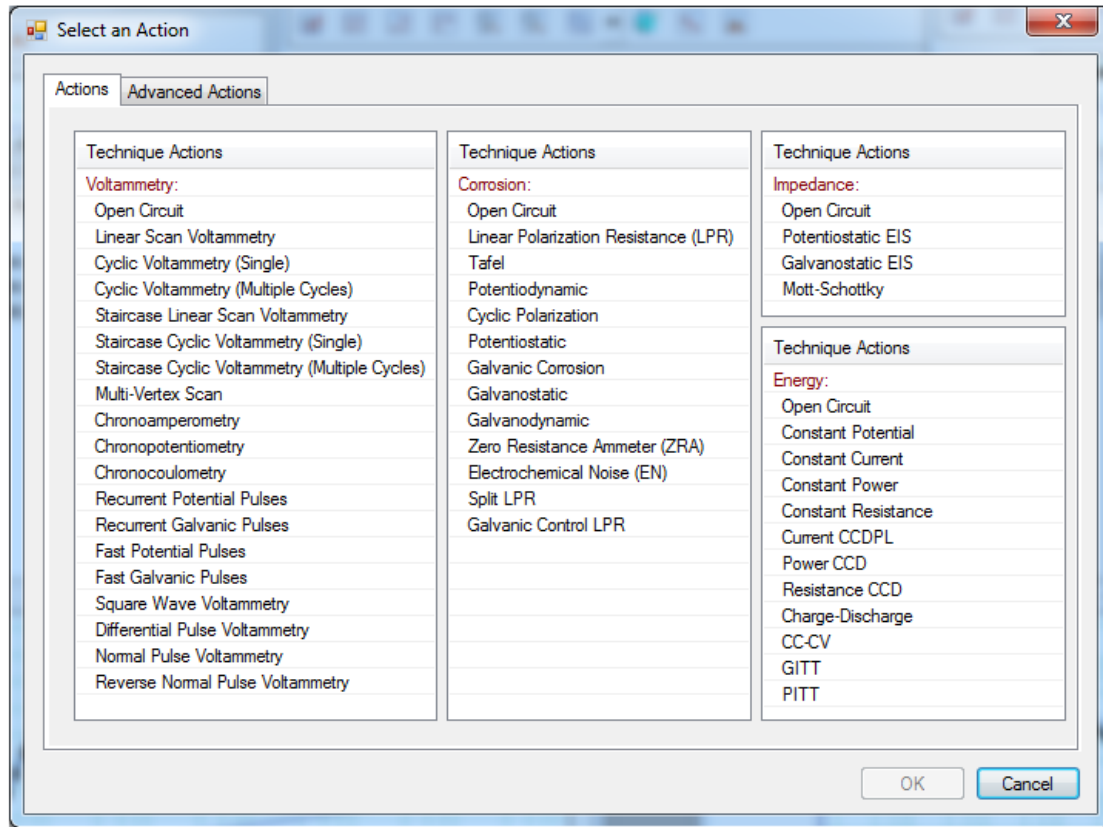


Figure 2-11: Different electrochemical experiments from potentiostat software.

After selecting the appropriate action, the experimental conditions will be added in another window where for example the applied potential, starting and ending applied frequency, duration of the selected test, the applied current, etc. can be entered. An example of this setup, for an impedance test, with 100 kHz starting frequency, 0.1 Hz ending frequency, and 10 mV applied potential is shown in Figure 2.12.

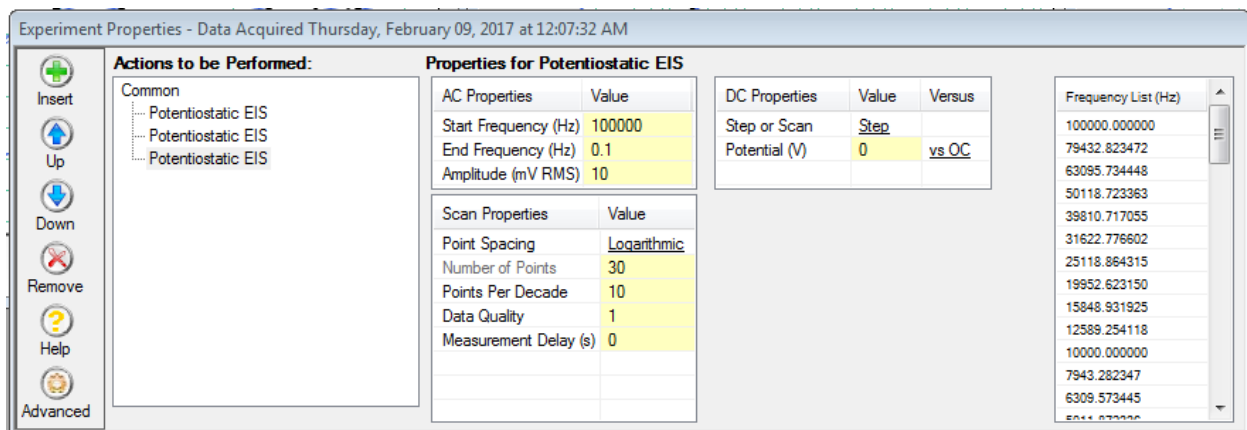


Figure 2-12: Impedance test experimental properties from potentiostat software

After determining the experimental conditions, appropriate ways to represent the data are selected from a list of available graph templates. Some examples of the available graphs and data are shown in Figure 2.13.

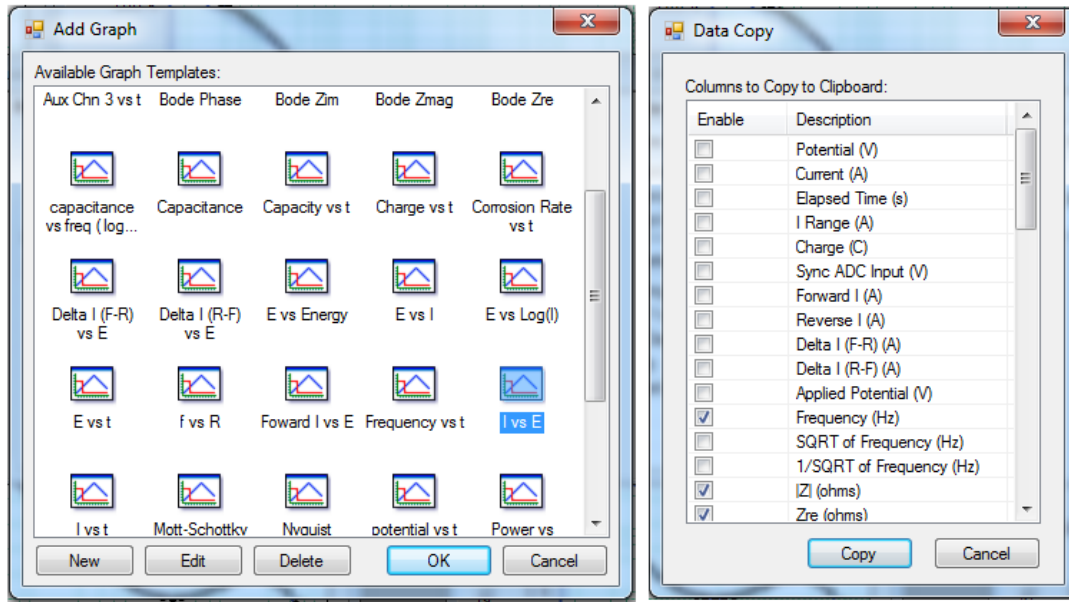


Figure 2-13: Examples of electrochemical data that can be extracted from the VersaSTAT-4 potentiostat

2.2.4. Characterization of electromechanical behavior as a function of temperature

Two different procedures are used to test actuators or membranes at different temperatures depending on the type of the experiment as follows.

2.2.4.1. Testing the actuation process in air at different temperatures

The procedure for this experiment is similar to the procedure described in 2.2.1. In addition to the steps in 2.2.1, the experiment is conducted in an in-house fabricated temperature-controlled chamber for thermal isolation. The actuators are mounted with a clearance of 5 cm of a manually temperature controlled resistive heater that will be used to raise the temperature inside the chamber. The temperature around the actuator is measured by a thermocouple when a uniform and stable temperature across the chamber is achieved. The actuation performance will be recorded and analyzed at the desired temperatures. The experimental setup is shown in Figure 2.14.

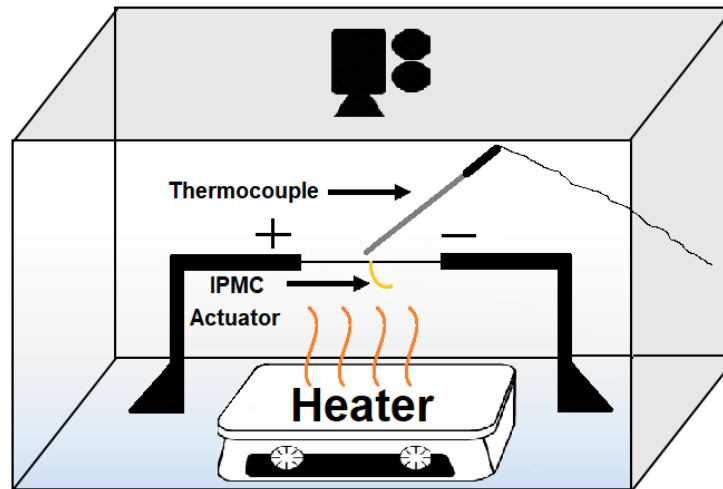


Figure 2-14: Actuation performance at different temperatures in air setup.

2.2.4.2. Testing electrochemical properties at different temperatures

For electrochemical characterizations as a function of temperature, the procedure is similar to the procedure in section 2.2.3. In addition to the steps in 2.2.3, hot glue is used to seal the edges of the glass substrates before submerging it into a temperature-controlled water bath. A hot plate (Corning 5×7 in² PC-420D) with temperature feedback control is used to achieve the desired temperature in the water bath and a mercury thermometer is used to measure the actual temperature to increase confidence. It is easier and more accurate to control and achieve the desired temperatures using a hot water bath, but this method is not suitable for actuation process as actuators shall operate in air.

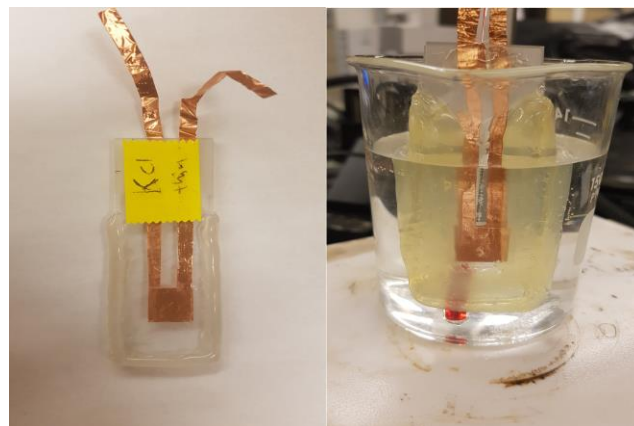


Figure 2-15: Water proof samples using hot glue to seal the edges of the glass substrates (left), submerged samples in hot water at the desired temperature to be tested (right).

2.2.5. Ion exchange procedure

For specific experiments, the proton counterions in acidic Nafion need to be substituted by other ions. The preparation of samples will start by exchanging the protons in Nafion with one of the counterions to be tested. This can be achieved by boiling Nafion membranes in 1.0 M sulfuric acid for 120 minutes, followed by boiling in DI water for 120 minutes. The membranes will be then exchanged from the proton form to one of the counterions forms by soaking in 0.5 M aqueous salt solution of the desired ion for two days at 80 °C, followed by eight days at 60 °C. One example is Nafion-Lithium (Nafion-Li) form, where in this case the Nafion membrane will be soaked in lithium chloride salt solution following the steps above. After that, the membrane will be rinsed thoroughly and soaked in DI water for 3 hours to remove any excess salt and then dehydrated in a vacuum oven (110 °C, -100 kPa) for 3 days. The dehydrated membrane will be then impregnated by soaking in EMI-Tf for 48 hours at 80 °C and then cut into $1 \times 1 \text{ cm}^2$ samples for testing.

CHAPTER 3. INFLUENCE OF IONIC LIQUID CONCENTRATION ON THE ELECTROMECHANICAL PERFORMANCE OF IONIC ELECTROACTIVE POLYMER ACTUATORS

Published in the journal of Organic Electronics¹

Wangyujue Hong^{2,3}, Abdallah Almomani^{2,4}, Reza Montazami^{2,3,5}

Abstract

We have investigated the influence of ionic liquid concentration on the electromechanical response of ionic electroactive polymer actuators. Actuators were fabricated from ionomeric membrane and doped with different concentrations of 1-ethyl-3-methylimidazolium trifluoromethanesulfonate ionic liquid. Samples were investigated for their electromechanical and electrochemical characteristics; and it was observed that the maximum electromechanical strain of approximately 1.4% is achieved at 22 wt% ionic liquid content. Increasing ionic liquid concentration results in saturation of the electrode-ionomer interface and formation of ionic double/multi layers, which in turn result in an inward accumulation of ions; hence, generate strain in an undesired direction that deteriorates the electromechanical response of the actuator.

¹ The publisher of this journal “Elsevier “, allows the students to include the work in their thesis or dissertation if this is not to be published commercially.

² Primary researchers and authors. Graduate student, graduate student, and academic advisor, respectively.

³ Department of Mechanical Engineering, Iowa State University.

⁴ Department of Aerospace Engineering, Iowa State University.

⁵ Author of correspondence.

3.1. Introduction

Recently, electroactive polymers have received immense attention and interest from the materials community because of their applicability to actuators, sensors and haptics [1–3]. Electroactive polymers are soft and lightweight; hence, enable the realization of biomimetic and micro-robotic devices. Among wide variety of electroactive polymers, ionic electroactive polymers (IEAP) have proven more practical for actuator applications due to their substantially low operation voltage (typically <5 V), light weight, relatively large strain, and bending (instead of linear) deformation [4,5].

IEAP actuators comprise of an ionomer membrane that is doped with an ion-rich electrolyte and coated with electrodes on each surface [6,7]. The electromechanical response is upon attraction/repulsion of ions and their accumulation at the oppositely charged electrode when subjected to an external electric field. Due to the volume difference between cations and anions, cathode and anode swell to different extents, thus a volume imbalance is generated in the actuator, which in turn causes a mechanical deformation. Change in the polarity of the electric field reverse the process and direction of bending [8–14].

Ions are sourced by either an aqueous electrolyte or ionic liquid (IL). Ionic liquids are preferred as their near zero vapor pressure allows longer shelf life, operation in air, and higher operation voltages without concerns about ionomer hydration or electrolysis of water in aqueous electrolytes [15–17]. Also, substantially higher ion concentration in ionic liquids, compare to that of aqueous electrolytes, and larger Van der Waals volume difference between molecular cations and anions (compare to atomic cations and anions in aqueous electrolytes) result in an enhanced performance of IEAP actuators doped with ionic liquids, compare to those doped with aqueous electrolytes. These characteristics along with scalable manufacturing and flexibility in design

allow integration of IEAP actuators in flexible organic electronics, micro-robotics, biomimetic devices and bioelectronics [18].

In the present study, we have demonstrated that the electromechanical performance of IEAP actuators is influenced by the concentration of the ionic liquid and that the concentration of ionic liquids can be tuned to achieve maximum actuation performance. Ionic liquids concentration in IEAP actuators was varied while electromechanical and electrochemical properties were characterized. It is shown that the ionic liquid concentration can be used as a means to control, improve and optimize actuation performance; and that at high concentrations of ionic liquid an ionic double/ multi-layer forms at the ionomer–electrode interface which deteriorate the actuation strain.

3.2. Materials and Methods

3.2.1. Sample Preparation

Commercially available Nafion membrane of 25 μm thickness (Ion Power Inc, DE-USA) was used as the ionomeric membrane. To fabricate IPMCs, nanocomposites of the polycation poly(allylamine hydrochloride) (PAH) (Sigma-Aldrich, MO-USA) and anionic functionalized gold nanoparticle (AuNPs) (~ 3 nm diameter, Purest Colloids Inc, NJ-USA) were grown on both sides of the Nafion membrane via LbL deposition of the ionic species, using a StratoSequence 6 (NanoStarta Inc, FL-USA) automated thin-film fabrication robot. The substrates were alternately immersed for 5 min each in aqueous solutions of PAH at a concentration of 10 mM at pH 4.0 and AuNPs at a concentration of 20 ppm at pH 9.0 with three rinsing steps for 1 min each in de-ionized water after each deposition step. IPMCs were then soaked with 1-ethyl-3-methylimidazolium trifluoromethanesulfonate (EMI-Tf molecular formula: $\text{C}_7\text{H}_{11}\text{F}_3\text{N}_2\text{O}_3\text{S}$) (Sigma-Aldrich, MO-USA) ionic liquid at 80 $^\circ\text{C}$ for various durations of time to intake desired concentrations of ionic

liquid. Ionic liquid content was measured as the weigh percentage (wt%) of dry weight of the membrane, and calculated from Equation (3-1).

$$w_e(\%) = \frac{w_f - w_d}{w_f} \times 100\% \quad (3-3-1)$$

where W_e (%) is the weight-percent of the electrolyte; and, W_d and W_f are the weights of dry and doped samples, respectively. Gold leaf electrodes of 50 nm thickness were then hot-pressed at 95 °C under 1000 lbf for 25 s on both sides of the membrane to form IEAP actuators.

3.2.2. Electrochemical characterization

Impedance spectroscopy and current flow were measured and recorded using a VersaSTAT-4 potentiostat (Princeton Applied Research, IL-USA). The impedance spectroscopy studies were carried at frequencies between 1.0E5 Hz and 0.1 Hz, and a potential difference (ΔV) of 10 mV. Current flow was monitored in response to a ± 4 V step potential over 60 s intervals. Electrical conductivity (σ) of the doped membranes was calculated from Equation (3-2),

$$\sigma = \frac{h}{RA} \quad (3-3-2)$$

based on the geometry of the membranes where h and A represent thickness and area of the membrane, respectively; and R is the resistance deduced from impedance spectroscopy measurements.

3.2.3. Electromechanical characterization

Actuators were cut into approximately 1.5×15 mm² pieces and tested under application of a 4 V step potential. Electromechanical response of the actuators was monitored and recorded using a charge-coupled device (CCD) video camera, mounted to an in-house fabricated microprobe station, at 30 fps. Individual frames were then analyzed to measure the radius of curvature as a

function of time ($r(t)$) and to calculate ($Q(t)$) and strain ($\varepsilon\%(t)$) values from Equations (3-3) and (3-4), respectively; where Q , ε and h are curvature, strain and thickness of the actuator, respectively.

$$Q(t) = \frac{1}{r(t)} \quad (3-3-3)$$

$$\varepsilon\%(t) = \frac{h}{2r(t)} \quad (3-3-4)$$

3.3. Results and discussions

3.3.1. Current flow

Current flow corresponding to a 4 V potential difference between the outer electrodes was measured and recorded as a function of time. As presented in Figure 3-1, magnitude of displaced charge (area under the curve) increases with the increasing concentration of ionic liquid in the samples; suggesting that first, current flow is due to mobilized ions; and second, more ions are displaced in samples containing higher concentration of ionic liquid. After approximately 55 s (see $55 < t < 60$ and $115 < t < 120$ on Figure 3-1) all curves have asymptotically reach the x-axis (approximately zero current) indicating that the system is fully charged.

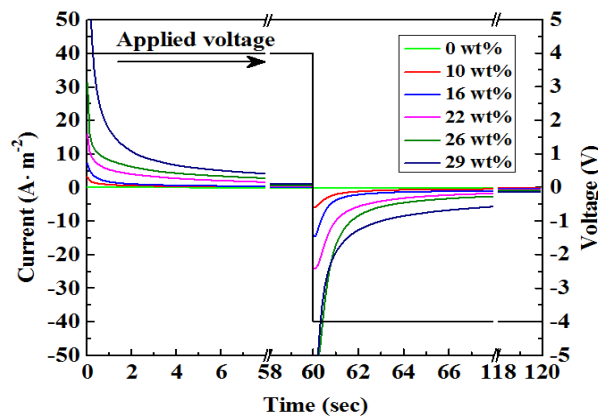


Figure 3-1: Charging and discharging currents for samples containing different.

3.3.2. Electromechanical Response

The electromechanical responses of IEAP actuators to an external electric signal of 4 V were monitored and recorded at a rate of 30 frames/second. Sequential digital images were used to deduce $r(t)$ and to calculate $Q(t)$ and $\varepsilon\%(t)$ of each IEAP actuator. Presented in Figure 3-2 is the maximum actuation curvature and strain as a function of ionic liquid concentration. The electromechanical response showed enhancement as the concentration of ionic liquid was increased from 0 to 22 wt%, and was followed by a sharp decline at higher concentrations. The initial incline between 0 and 22 wt% of ionic liquid is devoted to increased concentration of ions at the interface of the outer electrodes. As ion concentration is increased, so does the extent of the swelling at each electrode, resulting a larger volume imbalance between the two electrodes, which in turn results a larger mechanical actuation. Data suggest that above 22 wt% of ionic liquid intake, a secondary layer of charge is formed at the inner side of the initial ion layer (not at the electrode interface) which not only does not contribute toward actuation, it cancels some of the strain generated by the first ion layer which is at the electrode interface. Once this secondary ion layer is formed, addition of more ionic liquid worsens the electromechanical response.

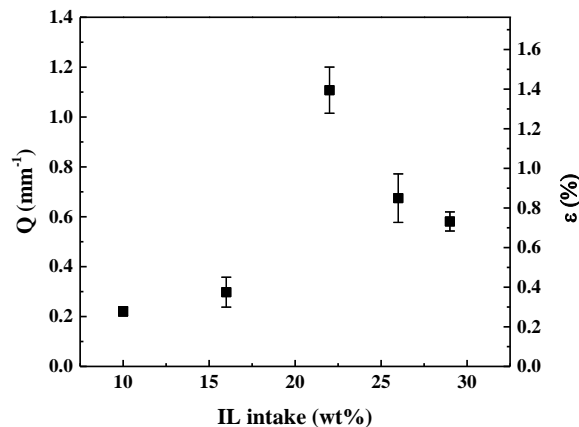


Figure 3-2: Actuation curvatures (primary y-axis) and strain (secondary y-axis) of IEAP actuators in response to a 4 V step potential is presented as a function of EMI-Tf ionic liquid concentration.

3.3.3. Electrochemical Studies

To investigate how does the concentration of ionic liquid affect the frequency response of the IEAP actuators, electrical impedance of the IEAP actuators was measured as a function of frequency. Electrochemical studies were conducted at lower voltage of 0.1 V, instead of 4 V applied for electromechanical response studies, to allow characterization over a broader frequency range, with required accuracy. It must be noted that using a higher, or different, applied potential results in different numerical values; however, trends and conclusions drawn from the experimental results would not be changed.

Presented in Figure 3-3 are the curves of Nyquist plot for the IEAP actuators. At higher frequencies (close to the origin of the x-axis) the electrochemical systems exhibited near-pure resistance behavior. Intersection of the semicircular plots with the x-axis, at high frequency regions manifests the solution resistance (R), as presented in the equivalent electrical circuit (Figure 3-5). Solution resistance depended on the ionic conductivity of the entire system including the transportation of ions between anode and cathode.

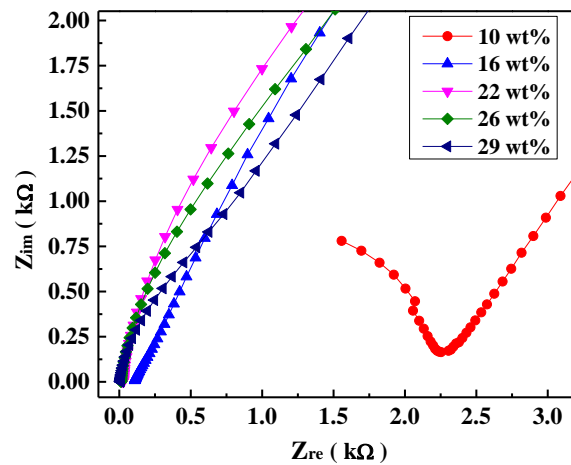


Figure 3-3: Nyquist plot of impedance magnitude of IEAP actuators containing various concentrations of ionic liquid. Solution resistance is deduced from the intersection of plots with the Z_{re} axis

Solution resistance of samples, presented in Figure 3-3, suggests that the addition of ionic liquids results in the reduction of solution resistance, an observation that is in agreement with expected effect of any ion-rich electrolyte, such as ionic liquids. Solution resistance and ionic conductivity of IPMCs are listed in Table 3-1.

Table 3-1: Solution resistance and ionic conductivity of IPMCs containing different concentrations of ionic liquid.

ILs (wt%)	h (μm)	A (cm^2)	R (Ω)	σ ($\text{S}\cdot\text{cm}^{-1}$)
10	25	1	2081.5	1.2E-6
16	25	1	99.5	2.5E-5
22	25	1	26.7	9.4E-5
26	25	1	11.5	2.2E-4
29	25	1	7.8	3.2E-4

Figure 3-4 presents electrical impedance magnitude $|Z|$ and phase angle (ϕ) of IEAP actuators as a function of ionic liquid concentration. At frequencies smaller than 100Hz the magnitude of electrical impedance is relatively independent of ionic liquid concentration; however, at faster frequencies for samples containing more than 10 wt% ionic liquids a sharp decrease in $|Z|$ is observed. It is only at very high frequencies that the magnitude of electrical impedance exhibits full dependence on ionic liquid concentration. In general, for an IEAP actuator to deliver a large strain and force output, a large capacitance is preferred. The electrical impedance ($Z = |Z| \exp(-j\phi)$) is a function of the phase angle ϕ , which itself depends on frequency, and can be deduced from $\tan \phi = 1/\omega R_S C_S$, where R_S and C_S are the system's net resistance and capacitance, respectively. Phase angles of $\phi = 90^\circ$ corresponds to a pure capacitor and $\phi = 0^\circ$ to a pure resistor (which would indicate the electrical impedance of the resistor is much larger than

that of the capacitor). Since the resistive component represents the electrical loss, a ϕ approaching 90° is preferred in order to achieve a high electrical efficiency of the actuator. A larger ϕ was observed for IEAP actuators containing higher concentrations of ionic liquid. At higher frequencies, the difference in phase angles as a function of ionic liquid concentration became more distinct, suggesting stronger capacitance-like behavior for samples with higher ionic liquid concentration.

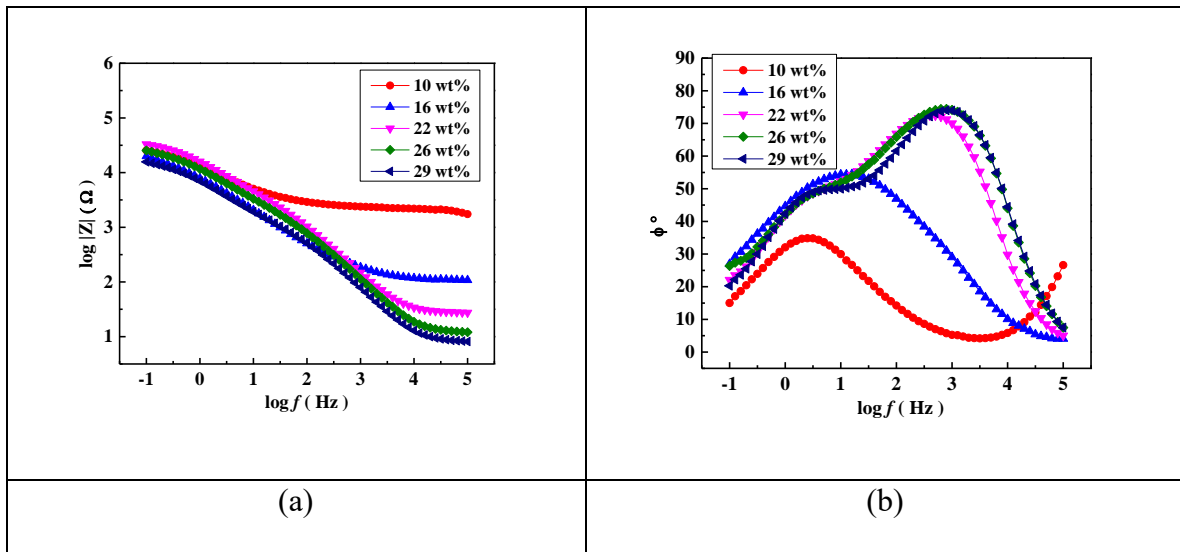


Figure 3-4 : (a) Impedance magnitude versus frequency; and, (b) phase angle versus frequency of IEAP actuator containing different ionic liquid concentration. At higher frequencies, impedance and phase angle exhibit higher dependency on ionic liquid concentration.

As a result of ion accumulation at the outer electrodes an electric double layer (EDL) capacitor is formed at the interface between the ionomeric polymer membranes (Nafion in this study) and the outer electrodes. This EDL capacitor and the solution (leakage) resistance of IEAP actuators can be used to model electrochemical behavior of such systems by an equivalent electrical circuit. Previously we have shown that due to a continuous contribution to the charging and discharging current of a diffuse layer, an ideal RC circuit does not fit the experimental results well at the low frequencies [19]. Therefore, a constant phase element, Warburg element (W), is introduced by the assumption of a semi-infinite linear diffusion process at the planar electrode[12,

20-22]. Presented in Figure 3-5 is the equivalent electrical circuit where the two C-W components present outer electrode-ionomeric membrane interfaces and R is the solution resistance. Data from the real part of impedance was used to test the model at low frequency range. Electrochemical behavior of this system at high frequency can be fitted with a simple RC circuit; however, at lower frequencies ($f < 100\text{kHz}$) the Warburg element is required to provide an accurate model.

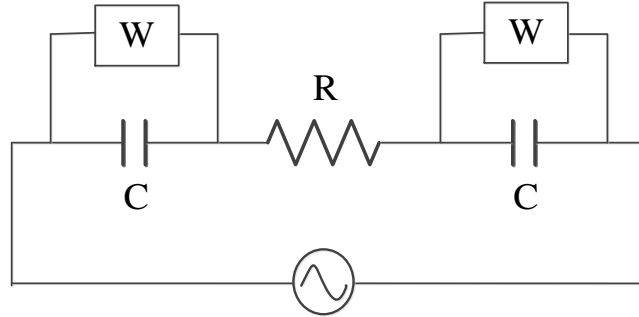


Figure 3-5 : Equivalent electric circuit with Warburg element.

As a constant phase element, the Warburg element has an explicit expression of $Z_w = (1/Y_0)(j\omega)^{-n}$, where Y_0 is a coefficient with unit of $\Omega^{-1} \cdot \text{s}^n$, ω is angular frequency (rad s^{-1}), and n is a unit-less coefficient and equal to 0.5.

Impedance of the equivalent circuit can be expressed as:

$$Z = R + 2 \times \frac{1}{j\omega C + Y_0(j\omega)^n} \quad (3-3-5)$$

Which can be expanded by Euler's equation to:

$$Z = R + \frac{2Y_0\omega^n \cos\left(\frac{n\pi}{2}\right)}{Y_0^2\omega^{2n} + \omega^2 C^2 + 2\omega^{n+1}CY_0 \sin\left(\frac{n\pi}{2}\right)} - j \frac{2\left[\omega C + Y_0\omega^n \sin\left(\frac{n\pi}{2}\right)\right]}{Y_0^2\omega^{2n} + \omega^2 C^2 + 2\omega^{n+1}CY_0 \sin\left(\frac{n\pi}{2}\right)} \quad (3-3-6)$$

where the net real resistance of the system (R_s) can be expressed as the sum of the leakage resistance (R) and real part of the impedance (Z_{re}):

$$R_s = R + \frac{2Y_0\omega^n \cos\left(\frac{n\pi}{2}\right)}{Y_0^2\omega^{2n} + \omega^2 C^2 + 2\omega^{n+1}CY_0 \sin\left(\frac{n\pi}{2}\right)} \quad (3-3-7)$$

which can be reorganized to:

$$\frac{1}{R_s - R} = \frac{Y_0\omega^n}{2\cos\left(\frac{n\pi}{2}\right)} + \frac{C^2\omega^{2-n}}{2Y_0\cos\left(\frac{n\pi}{2}\right)} + \omega C \tan\left(\frac{n\pi}{2}\right) \quad (3-3-8)$$

and for $n = 0.5$ can be rewritten as:

$$\frac{1}{R_s - R} = \frac{\sqrt{2} C^2}{2 Y_0} \omega^{1.5} + C\omega + \frac{\sqrt{2}}{2} Y_0 \omega^{0.5} \quad (3-3-9)$$

and simplified to:

$$y = ax^{1.5} + bx + \frac{b^2}{2a} x^{0.5} \quad (3-3-10)$$

where

$$a = \frac{\sqrt{2} C^2}{2 Y_0}, \quad b = C \quad (3-3-11)$$

Experimental data fitted with computational data are shown in Figure 3-6, confirming viability of the presented electrical equivalent circuit; and, that the net real resistance of the system decreases as concentration of ionic liquid increases.

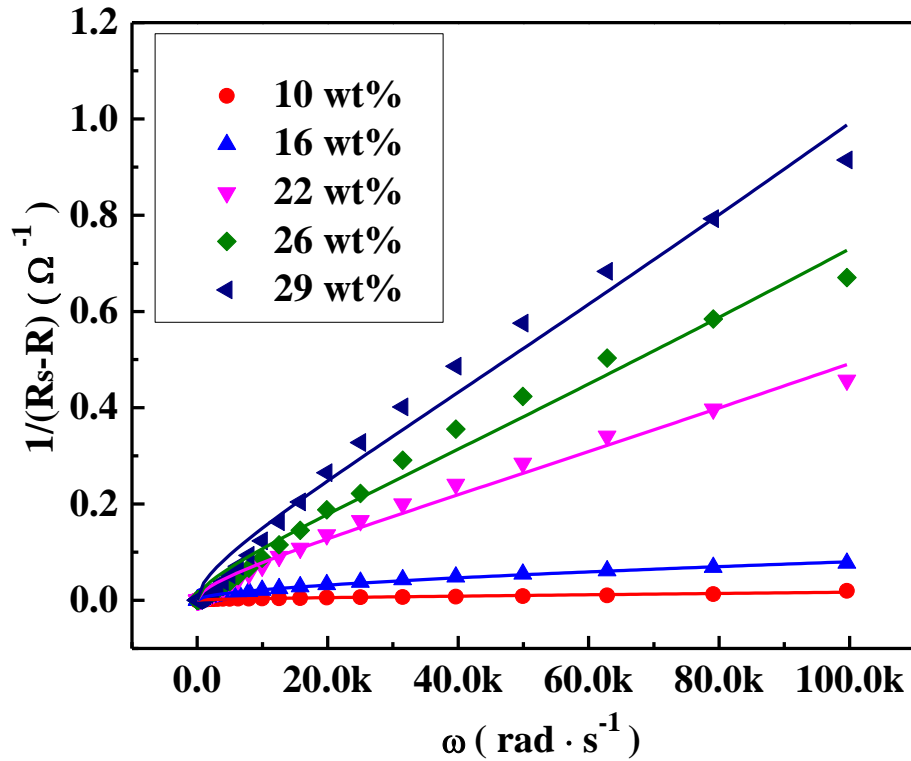


Figure 3-6: The plots of $1/(R_s - R)$ versus ω with various ILs intake and their corresponding fitting lines with $y = ax^{1.5} + bx + b^2x^{0.5}/(2a)$.

3.3.4. Discussion

It was observed in this study that the internal resistance of IEAP actuators is inversely proportional to the ionic liquid concentration. Samples containing higher concentrations of ionic liquid also exhibit more capacitor-like behavior, which in turn should result in larger electromechanical response. However, electromechanical studies indicated that there exists an optimum concentration of ions at which the electromechanical response is maximized, and that optimum concentration is not the highest ion concentration. The observed drop in electromechanical response beyond optimum concentration of ions is dedicated to formation of a saturated ion layer at outer electrodes interfaces. As a result, swelling due to accumulation of ions is shifted from the edge (which is most effective in generation of electromechanical response)

toward the center of the system (where its effect is no desired). Similar behavior is reported by Kwon and Ng [23] where the concentration of ionic liquid in gel electrolyte was varied. Our investigation suggests that for applications where high charge displacement is desired (e.g. super capacitors, sensors, etc.) increasing concentration of ionic liquids (or more generally electrolytes) may prove advantageous; however, for IEAP actuators where high electromechanical response is of interest, it is recommended to optimize the system by not passing ion concentration saturation threshold.

3.4. Conclusion

We fabricated and characterized IEAP actuators consisting of Nafion ionomeric membrane and EMI-Tf ionic liquid. We found that increasing concentration of ionic liquids in IEAP actuators results in enhanced electromechanical response, until the electrode-ionomer interface is saturated with the accumulated ions. Beyond the saturation point, ion accumulation is inward, forming a secondary layer of ions, and generates undesired strain that partially cancels the strain generated by the ion layer at the interface, which is desired for actuation. In short, optimum (not maximum) concentration of ionic liquids should be incorporated in IEAP actuators to achieve maximum electromechanical response.

Acknowledgment

This material is based upon work supported in part by a funding from Health Research Initiative and Presidential Initiative for Interdisciplinary Research at Iowa State University.

3.5. References

- [1] A. McDaid, S. Xie, and K. Aw, "A compliant surgical robotic instrument with integrated IPMC sensing and actuation," *International Journal of Smart and Nano Materials*, vol. 3, no. 3, pp. 188-203, 2012.
- [2] B. J. Akle, M. D. Bennett, and D. J. Leo, "High-strain ionomeric–ionic liquid electroactive actuators," *Sensors and Actuators A: Physical*, vol. 126, no. 1, pp. 173-181, 2006.
- [3] M. Shahinpoor, K. Kim, and D. Leo, "Ionic polymer-metal composites as multifunctional materials," (in English), *Polymer Composites*, vol. 24, no. 1, pp. 24-33, FEB 2003 2003.
- [4] K. Oguro, Y. Kawami, and H. Takenaka, "Bending of an ion-conducting polymer film-electrode composite by an electric stimulus at low voltage," *Journal of Micromachine Society*, vol. 5, no. 1, pp. 27-30, 1992.
- [5] K. Sadeghipour, R. Salomon, and S. Neogi, "Development of a novel electrochemically active membrane and 'smart' material based vibration sensor/damper," *Smart Materials and Structures* vol. 1, pp. 172-179, 1992.
- [6] C. Meis, N. Hashemi, and R. Montazami, "Investigation of spray-coated silver-microparticle electrodes for ionic electroactive polymer actuators," *JOURNAL OF APPLIED PHYSICS*, vol. 115, no. 13, p. 134302, 2014.
- [7] S. Liu et al., "Layer-by-layer self-assembled conductor network composites in ionic polymer metal composite actuators with high strain response," *Applied Physics Letters*, vol. 95, no. 2, p. 023505, 2009.
- [8] Y. Liu et al., "Ion transport and storage of ionic liquids in ionic polymer conductor network composites," *Applied Physics Letters*, vol. 96, no. 22, p. 223503, 2010.
- [9] S. Liu et al., "Influence of the conductor network composites on the electromechanical performance of ionic polymer conductor network composite actuators," *Sensors and Actuators A: Physical*, vol. 157, no. 2, pp. 267-275, 2010.
- [10] R. Montazami, S. Liu, Y. Liu, D. Wang, Q. Zhang, and J. R. Heflin, "Thickness dependence of curvature, strain, and response time in ionic electroactive polymer actuators fabricated via layer-by-layer assembly," *Journal of Applied Physics*, vol. 109, no. 10, p. 104301, 2011.
- [11] R. Montazami, D. Wang, and J. R. Heflin, "Influence of conductive network composite structure on the electromechanical performance of ionic electroactive polymer actuators," *International Journal of Smart and Nano Materials*, vol. 3, no. 3, pp. 204-213, 2012.
- [12] Y. Liu et al., "Equivalent circuit modeling of ionomer and ionic polymer conductive network composite actuators containing ionic liquids," *Sensors and Actuators A: Physical*, vol. 181, pp. 70-76, 2012.

- [13] J. Hou, Z. Zhang, and L. A. Madsen, "Cation/anion associations in ionic liquids modulated by hydration and ionic medium," *J Phys Chem B*, vol. 115, no. 16, pp. 4576-82, Apr 28 2011.
- [14] J. Hou, J. Li, D. Mountz, M. Hull, and L. A. Madsen, "Correlating morphology, proton conductivity, and water transport in polyelectrolyte-fluoropolymer blend membranes," *Journal of Membrane Science*, vol. 448, pp. 292-299, 2013.
- [15] B. J. Akle, M. D. Bennett, and D. J. Leo, "High-strain ionomeric-ionic liquid electroactive actuators," *Sensors and Actuators a-Physical*, vol. 126, no. 1, pp. 173-181, Jan 2006.
- [16] S. Nemat-Nasser, "Micromechanics of actuation of ionic polymer-metal composites," *Journal of Applied Physics*, vol. 92, no. 5, pp. 2899-2915, 2002.
- [17] J. Li, K. Wilmsmeyer, J. Hou, and L. Madsen, "The role of water in transport of ionic liquids in polymeric artificial muscle actuators," *Soft Matter*, vol. 5, no. 13, pp. 2596-2602, 2009.
- [18] H. Acar, S. Çınar, M. Thunga, M. R. Kessler, N. Hashemi, and R. Montazami, "Study of Physically Transient Insulating Materials as a Potential Platform for Transient Electronics and Bioelectronics," *Advanced Functional Materials*, 2014.
- [19] J. Lyklema, "Fundamentals of Interface and Colloid Science," ed: Academic Press: London, 1995.
- [20] J. Randles, "Kinetics of rapid electrode reactions," *Discussions of the faraday society*, vol. 1, pp. 11-19, 1947.
- [21] P. Delahay and D. Turner, "New instrumental methods in electrochemistry," *Journal of The Electrochemical Society*, vol. 102, no. 2, pp. 46C-47C, 1955.
- [22] A. J. Bard and L. R. Faulkner, *Electrochemical methods: fundamentals and applications*, 2nd ed. Wiley New York, 2000.
- [23] K.-S. Kwon and T. N. Ng, "Improving electroactive polymer actuator by tuning ionic liquid concentration," *Organic Electronics*, vol. 15, no. 1, pp. 294-298, 2014.

CHAPTER 4. ELECTROCHEMICAL AND MORPHOLOGICAL STUDIES OF IONIC POLYMER METAL COMPOSITES AS STRESS SENSORS

Published in the journal Measurement¹

Wangyujue Hong^{2,3}, Abdallah Almomani^{2,4}, Reza Montazami^{2,3,5}

Abstract

Ionic polymer metal composites (IPMCs) are the backbone of a wide range of ionic devices. IPMC mechanoelectric sensors are advanced nanostructured transducers capable of converting mechanical strain into easily detectable electric signal. Such attribute is realized by ion mobilization in and through IPMC nanostructure. In this study we have investigated electrochemical and morphological characteristics of IPMCs by varying the morphology of their metal composite component (conductive network composite (CNC)). We have demonstrated the dependence of electrochemical properties on CNC nanostructure as well as mechanoelectrical performance of IPMC sensors as a function of CNC morphology. It is shown that the morphology of CNC can be used as a means to improve sensitivity of IPMC sensors by 3-4 folds.

4.1. Introduction

Ionomers, especially Nafion, have been subject of numerous investigations for their ionic properties and applications in ionic-electric devices such as fuel cells [1-4], actuators [5-9], batteries [10-13], super capacitors [14] and sensors [15-18]. Among all such applications, ionic polymer sensors have received less attention mainly due to apparently inconsistent experimental

¹ The publisher of this journal "Elsevier", allows the students to include the work in their thesis or dissertation if this is not to be published commercially.

² Primary researchers and authors. Graduate student, graduate student, and academic advisor, respectively.

³ Department of Mechanical Engineering, Iowa State University.

⁴ Department of Aerospace Engineering, Iowa State University.

⁵ Author of correspondence.

results [19-22]. Similar to ionic polymer actuators, ionic polymer sensors are consisted of an ionomer membrane coated by conductive network composites (CNCs) on both sides, where the whole structure (also known as ionic polymer-metal composite (IPMC)) is doped by either aqueous or ionic liquid electrolyte. The functionality of ionomeric sensors relies on, supposedly, random displacement of ions (and charged ionic clusters if ionic liquids are used) throughout the CNC layers when an external mechanical stress is applied. Electric field generated due to the motion of charged species is collected by the CNC and is detectable by conventional electronics. Due to the presence and displacement of both cations and anions in IPMC, theoretically there should be a zero net charge as opposite fields generated by displacement of cations and anions are expected to be statistically very close to each other in magnitude and cancel one another. In reality, however, there is a non-zero detectable net electric field. This electric field (mechanoelectric signal) exists because, due to their volume, charge and interactions with the ionomer, motions of cations and anions are different when subjected to stress [17, 23].

Influence of CNC structure [24-27], ion density [28, 29], electrode properties [30-32] and chemical and ionic structure of ionomer membrane [33-35] on performance of IPMC actuators have been thoroughly investigated by others and us; similar studies on IPMC sensors, however, are not widely reported. To our best recollection, one of the first reports on Nafion-based sensors was published by Sadeghipour *et al.* in 1992 [36] where the concept was introduced. Later in 1995, Shahinpoor *et al.* investigated the response of IPMC sensor against large imposed displacements [37]. They published the first review paper of IPMC as biomimetic sensors and actuators in 1998, presenting an introduction to IPMC, its applications and the corresponding mathematical modeling [22]. In 1999 Ferrara *et al.* proposed the possibility of applying IPMC sensor as a pressure transducer in the human spine [18]. Over the same time period, studies on mathematical modeling

of IPMC sensors were also conducted and published [38-41]. All of the abovementioned studies considered the IPMC sensors doped with aqueous electrolytes; studies on the ionic liquid-doped IPMC sensors, however, are rare.

In this work, we have investigated the correlations between the mechanoelectric sensing performance of IPMC sensors and structural and morphological properties of ionic liquid-doped CNC layers. IPMC sensors were fabricated by layer-by-layer (LbL) (Figure 4-1a) deposition of CNC layers consisting of gold nanoparticles (AuNPs) and poly(allylamine hydrochloride) (PAH) on Nafion membranes. LbL fabrication technique was utilized to manipulate structural properties of CNC layers. IPMCs provide environments for storage and mobility of ions. Ion mobility through IPMC, due to the porous structure of CNC layers, is higher compared to dense ionomer membrane; thus, porosity and structural properties of IPMC is an influential factor in performance and attributes of the sensors. This work specifically contributes to the knowledge of ionic and electrical properties of ionic liquid-doped nanostructured IPMCs, as well as the potential applications of such structures as mechanoelectric sensors.

4.2. Experimental Section

4.2.1. Materials

Nafion membrane of 25 μm thickness (NR 211) was purchased from Ion Power, Inc (DE-USA). and was cut into pieces of 2.5 cm \times 5 cm. Poly(allylamine hydrochloride) (PAH) was purchased from Sigma Aldrich (MO-USA) and used to make 10 mM polycationic aqueous solution of pH 4; 1-ethyl-3-methylimidazolium trifluoromethanesulfonate (EMI-Tf) and sodium chloride (NaCl) were purchased from Sigma Aldrich (MO-USA) and used as received. 20-ppm aqueous dispersion of 3nm (diameter) negatively charged gold nanoparticles (AuNPs) of pH 9 were purchased from Purest Colloids, Inc (NJ-USA). and used without further modification. 3M

conductive copper tape was purchased from VWR International LLC (PN-USA) and used as current collector.

4.2.2. Methods

4.2.2.1. IPMC fabrication

An automated thin-film fabrication robot (StratoSequence 6, NanoStrata, Inc, FL-USA) was used to grow AuNPs/PAH CNCs of desired number of bilayers via LbL deposition technique. Nafion membrane was mounted on a glass frame and was alternately exposed to cationic (10 mM PAH aqueous solution) and anionic (20-ppm aqueous dispersion of AuNPs) species for 5 minutes each, with three steps of 1 minute each DI water rinsing after each deposition step. CNCs consisting of 2, 4, 6, 8 and 10 bilayers were obtained to investigate thin-film growth on ionomer membrane; CNCs consisting of 10, 20, 30 and 40 bilayers were obtained for electrochemical studies. Thin-film thicknesses (h , shown in Table 4-1) were measured using a contact profilometer as described in our earlier work [24].

Moreover, to further study the effect of ionic strength of polyelectrolyte on CNC morphology, 200 mM NaCl was added to PAH solution to manipulate its ionic strength and consequently its polymer chains configuration. 20 bilayer CNCs with and without NaCl were fabricated to investigate the influence of morphology on the sensing performance. The samples were labeled $(\text{AuNP/PAH-NaCl})_{20}$ and $(\text{AuNP/PAH})_{20}$, respectively, where the subscript 20 identifies the number of deposited bilayers constituting the CNCs. Presented in Figure 4-1b is an $(\text{AuNP/PAH})_{20}$ IPMC on a glass frame. Figure 4-1c, background, shows a SEM micrograph of the CNC coating and a schematic of the device is presented in the foreground. CNC coated ionomer membranes were then soaked in EMI-Tf ionic liquid at 80 °C to intake ~30 wt% ionic

liquids. Considering the high sensitivity of Nafion and EMI-Tf ionic liquid to humidity [42, 43], samples were then placed under vacuum (gauge pressure of \sim -100 kPa) at 115 °C for three days to dehydrate, and kept in desiccator until used.

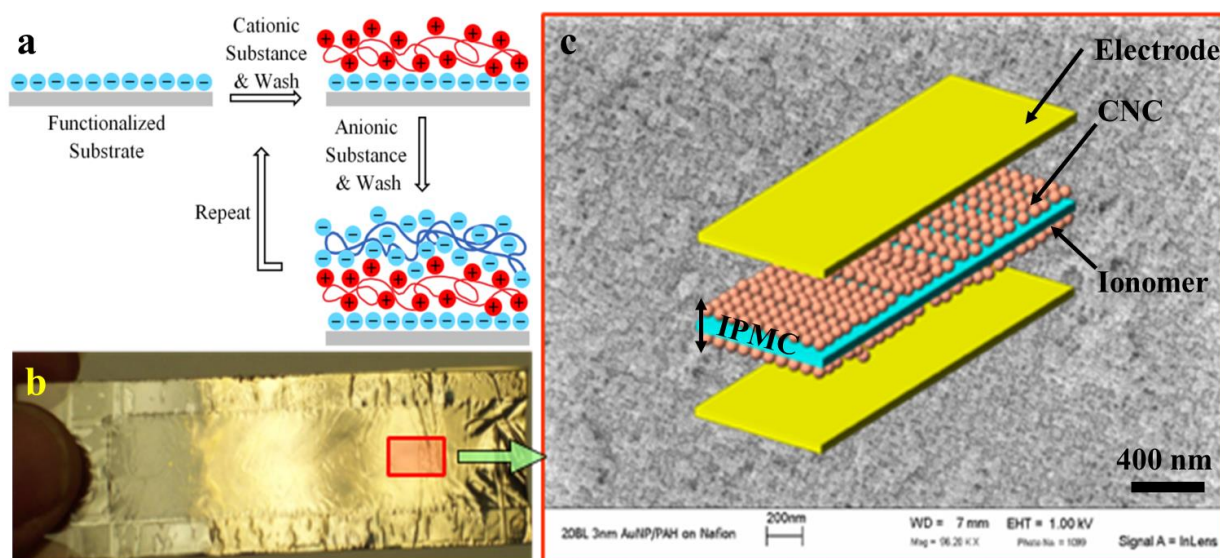


Figure 4-1: a) Schematic representation of layer-by-layer direct self-assembly of AuNP and PAH; b) CNC layer formed on Nafion ionomer, the membrane is mounted on a glass frame; c) foreground: schematic representation of IPMC and sensor structure, background: SEM micrograph of AuNP/PAH CNC nanostructure.

4.2.2.2. Optical characterization

Optical spectrum was acquired on CNCs to characterize the LbL self-assembled thin-films, using a PerkinElmer Lambda-25 UV/VIS Spectrometer.

4.2.2.3. Electrochemical characterization

Samples doped with ionic liquid were characterized for their electrochemical properties using a VersaSTAT-4 (Princeton Applied Research, IL-USA) potentiostat on 2-electrode mode. Impedance spectroscopy studies were carried at frequencies between 1.0E5 Hz and 1.0E-1 Hz,

and a potential difference (ΔV) of 10 mV. Electrical conductivity (σ) of the doped membranes was calculated from Equation 4-1,

$$\sigma = \frac{h}{RA} \quad (4-4-1)$$

where h and A are representing thickness and area of the membrane, respectively; and R is the resistance deduced from impedance spectroscopy measurements.

4.2.2.4. *Mechanoelectrical characterization*

Stress induced dynamic electric response was measured and recorded to study mechanoelectrical properties of the samples. Samples were cut into pieces of approximately 14 mm \times 17 mm. Copper tape was used as electrodes and the whole system was covered by electrical tape to form an isolated sample. The samples were placed flat and tested on an in-house made setup at frequency of 1Hz. A 12 kPa stress was generated and distributed uniformly across the sensor by reciprocating motion of a mass manipulated by a computer controlled stepper motor. A schematic representation of the setup is presented in Figure 4-2. Two ends of the sample were clamped and connected to an oscilloscope to monitor the generated electric signal, which was recorded via a LabVIEW interface over an extended period of time.

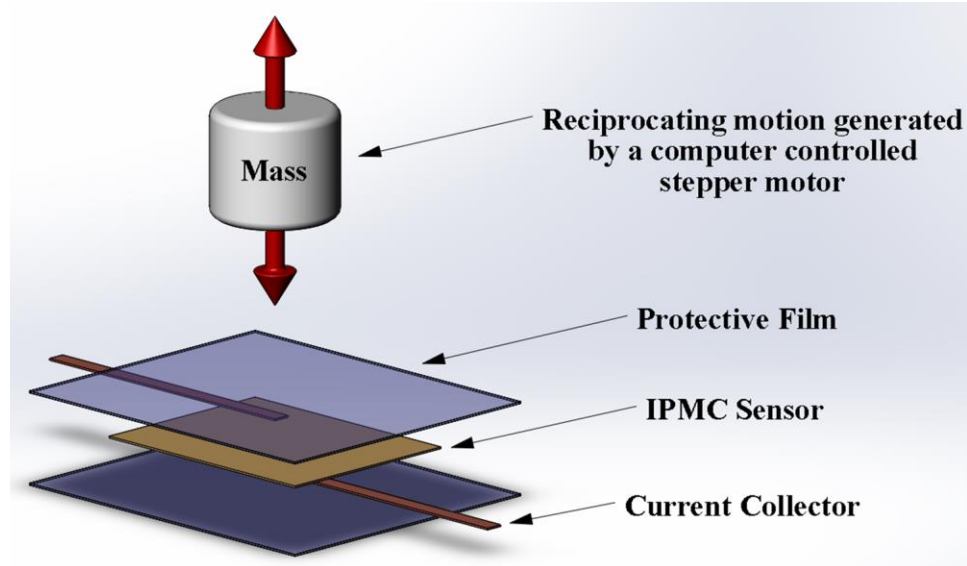


Figure 4-2: A schematic representation of the setup and operations for the mechano-electrical characterization (dimensions are not to scale). The IPMC sensor piece was covered by electrical tape, with copper tape used as electrodes to connect to an oscilloscope to monitor the generated electric signal. A 12 kPa stress was distributed evenly by a mechanical arm whose frequency was controlled at 1 Hz by a step motor.

4.3. Results and Discussion

4.3.1. Morphological characterization

Growth kinetics of CNC nanostructures, consisting of AuNP/PAH with and without addition of NaCl to the PAH solution, was investigated. Presented in Figure 4-3a is the plasmonic absorption band of 3 nm diameter AuNPs, centered at 514 nm. When paired with PAH to form LbL nanostructures, the absorbance peak shifted toward longer wavelengths (Figure 4-3b); which is an indication of the enhanced electromagnetic coupling between neighboring nanoparticles [44], and it is more evident in nanostructures of larger thicknesses because a more closely packed structure is formed. Increase in the absorbance intensity implies an increase in the thickness of the CNC film. The correlations of ionic strength of polyelectrolyte and film thickness in LbL self-assembly are discussed by several researchers including [45-48].

Intensity of the absorbance peaks of the AuNP/PAH bilayers showed a direct and linear dependence on the thickness of the nanostructures (Figure 4-3c). The linear correlation between thickness and peak absorbance amplitude is an indication of consecutive surface-charge buildup of AuNPs in the nanostructure[49]. Addition of NaCl to PAH resulted in formation of thicker and denser nanostructures; thus, the increase in absorbance intensity for CNCs consisting of larger number of bilayers is significantly more evident compared to that of samples without NaCl (Figure 4-3c); this is mainly due to an increase in ionic strength of the polycation which results in accumulation of more negatively charged AuNPs and formation of thicker and denser bilayers.

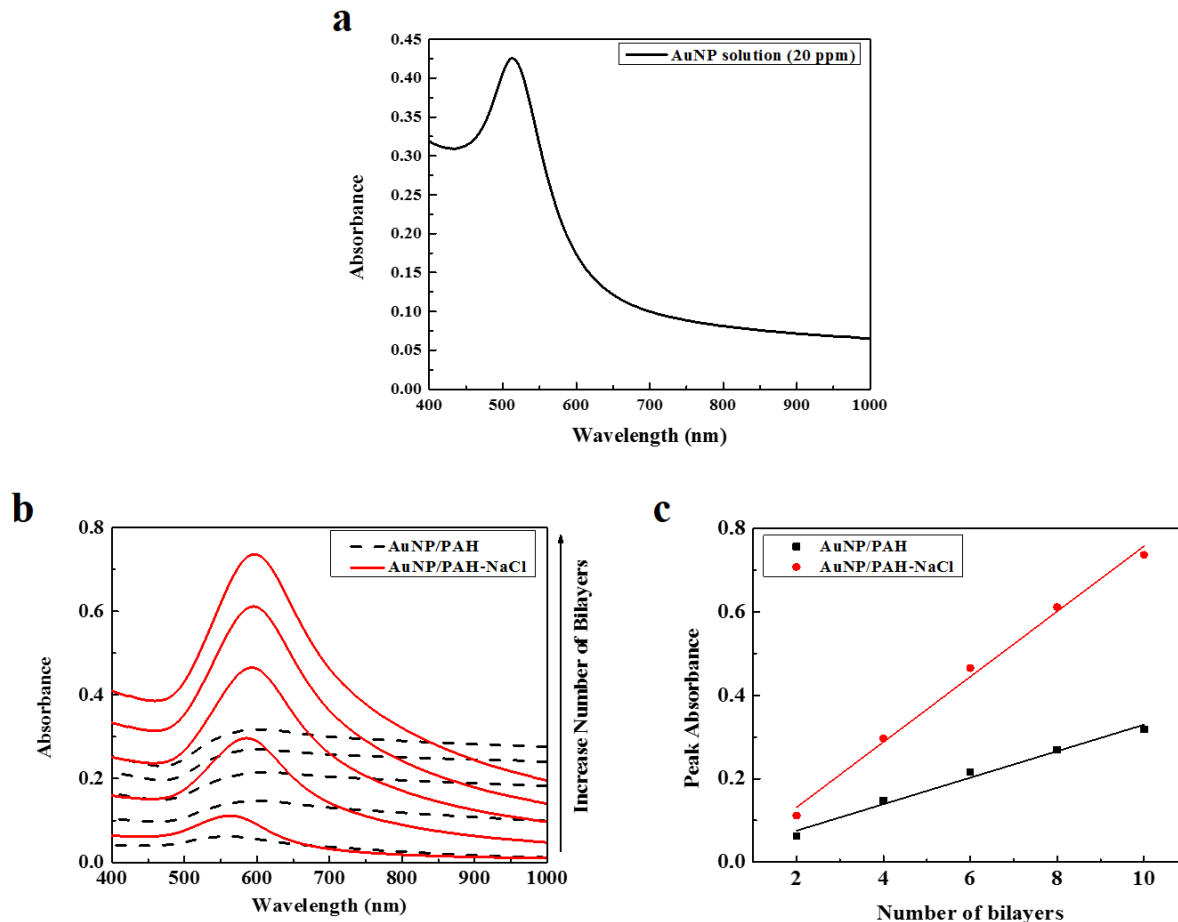


Figure 4-3: a) UV-Vis absorbance spectra of AuNP aqueous solution (20 ppm); b) UV-Vis absorbance spectra of 2, 4, 6, 8, and 10-bilayer AuNP/PAH and AuNP/PAH-NaCl nanostructures; c) plot of the absorbance peaks of CNCs consisting of different number of bilayers and morphology

4.3.2. Electrochemical analysis

To study thickness dependence of the frequency response in IPMC sensors and the corresponding electrical efficiency, the electrical impedances of sensors with CNC layers consisting of different number (0, 10, 20, 30 and 40) of bilayers were investigated as a function of frequency. Applied potential of 10 mV was selected so that the electric impedance can be characterized over a broad frequency range with required accuracy. Typically, the electrochemical responses of such ionic devices are nonlinear functions of the CNC morphology and applied voltage, thus different CNC structures (e.g. with or without NaCl) and changes in the applied voltage will affect the numerical values of the electrical impedance results; for example, the capacitance will increase with increase of applied voltage. However, these nonlinear effects will not change the trends and conclusions drawn from the experimental results [50].

Presented in Figure 4-4a are the curves of Nyquist plot for the IPMC sensors at higher frequencies, where the electrochemical systems exhibited near-pure resistance behavior. Solution resistance (R) is deduced by reading the Z_{re} value at the intersection of extended curves and the x-axis. As discussed in our previous works [10, 28], solution resistance depends on the ionic conductivity of the entire system including the transportation of ions between anode and cathode. Thicker CNC layers result in smaller solution resistances, indicating the presence of an ion-rich environment in thicker CNC nanostructures. Ionic conductivity of the IPMC sensors is calculated from Equation 4-1 and reported in Table 4-1 along with solution resistance and other characteristics of the IPMC sensors.

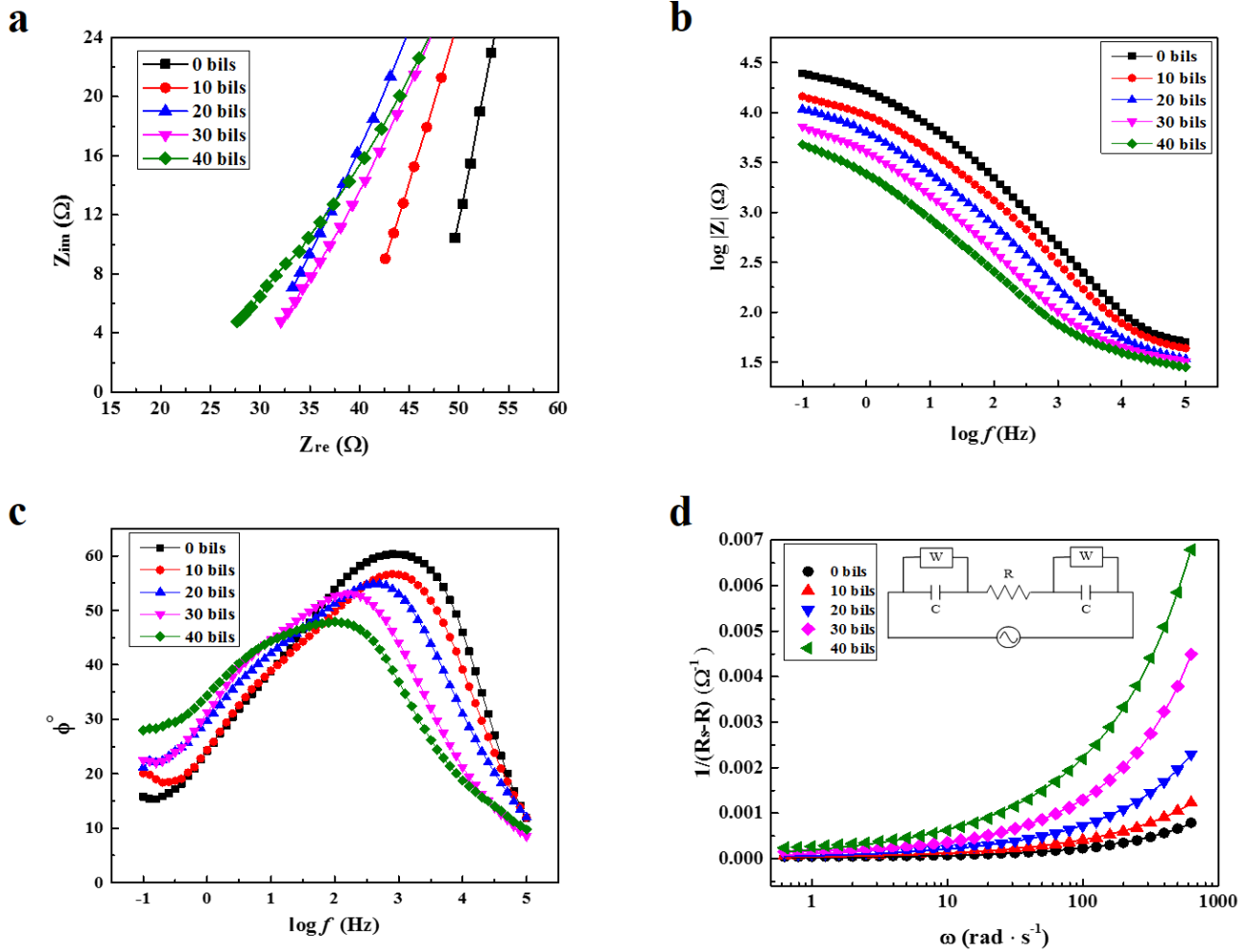


Figure 4-4: Electrochemical studies of IPMC sensors consisting of different thickness CNCs (without NaCl) a) Nyquist plot of impedance magnitude of IPMC sensors. Solution resistance values are deduced from the intersection of plots with the axis; b) Impedance magnitude as a function of frequency; c) phase angle as a function of frequency; d) plots of $1/(R_s - R)$ versus ω , and their corresponding fitting lines based on the equivalent circuit (inset).

Table 4-1: Solution resistance, ionic conductivity and electric double layer capacitance of IPMC sensors with various thicknesses of CNC layers.

Bilayers	0	10	20	30	40
$h(\mu\text{m})$	25.000	25.046	25.084	25.128	25.162
$A(\text{cm}^2)$	1	1	1	1	1

$R(\Omega)$	45.0	38.4	29.4	27.7	23.8
$\sigma(S.cm^{-1})$	5.56E-5	6.52E-5	8.53E-5	9.07E-5	10.58E-5
$C(F.cm^{-1})$	3.64E-7	3.62E-7	9.37E-7	2.32E-6	2.67E-6

Magnitude of electrical impedance $|Z|$ and phase angle (φ) for IPMC sensors consisting of different thickness CNCs as a function of frequency (f) are presented in Figures 4-4(b-c). As evident from Figure 4-4a, impedance $|Z|$ is inversely proportional to the thickness of CNC layer. This behavior is especially more evident at lower frequencies (0.1-100 Hz). In general, for an IPMC sensor to respond to an external mechanical stimulus and deliver an electric signal, a large capacitance is preferred. At the same low frequency range, phase angle, which is a function of frequency, exhibited a direct correlation to the thickness of the CNC nanostructure (Figure 4-4c), suggesting a stronger capacitance-like behavior for samples with thicker CNC layer; this characteristic is hindered at higher frequencies. To achieve high electrical efficiency in IPMC sensors, larger phase angles are preferred; which, can be realized by increasing the thickness of the CNC layers in sensors for low frequency (<100 Hz) applications.

An equivalent circuit, as shown in Figure 4-4d-inset, was introduced to study the electrochemical behavior of IPMC sensors at lower frequency boundaries, between 0.1 and 100 Hz, as a function of thickness of the CNC layer. Briefly, an electric double layer (EDL) capacitor (C) is formed at the interface between the outer electrodes and electrolyte, with a Warburg impedance element (W) connected in parallel to represent diffusion controlled charge transfer process in pseudo-capacitors. Both elements are then connected with a solution resistor (R) in series to represent the bulk resistance between two electrodes. The net real resistance of the system

(R_s) can be expressed as the sum of the solution resistance (R) and real part of the impedance (Z_{re})

as $R_s = R + \frac{2Y_0\omega^n \cos(n\pi/2)}{Y_0^2\omega^{2n} + \omega^2 C^2 + 2\omega^{n+1} C Y_0 \sin(n\pi/2)}$, which can be reorganized to $\frac{1}{R_s - R} = \frac{Y_0\omega^n}{2\cos(n\pi/2)} + \frac{C^2\omega^{2-n}}{2Y_0\cos(n\pi/2)} + \omega C \tan(\frac{n\pi}{2})$. Take $n = 0.5$ for a Warburg element and rewrite the equation to $\frac{1}{R_s - R} = \frac{\sqrt{2}}{2} \frac{C^2\omega^{1.5}}{Y_0} + C\omega + \frac{\sqrt{2}}{2} Y_0\omega^{0.5}$. More details of this model is presented in our previous study

[28]. Experimental data (symbol) fitted with computational data (solid line) are shown in Figure 4-4d, confirming viability of the presented equivalent circuit. The computational data of the EDL capacitor (represented as C in the circuit) at each sample was deduced and is listed in Table 4-1. A general upward trend was observed with increasing thickness of CNC layer, confirming the hypothesis that a thicker CNC layer has a larger ion storage volume and can withhold more mobile ions at the electrodes [24].

4.3.3. Mechanoelectrical sensing performance

When mechanically deformed, IPMC sensors generate a weak yet detectable electric potential, which is the core of the “sensing” concept of such systems. Mechanism and theory of such mechanoelectrical behavior of systems doped with aqueous electrolytes have been studied thoroughly and reported [16, 17, 22, 38]. It is hypothesized that prior to application of mechanical stress, and the consequent deformation, the cations and anions are distributed uniformly over the inner surface of ionic cluster phase of ionomer. This steady state of zero net charge, however, is disturbed and distorted by the imposed deformation. Consequently, ions are displaced producing an effective dipole in each cluster [5, 25, 38, 50]; as a result, an electric field is generated that is analyzed as the dynamic sensing response. In case of Nafion, the ionomer studied in this work, anions are restrained and only cations are mobilized. When impacted, while anions are fixed, cations move away from the impacted side and toward the other side which is stretched due to the

impact. This results in polarization of electric charge across the sensor, rendering the impacted side as the anode and the stretched side as the cathode [18, 51-53]. During the experimental testing, the positive (red) terminal of the voltmeter was connected to the cathode to read the sensed signal as positive. Three sets of samples (bare Nafion (AuNP/PAH)₀, (AuNP/PAH)₂₀ and (AuNP/PAH-NaCl)₂₀), were studied for the mechano-electrical characterization. Sample selection was in such way that the role of CNC and its morphology can be examined. Samples were subjected to cyclic mechanical stress of 12 kPa at 1 Hz for over 500 cycles, until sensing signals were stable in amplitude. Presented in Figure 4-5 is the mechano-electrical response of the three sets of samples; insets shown zoomed in signals in the beginning and the end of the testing period. Initially, signals generated by the samples with CNC coating were 5 to 11 folds stronger than that of the uncoated samples. Amplitude of all signals declined overtime and reached a stable state where the signals from coated samples were approximately 4 folds stronger than the uncoated sample. Samples with and without NaCl in the CNC structure reached approximately the same stable plateau. The dynamic response was observed to be highly repeatable with a bandwidth of 1 Hz for all three samples. Each peak rises almost instantaneously when the pressure is applied, and recovers when the pressure is withdrawn. To confirm reproducibility and statistical significance of the collected data, three runs were conducted on each of the three sets of samples, and the standard deviation of each data set was calculated. For the three sets of samples ((AuNP/PAH)₀, (AuNP/PAH)₂₀ and (AuNP/PAH-NaCl)₂₀), the standard deviation range (minimum/maximum) was found to be (6.7E-6/1.7E-3), (0/4.7E-3) and (0/7.5E-3), respectively.

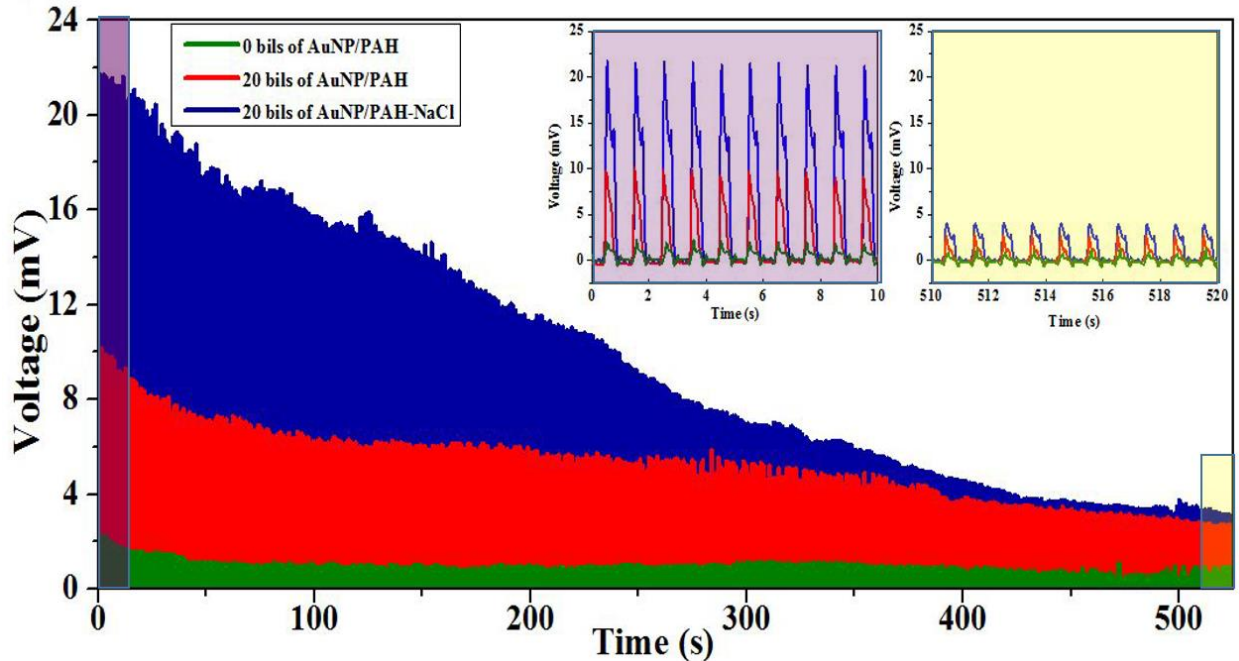


Figure 4-5: Mechanoelectric sensing in repose to cyclic 12 kPa stress at 1 Hz. Insets show the zoomed in plots at the first and last 10 seconds of the experiment.

Experimental data indicates that there is a strong correlation between the morphology of CNC layers and mechanoelectrical response in IPMC sensors. A higher concentration of AuNPs in CNC results in higher porosity that facilitates higher ion mobility under mechanical impact. This enhanced ion mobility, however, is declined to a common and stable plateau for IPMC sensors regardless of the nanostructure of the CNC. This observation may be due to loss of elasticity, or creep of the IPMC at microscale. For samples without CNC the signal amplitude is considerably weaker. Overall, the CNC layer results in at least 3-4 folds' increase in the strength of the sensing response; no dependence was observed between the structure of IPMC and the response time of the sensors.

4.4. Conclusions

We reported the study of correlations between structural properties of IPMC sensors and their electrochemical and mechanoelectrical properties and performance. It was demonstrated that

changes in nanostructure and morphology of CNC layers could be utilized as a means to control and enhance the sensitivity of mechanoelectric IPMC sensors by at least 3 to 4 folds. Initially optimized samples exhibited 11 folds' increase in their sensitivity to mechanical strain; the overall amplitude of the electrical signal, however, declined over hundreds of cycles, most probably due to creep formation and mechanical failure of the IPMC. Better casing and more robust IPMCs are expected to overcome this issue. It is foreseen that future work would involve exploration of effective techniques to reduce the stabilization time of such sensor systems.

Acknowledgements

The presented work is supported in part by grants from Health Research Initiative (HRI), Presidential Initiative for Interdisciplinary Research (PIIR), and the Department of Mechanical Engineering at Iowa State University.

4.5. References

- [1] L. T. Wagner, J. Yang, S. Ghobadian, R. Montazami, and N. Hashemi, "A microfluidic reactor for energy applications," *Open Journal of Applied Biosensor*, vol. 1, no. 3, pp. 21-25, 2012.
- [2] K. Schmidt-Rohr and Q. Chen, "Parallel cylindrical water nanochannels in Nafion fuel-cell membranes," *Nature materials*, vol. 7, no. 1, pp. 75-83, 2008.
- [3] K. Adjemian, S. Lee, S. Srinivasan, J. Benziger, and A. Bocarsly, "Silicon oxide nafion composite membranes for proton-exchange membrane fuel cell operation at 80-140 C," *Journal of the Electrochemical Society*, vol. 149, no. 3, pp. A256-A261, 2002.
- [4] D. Spry, A. Goun, K. Glusac, D. E. Moilanen, and M. Fayer, "Proton transport and the water environment in nafion fuel cell membranes and AOT reverse micelles," *Journal of the American Chemical Society*, vol. 129, no. 26, pp. 8122-8130, 2007.
- [5] S. Liu et al., "Layer-by-layer self-assembled conductor network composites in ionic polymer metal composite actuators with high strain response," *Applied Physics Letters*, vol. 95, no. 2, p. 023505, 2009.
- [6] A. A. Amiri Moghadam, W. Hong, A. Kouzani, A. Kaynak, R. Zamani, and R. Montazami, "Nonlinear dynamic modeling of ionic polymer conductive network composite actuators

- using rigid finite element method," *Sensors and Actuators A: Physical*, vol. 217, no. 0, pp. 168-182, 2014.
- [7] C. Jo, D. Pugal, I.-K. Oh, K. J. Kim, and K. Asaka, "Recent advances in ionic polymer–metal composite actuators and their modeling and applications," *Progress in Polymer Science*, vol. 38, no. 7, pp. 1037-1066, 2013.
- [8] S. Y. Jung, S. Y. Ko, J.-O. Park, and S. Park, "Enhanced ionic polymer metal composite actuator with porous nafion membrane using zinc oxide particulate leaching method," *Smart Materials and Structures*, vol. 24, no. 3, p. 037007, 2015.
- [9] K. Surana, P. K. Singh, B. Bhattacharya, C. Verma, and R. Mehra, "Synthesis of graphene oxide coated Nafion membrane for actuator application," *Ceramics International*, vol. 41, no. 3, pp. 5093-5099, 2015.
- [10] R. Zhang, Y. Chen, and R. Montazami, "Ionic Liquid-Doped Gel Polymer Electrolyte for Flexible Lithium-Ion Polymer Batteries," *Materials*, vol. 8, no. 5, pp. 2735-2748, 2015.
- [11] I. Bauer, S. Thieme, J. Brückner, H. Althues, and S. Kaskel, "Reduced polysulfide shuttle in lithium–sulfur batteries using Nafion-based separators," *Journal of Power Sources*, vol. 251, pp. 417-422, 2014.
- [12] X. Yu, J. Joseph, and A. Manthiram, "Polymer lithium–sulfur batteries with a Nafion membrane and an advanced sulfur electrode," *Journal of Materials Chemistry A*, vol. 3, no. 30, pp. 15683-15691, 2015.
- [13] B. Jiang, L. Wu, L. Yu, X. Qiu, and J. Xi, "A comparative study of Nafion series membranes for vanadium redox flow batteries," *Journal of Membrane Science*, vol. 510, pp. 18-26, 2016.
- [14] C. K. Landrock and B. Kaminska, "New Capacitive Storage Device," in *PowerMEMS 2009 Conference Proceedings*, 2009, pp. 360-363.
- [15] B. Paola, L. Fortuna, P. Giannone, S. Graziani, and S. Strazzeri, "IPMCs as vibration sensors," in *Instrumentation and Measurement Technology Conference Proceedings, 2008. IMTC 2008. IEEE*, 2008, pp. 2065-2069: IEEE.
- [16] H. Lei, M. A. Sharif, and X. Tan, "Dynamics of omnidirectional IPMC sensor: Experimental characterization and physical modeling," *IEEE/ASME Transactions on Mechatronics*, vol. 21, no. 2, pp. 601-612, 2016.
- [17] D. Pugal, K. Jung, A. Aabloo, and K. J. Kim, "Ionic polymer–metal composite mechano-electrical transduction: review and perspectives," *Polymer international*, vol. 59, no. 3, pp. 279-289, 2010.
- [18] L. Ferrara et al., "Use of ionic polymer-metal composites (IPMCs) as a pressure transducer in the human spine," in *1999 Symposium on Smart Structures and Materials*, 1999, pp. 394-401: International Society for Optics and Photonics.

- [19] Z. Chen, X. Tan, A. Will, and C. Ziel, "A dynamic model for ionic polymer–metal composite sensors," *Smart Materials and Structures*, vol. 16, no. 4, p. 1477, 2007.
- [20] K. J. Kim and M. Shahinpoor, "A novel method of manufacturing three-dimensional ionic polymer–metal composites (IPMCs) biomimetic sensors, actuators and artificial muscles," *Polymer*, vol. 43, no. 3, pp. 797-802, 2002.
- [21] A. Keshavarzi, M. Shahinpoor, K. J. Kim, and J. W. Lantz, "Blood pressure, pulse rate, and rhythm measurement using ionic polymer-metal composite sensors," in *1999 Symposium on Smart Structures and Materials*, 1999, pp. 369-376: International Society for Optics and Photonics.
- [22] M. Shahinpoor, Y. Bar-Cohen, J. Simpson, and J. Smith, "Ionic polymer-metal composites (IPMCs) as biomimetic sensors, actuators and artificial muscles-a review," *Smart Materials and Structures*, vol. 7, no. 6, p. R15, 1998.
- [23] C. Bonomo, L. Fortuna, P. Giannone, and S. Graziani, "A method to characterize the deformation of an IPMC sensing membrane," *Sensors and Actuators A: Physical*, vol. 123, pp. 146-154, 2005.
- [24] R. Montazami, S. Liu, Y. Liu, D. Wang, Q. Zhang, and J. R. Heflin, "Thickness dependence of curvature, strain, and response time in ionic electroactive polymer actuators fabricated via layer-by-layer assembly," *Journal of Applied Physics*, vol. 109, no. 10, p. 104301, 2011.
- [25] R. Montazami, D. Wang, and J. R. Heflin, "Influence of conductive network composite structure on the electromechanical performance of ionic electroactive polymer actuators," *International Journal of Smart and Nano Materials*, vol. 3, no. 3, pp. 204-213, 2012.
- [26] B. J. Akle, M. D. Bennett, D. J. Leo, K. B. Wiles, and J. E. McGrath, "Direct assembly process: a novel fabrication technique for large strain ionic polymer transducers," *Journal of Materials Science*, vol. 42, no. 16, pp. 7031-7041, 2007.
- [27] A. Khan, R. Jain, and M. Naushad, "Development of sulfonated poly (vinyl alcohol)/polypyrrole based ionic polymer metal composite (IPMC) actuator and its characterization," *Smart Materials and Structures*, vol. 24, no. 9, p. 095003, 2015.
- [28] W. Hong, A. Almomani, and R. Montazami, "Influence of ionic liquid concentration on the electromechanical performance of ionic electroactive polymer actuators," *Organic Electronics*, vol. 15, no. 11, pp. 2982-2987, 2014.
- [29] K.-S. Kwon and T. N. Ng, "Improving electroactive polymer actuator by tuning ionic liquid concentration," *Organic Electronics*, vol. 15, no. 1, pp. 294-298, 2014.
- [30] C. Meis, N. Hashemi, and R. Montazami, "Investigation of spray-coated silver-microparticle electrodes for ionic electroactive polymer actuators," *Text* 2014/04/01 2014.

- [31] M. Shahinpoor and K. J. Kim, "The effect of surface-electrode resistance on the performance of ionic polymer-metal composite (IPMC) artificial muscles," *Smart Materials and Structures*, vol. 9, no. 4, p. 543, 2000.
- [32] L. Lu, J. Liu, Y. Hu, Y. Zhang, and W. Chen, "Graphene-Stabilized Silver Nanoparticle Electrochemical Electrode for Actuator Design," *Advanced materials*, vol. 25, no. 9, pp. 1270-1274, 2013.
- [33] W. Hong, C. Meis, J. R. Heflin, and R. Montazami, "Evidence of counterion migration in ionic polymer actuators via investigation of electromechanical performance," *Sensors and Actuators B: Chemical*, vol. 205, no. 0, pp. 371-376, 2014.
- [34] Q. He, M. Yu, D. Yu, Y. Ding, and Z. Dai, "Significantly enhanced actuation performance of IPMC by surfactant-assisted processable MWCNT/Nafion composite," *Journal of Bionic Engineering*, vol. 10, no. 3, pp. 359-367, 2013.
- [35] J. Hou, Z. Zhang, and L. A. Madsen, "Cation/anion associations in ionic liquids modulated by hydration and ionic medium," *The Journal of Physical Chemistry B*, vol. 115, no. 16, pp. 4576-4582, 2011.
- [36] K. Sadeghipour, R. Salomon, and S. Neogi, "Development of a novel electrochemically active membrane and 'smart' material based vibration sensor/damper," *Smart Materials and Structures*, vol. 1, no. 2, p. 172, 1992.
- [37] M. Shahinpoor, "New effect in ionic polymeric gels: the ionic flexoelectric effect," in *Smart Structures & Materials' 95*, 1995, pp. 42-53: International Society for Optics and Photonics.
- [38] S. Nemat-Nasser and J. Y. Li, "Electromechanical response of ionic polymer-metal composites," *Journal of Applied Physics*, vol. 87, no. 7, pp. 3321-3331, 2000.
- [39] C. Bonomo, L. Fortuna, P. Giannone, S. Graziani, and S. Strazzeri, "A model for ionic polymer metal composites as sensors," *Smart materials and structures*, vol. 15, no. 3, p. 749, 2006.
- [40] K. Newbury, "Characterization, Modeling, and Control of Ionic Polymer Transducers," Virginia Polytechnic Institute and State University, 2002.
- [41] K. M. Newbury and D. J. Leo, "Electromechanical modeling and characterization of ionic polymer benders," *Journal of Intelligent Material Systems and Structures*, vol. 13, no. 1, pp. 51-60, 2002.
- [42] I. Must, U. Johanson, F. Kaasik, I. Põldsalu, A. Punning, and A. Aabloo, "Charging a supercapacitor-like laminate with ambient moisture: from a humidity sensor to an energy harvester," *Physical Chemistry Chemical Physics*, vol. 15, no. 24, pp. 9605-9614, 2013.
- [43] I. Must et al., "Ionic liquid-based actuators working in air: The effect of ambient humidity," *Sensors and Actuators B: Chemical*, vol. 202, pp. 114-122, 2014.

- [44] X. Hu, W. Cheng, T. Wang, Y. Wang, E. Wang, and S. Dong, "Fabrication, Characterization, and Application in SERS of Self-Assembled Polyelectrolyte–Gold Nanorod Multilayered Films," *The Journal of Physical Chemistry B*, vol. 109, no. 41, pp. 19385-19389, 2005/10/01 2005.
- [45] Y. Lvov, G. Decher, and H. Moehwald, "Assembly, structural characterization, and thermal behavior of layer-by-layer deposited ultrathin films of poly(vinyl sulfate) and poly(allylamine)," *Langmuir*, vol. 9, no. 2, pp. 481-486, 1993/02/01 1993.
- [46] S. L. Clark, M. F. Montague, and P. T. Hammond, "Ionic Effects of Sodium Chloride on the Templated Deposition of Polyelectrolytes Using Layer-by-Layer Ionic Assembly," *Macromolecules*, vol. 30, no. 23, pp. 7237-7244, 1997/11/01 1997.
- [47] S. T. Dubas and J. B. Schlenoff, "Factors Controlling the Growth of Polyelectrolyte Multilayers," *Macromolecules*, vol. 32, no. 24, pp. 8153-8160, 1999/11/01 1999.
- [48] W. Chen and T. J. McCarthy, "Layer-by-Layer Deposition: A Tool for Polymer Surface Modification," *Macromolecules*, vol. 30, no. 1, pp. 78-86, 1997/01/01 1997.
- [49] S. Ghannoum, Y. Xin, J. Jaber, and L. I. Halaoui, "Self-Assembly of Polyacrylate-Capped Platinum Nanoparticles on a Polyelectrolyte Surface: Kinetics of Adsorption and Effect of Ionic Strength and Deposition Protocol," *Langmuir*, vol. 19, no. 11, pp. 4804-4811, 2003/05/01 2003.
- [50] S. Liu et al., "Influence of the conductor network composites on the electromechanical performance of ionic polymer conductor network composite actuators," *Sensors and Actuators A: Physical*, vol. 157, no. 2, pp. 267-275, 2010.
- [51] K. Park, M.-K. Yoon, S. Lee, J. Choi, and M. Thubrikar, "Effects of electrode degradation and solvent evaporation on the performance of ionic-polymer–metal composite sensors," *Smart Materials and Structures*, vol. 19, no. 7, p. 075002, 2010.
- [52] S. Nemat-Nasser, "Micromechanics of actuation of ionic polymer-metal composites," *Journal of Applied Physics*, vol. 92, no. 5, pp. 2899-2915, 2002.
- [53] A. Keshavarzi, M. Shahinpoor, K. J. Kim, and J. W. Lantz, "Blood pressure, pulse rate, and rhythm measurement using ionic polymer-metal composite sensors," in *Smart Structures and Materials 1999: Electroactive Polymer Actuators and Devices*, 1999, vol. 3669, pp. 369-376.

CHAPTER 5. SOFT IONIC ELECTROACTIVE ACTUATORS WITH TUNABLE NON-LINEAR ANGULAR DEFORMATION

Published in the journal of Materials¹

Wangyujue Hong^{2,3}, Abdallah Almomani^{2,4}, Yuanfen Chen^{2,3}, Reihaneh Jamshidi^{2,3}, Reza Montazami^{2,3,5}

Abstract

The most rational approach to fabricate soft robotics is the implementation of soft actuators. Conventional soft electromechanical actuators exhibit linear or circular deformation, based on their design. This study presents the use of conjugated polymers, Poly(3,4-ethylenedioxythiophene)-poly(styrenesulfonate) (PEDOT:PSS) to locally vary ion permeability of the ionic electroactive polymer actuators and manipulate ion motion through means of structural design to realize intrinsic angular deformation. Such angular deformations are closer to biomimetic systems and have potential applications in bio-robotics. Electrochemical studies reveal that the mechanism of actuation is mainly associated with the charging of electric double layer (EDL) capacitors by ion accumulation and the PEDOT:PSS layer's expansion by ion interchange and penetration. Dependence of actuator deformation on structural design is studied experimentally and conclusions are verified by analytical and finite element method modeling. The results suggest that the ion-material interactions are considerably dominated by the design of the drop-cast PEDOT:PSS on Nafion.

¹ This is an open access journal, and the publisher "Multidisciplinary Digital Publishing Institute", allows the authors to re-use the material without obtaining permission.

² Primary researchers and authors. Graduate student, graduate student, graduate student, graduate student, and academic advisor, respectively.

³ Department of Mechanical Engineering, Iowa State University.

⁴ Department of Aerospace Engineering, Iowa State University.

⁵ Author of correspondence.

5.1. Introduction

The field of robotics is currently dominated by “hard robots” consisting of hard materials, mainly metallic or composite structures, paired with either (or both) ceramic actuators or electric motors as drive trains. Although hard robots sometimes have biomimetic design and limb-like structures similar to those in animals (e.g., “Big Dog” constructed by Boston Robotics [1]), hard robots often use wheels and rotary motors for motion, which distance them from biomimetic design and deters their integration with biomimetic systems. Soft actuators, on the other hand, have enabled soft robotics that can move and be manipulated, exhibiting biomimetic physical and mechanical attributes similar to those of Mollusca [2-6]. The ultimate advantages of soft actuators are that (1) they can easily conform to curvilinear structures, like biological muscles; and (2) since actuation is an intrinsic property of the actuator, micro-scale systems are practical to design and fabricate.

Electroactive polymer actuators, and in particular ionic electroactive polymer (IEAP) actuators, have attracted enormous interest and attention from the soft-robotic community and have been subject to extensive studies over the past several years [7-13]. Depending on the design, IEAP actuators can exhibit either linear or circular deformation. Linear IEAP actuators have a minuscule electromechanical response, which is not adequate for locomotion; circular deformation, however, is substantial. IEAP actuators consist of an ionomeric membrane at the core, covered with conductive network composite (CNC) layers and metal electrodes on each side to enhance ionic mobility and electric conductivity. IEAP actuators are doped with electrolytes, typically ionic liquids, to provide the ion-rich environment required for actuation. IEAP actuators’ performance and attributes depend on many factors, including the thickness and chemical structure of the ionomeric membrane [14]; the thickness, density, porosity, and electric conductivity of CNC layers

[15-19]; the thickness and electric conductivity of metal electrodes [20]; and the type, mobility, and prevalence of mobile ions [14, 17, 21-23]. IEAP actuators exhibit two physical deformations: cationic and anionic. Under an applied electric field cations and anions compete to reach the electrodes of opposite charge. There is often (depending on chemical composition of the electrolyte [24], CNC, and ionomeric membrane) a time lag between the accumulation of different ions at the electrodes. Therefore, in our case the actuator initially bends toward anode, which is due to accumulation of cations and called cationic deformation, then follows a bending toward cathode, which is due to accumulation of anions and called anionic deformation. This behavior is previously explored and discussed in detail [15-19].

Circular-bending soft actuators can be used to mimic a Venus flytrap [25], flap wings [26, 27], create artificial muscles [12, 28], and propel fish robots [29, 30]. But, circular actuation can also be considered a disadvantage of IEAP actuators concerning soft bio-robotic applications, as it is distinctly different from most biological systems. Although vertebrates and invertebrates have many muscles with circular or sinusoidal motion (e.g., tongue, abdominal muscles, etc.), they are not used for locomotion. Locomotor muscles are usually integrated with skeleton or exoskeleton structures to form limbs. Some robotics applications like microgrippers [8, 31] and miniaturized five fingered robots [7] would have worked more efficiently with angular (limb-like) rather than circular motion. To achieve angular motion, some researchers controlled individual segments of the IEAP actuators, moving them in different directions [32, 33]. A snake-like swimming robot is one example of this technique [34].

In this work, IEAP actuators with angular deformation, mimicking the limb-like motion in biological systems, are presented and studied. The limb-like motion is achieved intrinsically and without utilization of skeleton-like structures. Patterns of a conjugated polymer were deposited on

the ionomeric membrane to introduce regions with selective ion permeability to manipulate deformation. Poly(3,4-ethylenedioxythiophene)-poly(styrenesulfonate) (PEDOT:PSS) was used in fabrication of patterns because of its high conductivity and facile processing [35-43]. Dependence of deformation on the patterns of conjugated polymers is studied as well as morphological asymmetry in patterns and their influence on the cationic and anionic deformations. Electromechanical and electrochemical studies are accompanied and verified by analytical and finite element method (FEM) modeling. This study is expected to provide a cornerstone for utilization of advanced manufacturing techniques such as 3D printing in fabrication of soft actuators [44, 45].

5.2. Experimental

5.2.1. Materials

Commercially available Nafion membrane, 25 μm thick, (Ion Power, Inc., New castle, DE, USA) was used as the ionomeric membrane; 1-ethyl-3-methylimidazolium trifluoromethanesulfonate (EMI-Tf, molecular formula: $\text{C}_7\text{H}_{11}\text{F}_3\text{N}_2\text{O}_3\text{S}$) ionic liquid (Sigma Aldrich, St. Louis, MO, USA) was used as received; poly(3,4-ethylenedioxythiophene)-poly(styrenesulfonate) (PEDOT:PSS) (3.0%–4.0% in H_2O , high-conductivity grade) (Sigma Aldrich, St. Louis, MO, USA) was diluted by mixing with de-ionized (DI) water at 1:1 ratio and was used for fabrication of conductive polymer patterns. Gold leaf, 50 nm thick, (24K, transfer, LA Gold Leaf, Azusa, CA, USA) was used as the outer electrodes.

5.2.2. Sample Fabrication

Nafion, in its acidic form, was first cut and soaked in EMI-Tf at 80 $^\circ\text{C}$ for 30 min to intake ~25 wt % of ionic liquid. Ionic liquid content was calculated as the weight percentage (wt %) of the dry weight of the membrane using Equation (5-1):

$$W_e (\%) = \frac{W_f - W_d}{W_f} \times 100\% \quad (5-5-1)$$

where $W_e (\%)$ is the weight percent of the electrolyte; and W_d and W_f are the weights of dry and doped Nafion, respectively [23]. The doped Nafion membrane was then placed between two sheets of filter paper overnight to flatten. Diluted PEDOT:PSS aqueous solution was drop-cast on the Nafion membrane over a vinyl mask at the concentration rate of $0.56 \mu\text{L}/\text{mm}^2$. Schematic representations of each pattern are provided in Figure 5-1. The coated and uncoated strips are equal in width and 3 mm each. The drop-cast patterns were dried slowly on a hot plate at $40 \text{ }^\circ\text{C}$ for 48 h to allow for complete solvent (DI water) evaporation, and prevent anisotropic shrinkage of samples. Employing this method, flat and smooth samples were obtained and no anisotropic shrinkage was observed. The coated samples were then dried under vacuum at 60 mmHg at room temperature for 24 h for further dehydration. Gold leaf electrodes were then hot-pressed at $95 \text{ }^\circ\text{C}$ under 1000 lb_f for 40 s on both sides of the membrane to form an IEAP actuator.

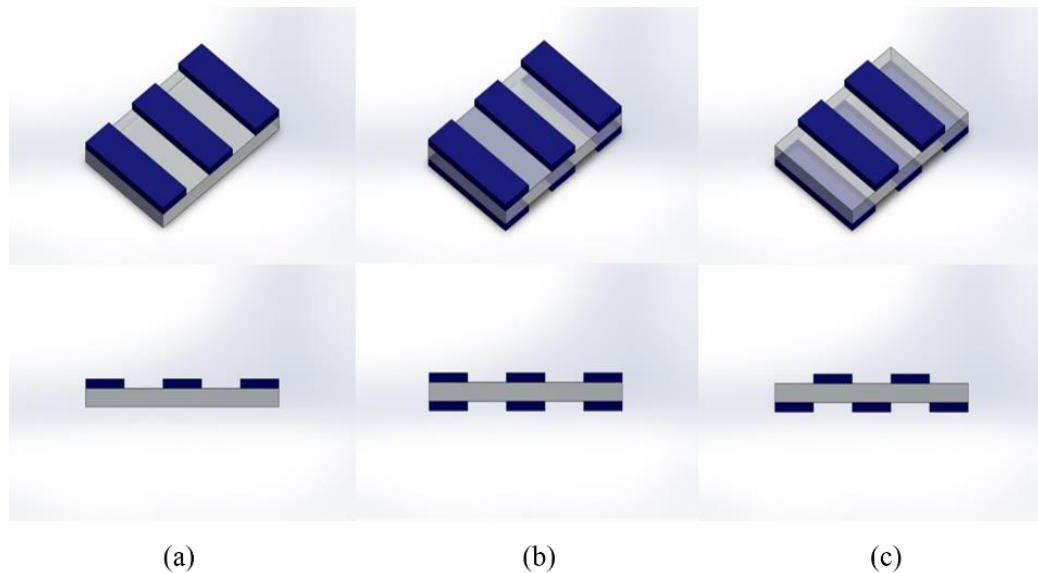


Figure 5-1 : Angled (top row) and side (bottom row) views of patterned samples; (a) 1S, (b) 2SS, and (c) 2SA. Gold leaf electrodes are not shown in the sketch to give a better view of the patterns. Not to scale.

5.2.3. Sample nomenclature

Sample nomenclature is shown in Table 5-1.

Table 5-1 The abbreviation and its definition of each sample used in this work.

Samples for Electromechanical Characterizations	
Name	Definition
1S	Pattern deposited on one side, Figure 5-1a
2SS	Symmetric patterns on both sides, Figure 5-1b
2SA	Asymmetric patterns on both sides, Figure 5-1c
2SA2	2SA sample with 2 strip-patterned side attached to anode
2SA3	2SA sample with 3 strip-patterned side attached to anode
Samples for Electrochemical Characterizations	
Name	Definition
BNafion	Bare Nafion doped with ionic liquid
Nafion/1s-PEDOT:PSS	PEDOT:PSS drop-cast on one side (full coverage, no pattern)
Nafion/2s-PEDOT:PSS	PEDOT:PSS drop-cast on both sides (full coverage, no pattern)
Sample for Morphological Characterizations	
Name	Definition
Nafion/1s-PEDOT:PSS/Au	PEDOT:PSS drop-cast on one side (full coverage, no pattern), with gold leaf electrodes hot-pressed on both sides

5.2.4. Electrochemical characterizations

Impedance spectroscopy, current flow, and cyclic voltammetry studies were conducted on a VersaSTAT-4 potentiostat (Princeton Applied Research, Oak Ridge, TN, USA) in two-electrode mode. The impedance spectroscopy studies were carried out at frequencies between 1.0×10^5 Hz and 1.0×10^{-1} Hz, and a potential difference (ΔV) of 10 mV. Current flow was studied as a function of ± 4 V step function, each over a 600 s interval. Cyclic voltammetry was carried out in ± 4 V potential window at a scan rate of 50 mV/s.

5.2.5. Electromechanical Characterizations

Actuators of 1×15 mm² dimension were cut perpendicularly to the longitudinal direction of the PEDOT:PSS strips. Electromechanical responses of actuators as a function of a 4 V step

function were monitored and recorded using a charge-coupled device (CCD) video camera, mounted to an in-house-constructed microprobe station, at 30 frames per second.

5.2.6. Morphological and mechanical characterizations

Surface analysis was conducted using scanning electron microscopy (SEM) (Jeol. JCM-6000 NeoScope, Peabody, MA, USA) to characterize morphology of the specimens, including film thickness and layer adhesion. The SEM image of the cross-section of Nafion/1s-PEDOT:PSS/Au sample is shown in Figure 5-2, indicating well interlayer adhesion between Nafion membrane and PEDOT:PSS layer after hot-press, with no observable separation in between.

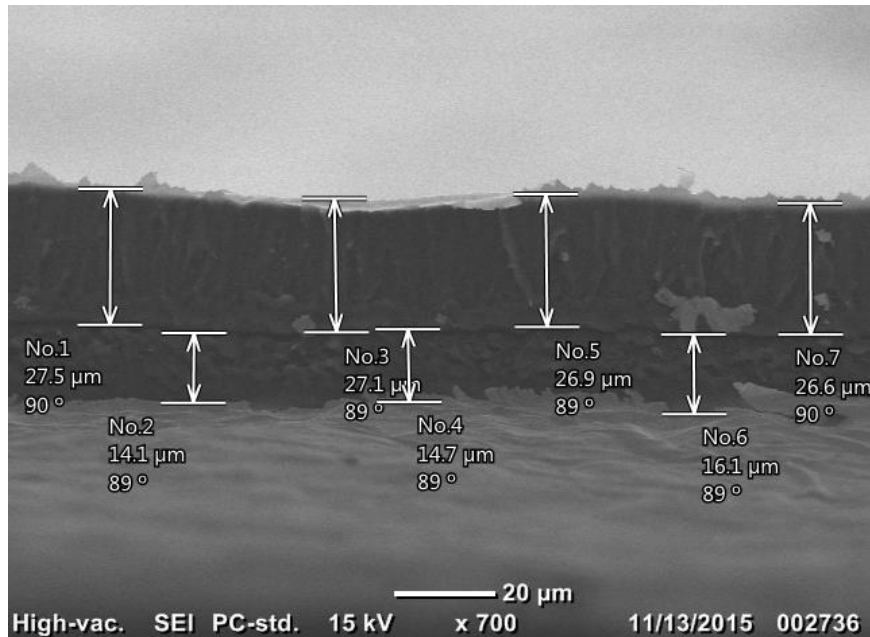


Figure 5-2: SEM image of the cross-section of specimen Nafion/1s-PEDOT:PSS/Au, indicating well interlayer adhesion between layers.

The elastic modulus of each constituent layer of IEAP actuator was measured/calculated using a dynamic mechanical analyzer (DMA-1, Mettler Toledo, Columbus, OH, USA), loaded with tension clamps and operated in static modes. More information is included in Section 1, Supporting Information.

5.2.7. Finite element modeling

ABAQUS finite element software (ABAQUS/CAE 2016, Dassault Systèmes Simulia Corp., Johnston, RI, USA) was used to model the electromechanical responses of IEAP actuators and study the effect of various patterns on the actuation performance, and verify the experimental results. Details of the simulation procedures are presented in Section 2 of the Supporting Information.

5.3. Results

5.3.1. Cyclic Voltammetry

Cyclic voltammograms of bare and coated specimens obtained in a potential range of ± 4 V at a sweep rate of 50 mV/s are shown in Figure 5-3. Both voltammograms of specimens BNafion and Nafion/2s-PEDOT:PSS show reversible curves, revealing a reversible redox reaction at the electrode. When compared with BNafion, two additional significant current peaks are observed at ± 1.5 V for Nafion/2s-PEDOT:PSS which are characteristic to PEDOT:PSS [38]. Additionally, another pair of current peaks are observed at ± 0.8 V for both bare and coated Nafion, which correspond to ion drift across the Nafion membrane [46].

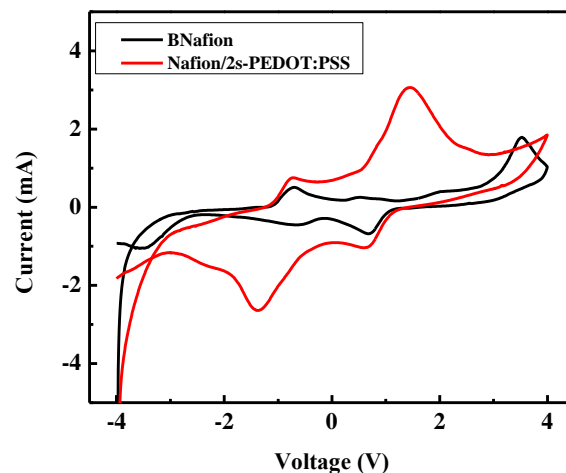


Figure 5-3: Cyclic voltammograms of different specimens measured at 50 mV/s.

5.3.2. Equivalent circuit modeling

Electric double layer (EDL) formation in IEAP actuators is a known phenomenon well-studied by others and us as well [17-19, 22, 38, 47]. To investigate how the presence of PEDOT:PSS layers affect the formation of the EDL at the electrode, electrical impedance was studied as a function of frequency. Electrochemical studies were conducted at 10 mV and at a varying frequency to allow characterization over a broader frequency range. The electrochemical behavior of the system can be analyzed by fitting the electrical impedance with an equivalent electric circuit; as authors have previously shown for similar actuators with metallic colloid coatings [22, 23, 48]. The EDL capacitors in series with the resistance of bulk Nafion layer R_b can be used to model the electrochemical behavior of such systems. The continuous contribution of a diffuse layer makes the pseudo-EDL capacitor very different from an ideal capacitor. Therefore, a constant phase element (CPE) was introduced in parallel with the EDL capacitor, as shown in Figure 5-4. The impedance of the introduced CPE, W_{CPE} , is defined as:

$$W_{CPE} = \frac{1}{Y_0} (j\omega)^{-n} \quad (5-2)$$

where ω is angular frequency, and the property of a CPE is defined by two values, Y_0 and n . n is a unitless exponent taking values between 0 and 1. As $n = 0$, CPE is identical to a resistor with $Y_0 = 1/R$, and when $n = 1$, CPE is identical to a capacitor with $Y_0 = C$.

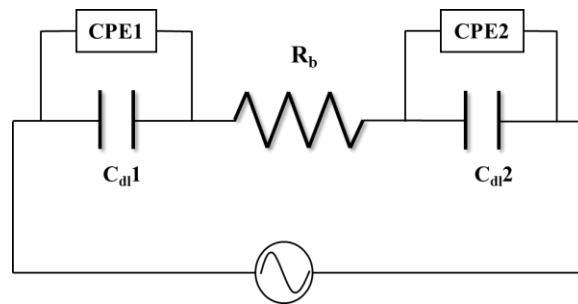


Figure 5-4: Equivalent circuit with a constant phase element

Considering the symmetric structure of BNafion and Nafion/2s-PEDOT:PSS, the impedance of two EDL capacitors and CPEs were set equally, that is, $C_{dl1} = C_{dl2}$, and $W_{CPE1} = W_{CPE2}$. Figure 5-5 **Error! Reference source not found.**a–f present the experimental data and the fittings (solid curves) of the electric impedance magnitudes and phase angles of BNafion, Nafion/1s-PEDOT:PSS, and Nafion/2s-PEDOT:PSS. The model and the impedance spectrum in the entire frequency range are in good agreement. Table 5-2 summarizes the fitting parameters for the three actuators. The bulk membrane resistance, R_b , is found to increase from 89.9 Ω (BNafion) to 171.7 Ω (Nafion/2s-PEDOT:PSS), primarily due to the indirect contact between the ionomer and the external electrode [9]. The PEDOT:PSS layers on both sides of Nafion/2s-PEDOT:PSS cause a significant drop in the capacitance of the EDL capacitor C_{dl} compared to BNafion (from 3.24 to 0.12 μF).

In samples with the PEDOT:PSS layer casted only on one side of the Nafion membrane, an asymmetric charging behavior is induced by its morphological asymmetry. As presented in **Error! Reference source not found.**, the capacitance C_{dl} improved on one side, while it dropped on the other side. The largest (12.78 μF) and smallest (3.52×10^{-3} μF) capacitances of C_{dl} both occurred in the same specimen, but at different electrodes, indicating a highly imbalanced storage of ions at the external electrodes. The higher capability of the ions storage could happen in either the uncoated or PEDOT:PSS coated side, which will be discussed in the next sections with other experimental results.

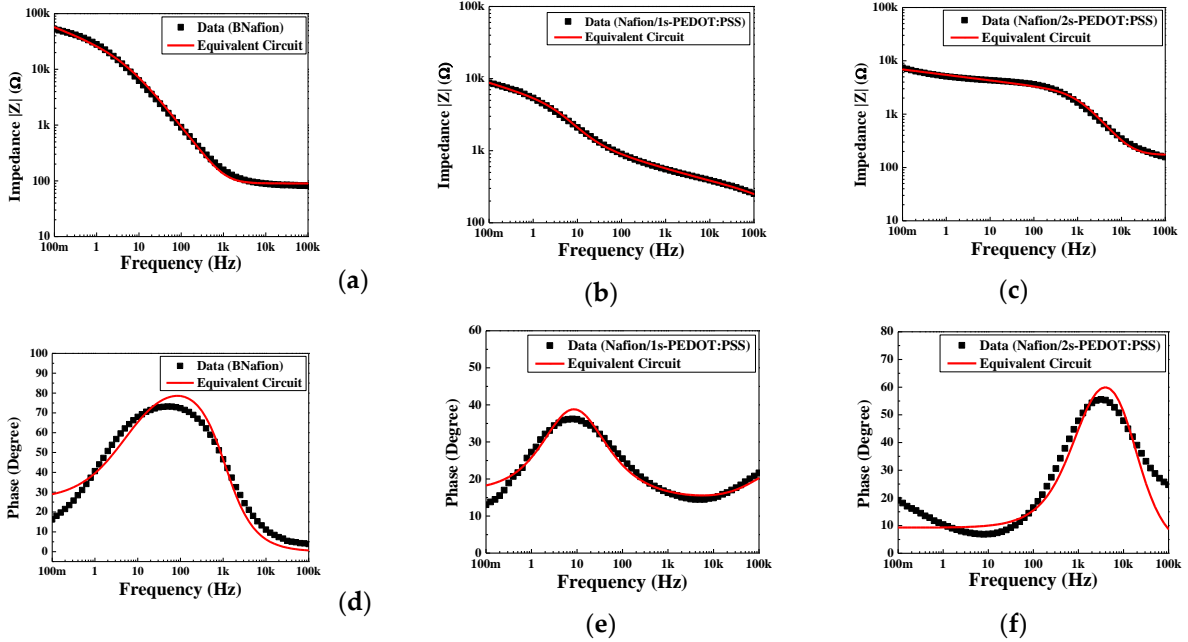


Figure 5-5: Impedance magnitudes of (a) BNafion, (b) Nafion/1s-PEDOT:PSS, and (c) Nafion/2s-PEDOT:PSS; and phase of (d) BNafion, (e) Nafion/1s-PEDOT:PSS, and (f) Nafion/2s-PEDOT:PSS fitted by equivalent circuit with constant phase element shown in Figure 5-4.

Table 5-2: Fitting parameters for different specimens.

Circuit Element	BNafion	Nafion/ 1s-PEDOT:PSS	Nafion/ 2s-PEDOT:PSS
R_b (Ω)	89.9	118.9	171.7
$CPE1$	Y_0 (Ω ⁻¹ · cm ⁻² · s ⁿ)	3.90×10^{-5}	1.95×10^{-4}
	n	0.29	0.18
$CPE2$	Y_0 (Ω ⁻¹ · cm ⁻² · s ⁿ)	3.90×10^{-5}	3.50×10^{-4}
	n	0.29	0.21
C_{dl1} (μF)	3.24	12.78	0.12
C_{dl2} (μF)	3.24	3.52×10^{-3}	0.12

5.3.3. Charging and discharging

To further investigate how the morphological asymmetry affects the charging/discharging behavior under a step voltage, current flow corresponding to a 4 V potential difference between

the external electrodes was measured and recorded as a function of time (Figure 5-6a). Figure 5-6b presents the corresponding charge density stored in the specimen as a function of time. Each step function was set to 600 s; a much larger time range for the strain generated in these actuators that have already reached saturation [47]. The side with the casted PEDOT:PSS layer in Nafion/1s-PEDOT:PSS is connected to the working electrode, which experiences a higher potential in the charging process and a lower potential in the following discharging process. According to the cyclic voltammetry results, an electrochemical reaction occurs in the PEDOT:PSS layer when it is under a ± 4 V voltage. The larger charging/discharging current in Nafion/2s-PEDOT:PSS (compared with BNafion) is due to the inserted/ejected electrons and the corresponding ion interchange. The charge density (area under the curve) difference between charging and discharging of symmetric samples (BNafion and Nafion/2s-PEDOT:PSS) is attributed to the random distribution of ions when charging is initiated compare to when discharging is initiated where, hypothetically, all ions are at the opposite electrode. While discharging, ions are traveling a longer path-length to reach the matching electrode, and this results in a larger current density. Additionally, a significantly larger magnitude of displaced charge (area under the curve) was observed in Nafion/1s-PEDOT:PSS. The highest charge density was observed when the PEDOT:PSS layer was connected to the higher potential in the charging process (Figure 5-6b, red curve, 0–600 s). This was followed by a less significant charge density during the discharging process (same plot, 600–1200 s). This phenomenon can be partially explained by the promoted ions' drift, due to the better contact between the ionomer and the external electrode on the uncoated side. When at the higher potential, electrons will be ejected from PEDOT and positive charge carriers will be introduced to make the material electrically conducting, while at the lower potential, PEDOT will be reduced and partially loses its conductivity [49]. This also can explain

the slightly decreased charge density of Nafion/1s-PEDOT:PSS during the discharging process. Overall Nafion/1s-PEDOT:PSS reveals the highest charge storage capacity.

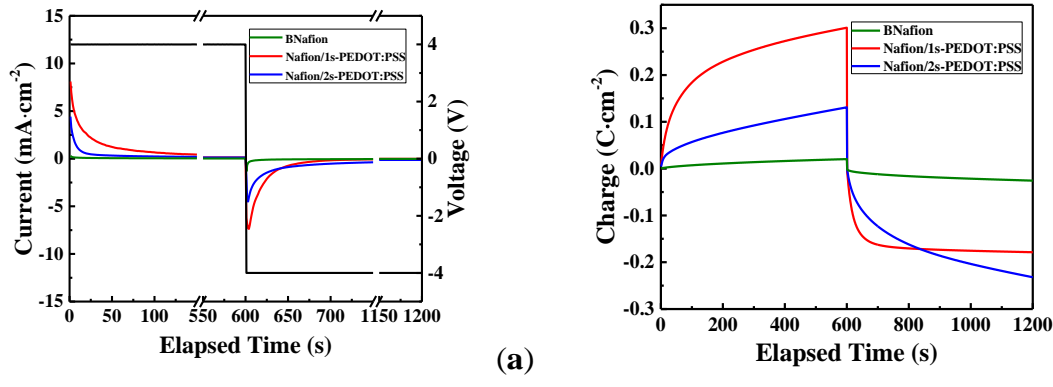


Figure 5-6 : (a) Charging/discharging currents and (b) charge density versus time for different specimens under one cycle of a 4 V square wave.

5.3.4. Electromechanical response

The electromechanical response of IEAP actuators with different PEDOT:PSS patterns was studied. Actuator 1S was first tested under a 4 V step function with the cathode connected to the PEDOT:PSS coated side. The cationic response was homogenous and circular toward the uncoated side. This behavior is similar to that of the actuators consisting of uniform CNC layers as reported previously [17-19, 22, 47]. However, as time progressed, this uniform actuation was canceled by the dominating anionic strain, which consists of a sharp, angular bending. Thus, the actuator exhibited a limb-like deformation. The schematic representation of the pattern and the images of the experimental results are shown in Figure5-7a.

To further explore how different patterns affect the actuation performance, a 4 V step function was applied to the other two actuators, 2SS and 2SA; experimental results are presented in Figure5-7b–d. The electromechanical response of the asymmetric 2SA actuator was studied under different polarities, 2SA2, and 2SA3. The 2SS actuator exhibited a rectangular, limb-like, deformation in both cationic and anionic deformations (Figure 5-7b), while 2SA actuators

exhibited a more complex behavior, indicating a dependency on the electrode polarity (Figure 5-7c,d). In anionic motion, 2SA2 deformed into rectangle-like shape when actuator 2SA3 deformed into a triangle-like shape. Meanwhile, both cases have noticeable anionic deformation (strain) but almost negligible cationic deformation.

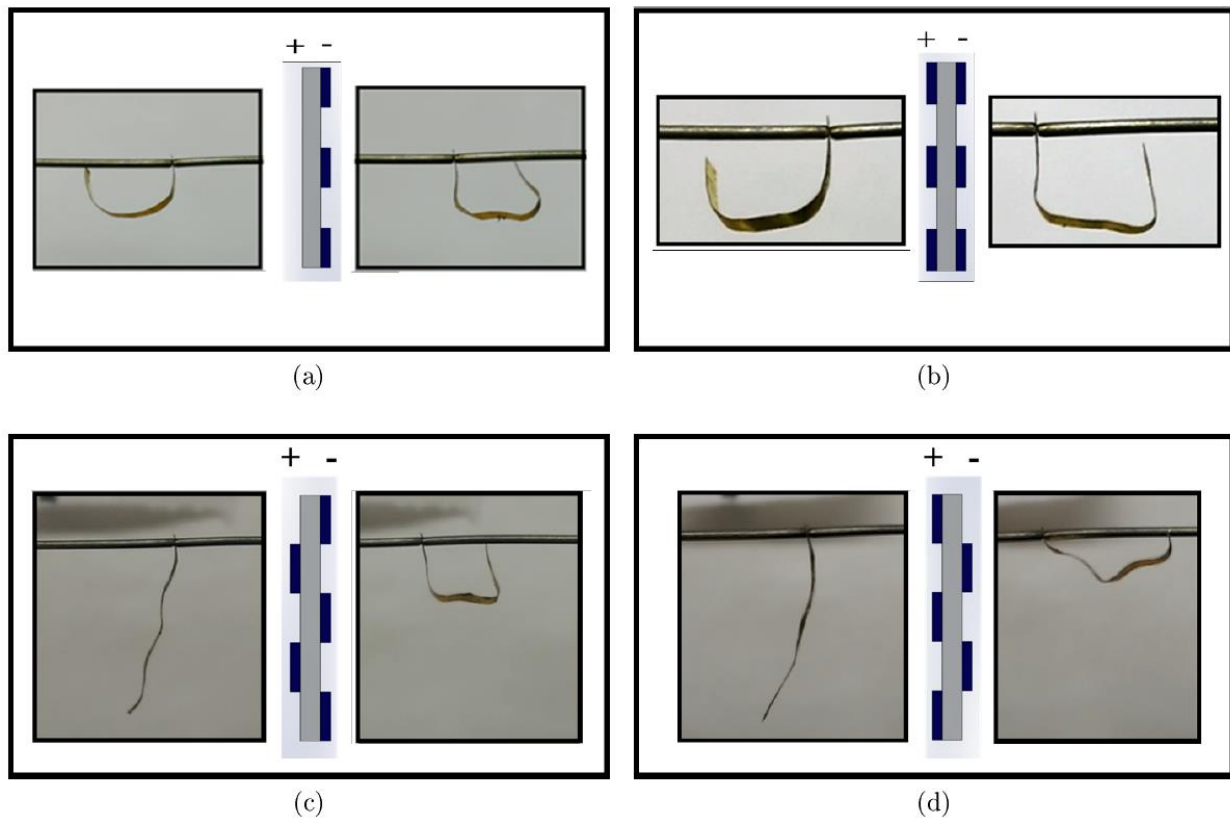


Figure 5-7 : Schematic representation and experimental actuation performance for (a) 1S, (b) 2SS, (c) 2SA2, and (d) 2SA3. Left picture is the cationic response and right picture is the anionic response.

5.4. Discussion and simulation

5.4.1. Discussion

Our experimental results suggest that the PEDOT:PSS layers as the CNC considerably affect the actuation behavior.

First, impedance data and the corresponding equivalent circuit modeling indicate that in Nafion/1s-PEDOT:PSS, ions are more likely to accumulate and act at the interface of one

electrode, while depleted on the interface of the other electrode. However, when the PEDOT:PSS layer is casted on both sides of Nafion, a completely different phenomenon occurs and fewer ions move to charge the EDL capacitors. Consequently, fewer ions will accumulate at the outer electrodes; which in turn hinders mechanical deformation of the actuator.

Secondly, Nafion/1s-PEDOT:PSS exhibits the highest charge density under a 4 V square function. Since the main cause of the actuation is the accumulation and depletion of charged ions at the interfaces of the electrodes, the existence of PEDOT:PSS layer casted on only one side of Nafion would, most likely, enhance the actuation.

Additionally, electromechanical responses suggest that the actuation performance varies significantly with the existence of the PEDOT:PSS layer. Experimental results for actuators 1S, 2SA2, and 2SA3 all reveal an enhancement in the strain generation when the PEDOT:PSS layer only exists on the convex side, and an inhibition when it only exists on the concave side. Before the application of an electric potential, EMI-Tf ions are only distributed in the Nafion membrane, and presumably none in the PEDOT:PSS layer. Cyclic voltammetry results reveal that an electrochemical redox occurs in the PEDOT:PSS layer at ± 1.5 V. Therefore, this enhancement-on-convex and inhibition-on-concave phenomenon may be caused by: (i) the expansion of the PEDOT:PSS layer due to the ion interchange and penetration to maintain charge neutrality; and (ii) ion accumulation and/or depletion at the electrodes. Experimental results for actuator 2SS, however, exhibit a completely reversed trend, that no matter whether in the convex or concave side, the PEDOT:PSS layer always hinders the actuation. That is, the existence of the PEDOT:PSS layer does not contribute considerably to expansion. Although, charging results reveal a relatively larger charging density in Nafion/2s-PEDOT:PSS than in BNafion, due to the electrochemical

redox of PEDOT layers, this phenomenon could be explained by fewer ions moving to charge the EDL capacitors at the interfaces of electrodes.

Considering the structures of the actuators investigated in this study, segments of the actuators can be categorized under three possible structures: (1) uncoated membrane (BNafion); (2) single-side coated membrane (Nafion/1s-PEDOT:PSS); and (3) double-side coated membrane (Nafion/2s-PEDOT:PSS). Following scrutinizing the electromechanical response of actuators on the segment scale, it is concluded that: (1) for asymmetric segments, volume expansion occurs in the PEDOT:PSS layer due to ion interchange and ion accumulation/depletion at the interfaces of external electrodes; (2) the PEDOT:PSS layer does not contract; and (3) for symmetric segments, volume expansion occurs, but fewer ions move toward the electrodes than that of the uncoated segment. Therefore, deformation is enhanced on the uncoated segments and hindered on the coated segments.

5.4.2. Finite element simulation

The conclusions drawn from experimental observations (Section 4.1) were examined and verified by FEM static analyses. The electromechanical response of IEAP actuators with different CNC patterns was modeled on ABAQUS/CAE using FEM (Section 2, Supporting Information). Figure 5-8 shows two different hypotheses for actuator 1S's displacement distribution during cationic response; those are, cations are mainly accumulated in the PEDOT:PSS layer Figure 5-8a or Nafion Figure 5-8b. It confirms that in asymmetric segments, deformation mainly occurs on the PEDOT:PSS layer during the cationic response. Otherwise, instead of a homogeneous and circular deformation, a rectangular deformation occurs, which does not match the experimental results. It confirms that the largest capability of ions storage in Nafion/1s-PEDOT:PSS should locate at the coated side.

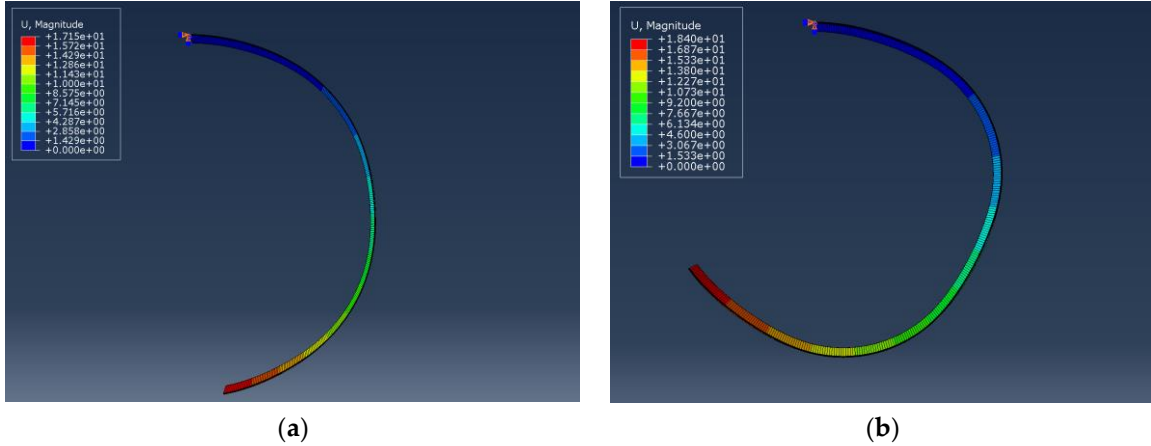
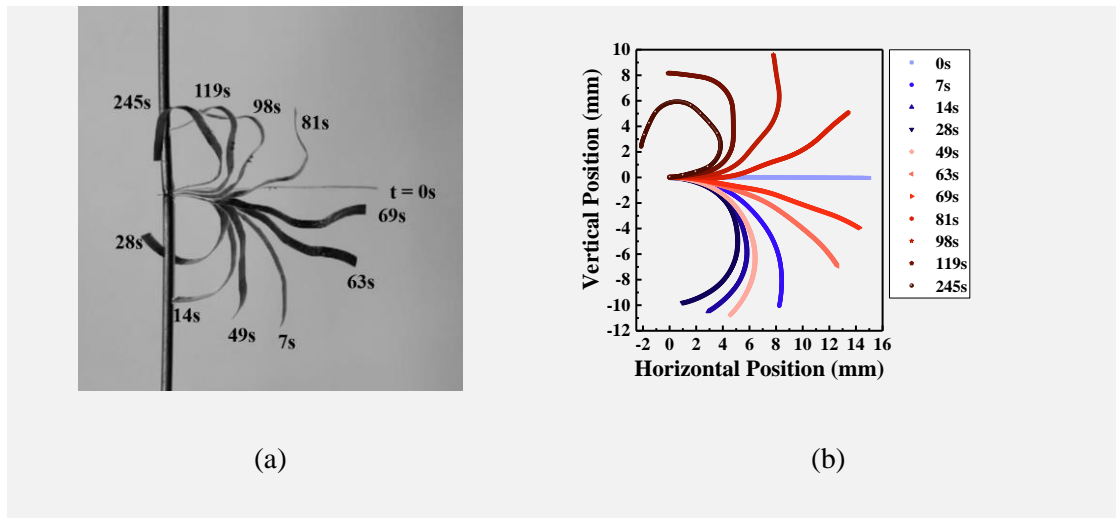
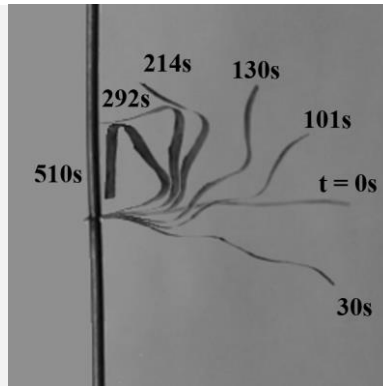


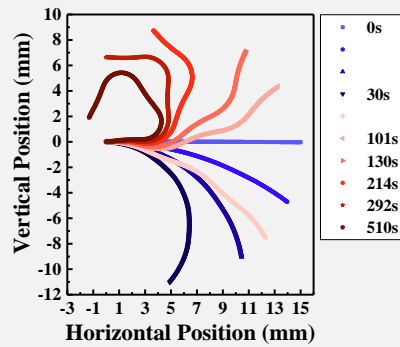
Figure 5-8: Displacement distribution of actuator 1S during cationic response under different hypotheses. When the total number of the movable ions in the actuator is fixed, the volume ratios of cations in the PEDOT:PSS layer (attached to the cathode) and the Nafion sub-layer (Supporting Information) are (a) 2:1 and (b) 1:2, respectively.

Figure 5-9 presents overlay images of experimental (5-9 a,c,e,g) and the corresponding simulated (5-9 b,d,f,h) results. Experimental results are collected under a 4 V step function and figures are extracted from video recordings. Simulations are the corresponding increments from static steps where blue and red gradation represents cationic and anionic strains, respectively. Experimental and simulated data are in good agreement, verifying the conclusive remarks made in Section 4.1.

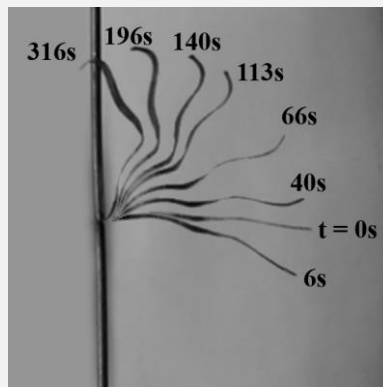




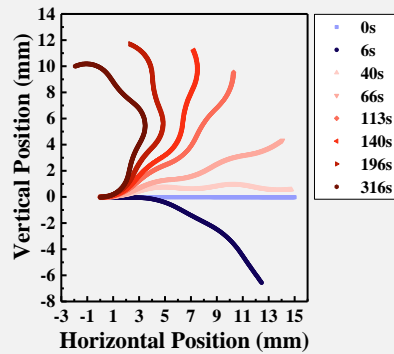
(c)



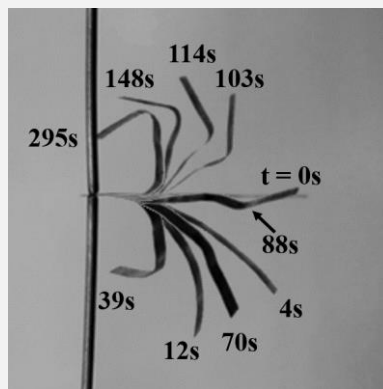
(d)



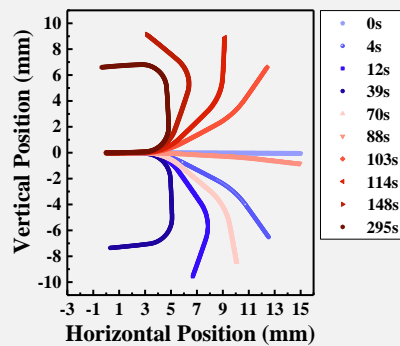
(e)



(f)



(g)



(h)

Figure 5-9: Comparison of experimental bending displacement in response to a 4 V step input (left column) and the corresponding results produced by the static theoretical model via ABAQUS (right column). Figure (a) and (b) represent actuator 1S, (c) and (d) represent actuator 2SA2, (e) and (f) represent actuator 2SA3, and (g) and (h) represent actuator 2SS. The top electrode is the cathode and the bottom electrode is the anode.

In addition, as suggested by Hou et al., a simple aggregation model happened when EMI-Tf ionic liquid was absorbed into an ionic polymer membrane (Nafion), indicating an excess of negatively charged triple ions, $(\text{Tf}^- - \text{EMI}^+ - \text{Tf}^-)$ [24]. Without loss of generality, let EMI-Tf in Nafion membrane is in the format of (EMI^+) and $(\text{Tf}^- - \text{EMI}^+ - \text{Tf}^-)$. In an IEAP actuator, $15 \text{ mm} \times 1 \text{ mm}$ ($l \times w$) and EMI-Tf uptake $\sim 24 \text{ wt } \%$, the increased weight is around $1.91 \times 10^{-4} \text{ g}$. With the molecular weight of 260.23 g/mol in EMI-Tf, the molecular from EMI-Tf is $7.35 \times 10^{-7} \text{ mol} = 4.42 \times 10^{17}$. Therefore, the total mobile cations (EMI^+) and anion/anionic cluster $(\text{Tf}^- - \text{EMI}^+ - \text{Tf}^-)$ should be half of the total molecules inside, which equals to 2.21×10^{17} . Meanwhile, when $\Delta T \times \alpha$ is small, the change in volume by thermal expansion ΔV can be simplified to $3\alpha \cdot \Delta T \cdot V_0$, by excluding the higher orders, where V_0 is the volume before any expansion/contraction. Simulations shown Figure 5-9 confirm a change in volume $\Delta V = 1.83 \times 10^{-11} \text{ m}^3$ in cationic response. Given the molecular volume of cations (EMI^+) as 182 \AA [47], an order of magnitude estimation is that 1.0×10^{17} (EMI^+) cations are expected to contribute to the cationic response, which is almost half of the mobile cations inside Nafion membrane. In other words, based on the experiments and simulations indicated in Figure 5-9, approximately half of the ions from EMI-Tf contribute to actuation.

Simulations shown in Figure 5-9 set the volume ratio of cations and anions/anionic clusters based on the results reported by Hou et al. They characterized the diffusion ratio $D_{\text{cation}}/D_{\text{anion}}$ of EMI-Tf ionic liquid inside Nafion membranes as a function of water content χ_{water} [24]. They discovered that when 15–30 wt % EMI-Tf is absorbed in Nafion at very low water contents, the diffusion ratio falls in the range of 1.5–2.5. The diffusion coefficient D is inversely proportional to the size of diffusing particles as described by the Stokes-Einstein relation.

$$D = kT/(c\eta r_H) \quad (5-3)$$

here k is the Boltzmann constant, T is absolute temperature, c is a constant factor depending on the shape and relative size of the diffusion particle to its surrounding fluid, η is fluid viscosity, and r_H is the hydrodynamic radius of the diffusing particle [24, 50]. Since the cations and anions/anionic clusters exist in the same thermodynamic phase, D_{cation}/D_{anion} equals the reciprocal of their hydrodynamic radii ratio, which is proportional to the cubic root of the ions' volume distributed in the Nafion membrane. That is $D_{cation}/D_{anion} = r_{Hanion}/r_{Hcation} \sim (V_{anion}/V_{cation})^{1/3}$. The volume ratio of cations and anions/anionic clusters set in the simulation falls in the range of 1.5^3 – 1.7^3 , which is consistent with the results reported by Hou et al.

5.5. Conclusion

Intrinsic angular deformation of IEAP actuators was achieved by incorporating conjugated polymer, PEDOT:PSS, patterns in the structure of soft actuators. Electrochemical and electromechanical studies were performed and it was observed that instead of the homogeneous circular deformation exhibited by conventional IEAP actuators, ones with polymer patterns bend at specific locations on the actuator which resulted in apparently angular deformation with sharp angles of 90° and beyond. Electromechanical responses indicate that actuation performances are significantly affected by different polymer patterns. Meanwhile, according to an FEM static model, approximately half of the ions from EMI-Tf contribute to the actuation. With different patterns of PEDOT:PSS, deformation patterns can be manipulated and actuators whose behaviors are complex but intrinsically controllable can be fabricated.

Supplementary Materials: The following are available online at <http://www.mdpi.com/1996-1944/10/6/664/s1>, Figure S1: SEM images of specimen Nafion/1s-

PEDOT:PSS/Au, from middle point to edge ((a)–(c)) of PEDOT:PSS layer, Figure S2: Schematic of a bilayer laminate for the characterization of the elastic modulus of individual layer, Table S1: The thickness of each layer in IEAP actuator and its physical properties..

Acknowledgments: Authors would like to thank Ms. Sarah Kreutner for technical editing of the manuscript.

Author Contributions: W.H. and A.A. equally contributed to performing experiments, analysis of data, and writing the paper; Y.C. and R.J. contributed to performing data analysis; W.H., A.A. and R.M. conceived and designed the experiments.

Conflicts of Interest: The authors declare no conflict of interest.

5.6. References

- [1] M. Raibert, K. Blankespoor, G. Nelson, R. Playter, and T. Team, "Bigdog, the rough-terrain quadruped robot," in Proceedings of the 17th World Congress, 2008, vol. 17, no. 1, pp. 10822-10825: Proceedings Seoul, Korea.
- [2] S. Shian, K. Bertoldi, and D. R. Clarke, "Dielectric Elastomer Based "Grippers" for Soft Robotics," *Advanced Materials*, Sep 29 2015.
- [3] D. Yang et al., "Buckling of Elastomeric Beams Enables Actuation of Soft Machines," *Advanced Materials*, Sep 21 2015.
- [4] K. Asaka and H. Okuzaki, *Soft Actuators: Materials, Modeling, Applications, and Future Perspectives*. Japan: Springer, 2014, p. 507.
- [5] J. A. Rogers, "Materials science. A clear advance in soft actuators," *Science*, vol. 341, no. 6149, pp. 968-9, Aug 30 2013.
- [6] Y. Yu and T. Ikeda, "Soft Actuators Based on Liquid-Crystalline Elastomers," *Angewandte Chemie International Edition*, vol. 45, no. 33, pp. 5416-5418, 2006.
- [7] D. Chatterjee, N. Hanumaiah, Y. Bahramzadeh, and M. Shahinpoor, "Actuation and sensing studies of a miniaturized five fingered robotic hand made with ion polymeric metal composite (IPMC)," in *Advanced Materials Research*, 2013, vol. 740, pp. 492-495: Trans Tech Publ.
- [8] R. Lumia and M. Shahinpoor, "IPMC microgripper research and development," in *Journal of Physics: Conference Series*, 2008, vol. 127, no. 1, p. 012002: IOP Publishing.

- [9] K. Kim and M. Shahinpoor, "Special issue - Biomimetics, Artificial Muscles, and Nano-Bio 2004," (in English), *Journal of Intelligent Material Systems and Structures*, vol. 18, no. 2, pp. 101-101, FEB 2007 2007.
- [10] K. Choe, K. Kim, D. Kim, C. Manford, S. Heo, and M. Shahinpoor, "Performance characteristics of electro-chemically driven polyacrylonitrile fiber bundle actuators," (in English), *Journal of Intelligent Material Systems and Structures*, vol. 17, no. 7, pp. 563-576, JUL 2006 2006.
- [11] M. Shahinpoor, K. Kim, and D. Leo, "Ionic polymer-metal composites as multifunctional materials," (in English), *Polymer Composites*, vol. 24, no. 1, pp. 24-33, FEB 2003 2003.
- [12] M. Shahinpoor, "Ionic polymer-conductor composites as biomimetic sensors, robotic actuators and artificial muscles--a review," *Electrochimica Acta*, vol. 48, no. 14-16, pp. 2343-2353, 2003.
- [13] M. Shahinpoor and K. J. Kim, "Solid-state soft actuator exhibiting large electromechanical effect," *Applied Physics Letters*, vol. 80, no. 18, pp. 3445-3447, 2002.
- [14] W. Hong, C. Meis, J. R. Heflin, and R. Montazami, "Evidence of counterion migration in ionic polymer actuators via investigation of electromechanical performance," *Sensors and Actuators B: Chemical*, vol. 205, no. 0, pp. 371-376, 2014.
- [15] R. Montazami, D. Wang, and J. R. Heflin, "Influence of conductive network composite structure on the electromechanical performance of ionic electroactive polymer actuators," (in en), <http://mc.manuscriptcentral.com/ijsnm>, research-article 2012-09-18 2012.
- [16] R. Montazami, S. Liu, Y. Liu, D. Wang, Q. Zhang, and J. R. Heflin, "Thickness dependence of curvature, strain, and response time in ionic electroactive polymer actuators fabricated via layer-by-layer assembly," *Text* 2011/05/16 2011.
- [17] Y. Liu et al., "Ion transport and storage of ionic liquids in ionic polymer conductor network composites," *Applied Physics Letters*, vol. 96, no. 22, p. 223503, 2010.
- [18] S. Liu et al., "Influence of the conductor network composites on the electromechanical performance of ionic polymer conductor network composite actuators," *Sensors and Actuators A: Physical*, vol. 157, no. 2, pp. 267-275, 2010.
- [19] S. Liu et al., "Layer-by-layer self-assembled conductor network composites in ionic polymer metal composite actuators with high strain response," *Applied Physics Letters*, vol. 95, no. 2, p. 023505, 2009.
- [20] C. Meis, N. Hashemi, and R. Montazami, "Investigation of spray-coated silver-microparticle electrodes for ionic electroactive polymer actuators," *Text* 2014/04/01 2014.
- [21] A. A. Amiri Moghadam, W. Hong, A. Kouzani, A. Kaynak, R. Zamani, and R. Montazami, "Nonlinear dynamic modeling of ionic polymer conductive network composite actuators

- using rigid finite element method," *Sensors and Actuators A: Physical*, vol. 217, no. 0, pp. 168-182, 2014.
- [22] Y. Liu et al., "Equivalent circuit modeling of ionomer and ionic polymer conductive network composite actuators containing ionic liquids," *Sensors and Actuators A: Physical*, vol. 181, pp. 70-76, 2012.
- [23] W. Hong, A. Almomani, and R. Montazamia, "Influence of ionic liquid concentration on the electromechanical performance of ionic electroactive polymer actuators," vol. 15, no. 11, pp. 2982–2987, November 2014 2014.
- [24] J. Hou, Z. Zhang, and L. A. Madsen, "Cation/anion associations in ionic liquids modulated by hydration and ionic medium," *The Journal of Physical Chemistry B*, vol. 115, no. 16, pp. 4576-4582, 2011.
- [25] M. Shahinpoor, "Biomimetic robotic Venus flytrap (*Dionaea muscipula* Ellis) made with ionic polymer metal composites," *Bioinspiration & biomimetics*, vol. 6, no. 4, p. 046004, 2011.
- [26] K. Kim, "Ionic polymer-metal composite as a new actuator and transducer material," in *Electroactive Polymers for Robotic Applications*: Springer, 2007, pp. 153-164.
- [27] S. Lee, H. Park, S. D. Pandita, and Y. Yoo, "Performance improvement of IPMC (ionic polymer metal composites) for a flapping actuator," *International Journal of Control Au*
- K. Asaka, "Biomimetic soft robots with artificial muscles," in *Smart Materials, Nano-, and Micro-Smart Systems*, 2004, pp. 132-144: International Society for Optics and Photonics.
- [33] Y. Nakabo, T. Mukai, and K. Asaka, "Kinematic modeling and visual sensing of multi-DOF robot manipulator with patterned artificial muscle," in *Proceedings of the 2005 IEEE International Conference on Robotics and Automation*, 2005, pp. 4315-4320: IEEE.
- [34] N. Kamamichi, M. Yamakita, K. Asaka, and Z.-W. Luo, "A snake-like swimming robot using IPMC actuator/sensor," in *Proceedings 2006 IEEE International Conference on Robotics and Automation*, 2006. ICRA 2006., 2006, pp. 1812-1817: IEEE.
- [35] G. Di Pasquale, L. Fortuna, S. Graziani, M. La Rosa, A. Pollicino, and E. Umana, "A study on IP2C actuators using ethylene glycol or EmI-Tf as solvent," *Smart Materials and Structures*, vol. 20, no. tomation and Systems, vol. 4, no. 6, p. 748, 2006.
- [28] Y. Bar-Cohen, "Artificial muscles using electroactive polymers (EAP): capabilities, challenges and potential," 2005.
- [29] Z. Chen, S. Shatara, and X. Tan, "Modeling of biomimetic robotic fish propelled by an ionic polymer–metal composite caudal fin," *IEEE/ASME transactions on mechatronics*, vol. 15, no. 3, pp. 448-459, 2010.

- [30] X. Tan et al., "An autonomous robotic fish for mobile sensing," in 2006 IEEE/RSJ International Conference on Intelligent Robots and Systems, 2006, pp. 5424-5429: IEEE.
- [31] R. Jain, U. Patkar, and S. Majumdar, "Micro gripper for micromanipulation using IPMCs (ionic polymer metal composites)," *Journal of Scientific and Industrial Research*, vol. 68, no. 1, p. 23, 2009.
- [32] Y. Nakabo, T. Mukai, and 4, p. 045014, 2011.
- [36] X. Crispin et al., "The origin of the high conductivity of poly (3, 4-ethylenedioxythiophene)-poly (styrenesulfonate)(PEDOT-PSS) plastic electrodes," *Chemistry of Materials*, vol. 18, no. 18, pp. 4354-4360, 2006.
- [37] G. Di Pasquale, S. Graziani, and E. Umana, "From IPMC Transducers to All-Organic Transducers," in *Sensors*: Springer, 2014, pp. 251-254.
- [38] H. Okuzaki, S. Takagi, F. Hishiki, and R. Tanigawa, "Ionic liquid/polyurethane/PEDOT: PSS composites for electro-active polymer actuators," *Sensors and Actuators B: Chemical*, vol. 194, pp. 59-63, 2014.
- [39] S. Graziani, E. Umana, M. Xibilia, and V. De Luca, "Multi-input identification of IP2C actuators," in 2013 IEEE International Instrumentation and Measurement Technology Conference (I2MTC), 2013, pp. 1147-1151: IEEE.
- [40] S. Graziani, E. Umana, and M. Xibilia, "Identification and modeling of polymeric actuators: a comparison," in *Control & Automation (MED)*, 2012 20th Mediterranean Conference on, 2012, pp. 216-221: IEEE.
- [41] L. Fortuna, S. Graziani, M. La Rosa, D. Nicolosi, G. Sicurella, and E. Umana, "Modelling and design of all-organic electromechanic transducers," *The European Physical Journal Applied Physics*, vol. 46, no. 1, p. 12513, 2009.
- [42] L. Cavallini and P. Di Giamberardino, "Validation of IP 2 C devices as touch sensors," in *Control & Automation (MED)*, 2012 20th Mediterranean Conference on, 2012, pp. 48-53: IEEE.
- [43] S. Graziani, E. Umana, G. Di Pasquale, M. La Rosa, and G. Sicurella, "IP 2 C sensor modeling," in *Instrumentation and Measurement Technology Conference (I2MTC)*, 2012 IEEE International, 2012, pp. 1299-1302: IEEE.
- [44] A. Zolfagharian, A. Z. Kouzani, S. Y. Khoo, A. A. A. Moghadam, I. Gibson, and A. Kaynak, "Evolution of 3D printed soft actuators," *Sensors and Actuators A: Physical*, vol. 250, pp. 258-272, 2016.
- [45] F. Momeni, X. Liu, and J. Ni, "A review of 4D printing," *Materials & Design*, vol. 122, pp. 42-79, 2017.

- [46] T.-G. Noh, Y. Tak, J.-D. Nam, and H. Choi, "Electrochemical characterization of polymer actuator with large interfacial area," *Electrochimica Acta*, vol. 47, no. 13, pp. 2341-2346, 2002.
- [47] S. Liu et al., "Influence of imidazolium - based ionic liquids on the performance of ionic polymer conductor network composite actuators," *Polymer International*, vol. 59, no. 3, pp. 321-328, 2010.
- [48] W. Hong, A. Almomani, and R. Montazami, "Electrochemical and morphological studies of ionic polymer metal composites as stress sensors," *Measurement*, vol. 95, pp. 128-134, 2017.
- [49] E. Smela, "Conjugated polymer actuators for biomedical applications," *Advanced materials*, vol. 15, no. 6, pp. 481-494, 2003.
- [50] J. T. Edward, "Molecular volumes and the Stokes-Einstein equation," *J. chem. Educ*, vol. 47, no. 4, p. 261, 1970.

5.7. Supporting information for: Soft Ionic Electroactive Actuators with Tunable Non-Linear Angular Deformation

5.7.1. Morphological and mechanical characterizations.

Figures S1a - S1c show a wedge-shaped thickness profile of the casted PEDOT:PSS layer. Similar to a trapezoid, the highest concentration is in the center, and gradually tapers off along the edge, due to the imperfect fabrication process of the simple drop-casting technique.

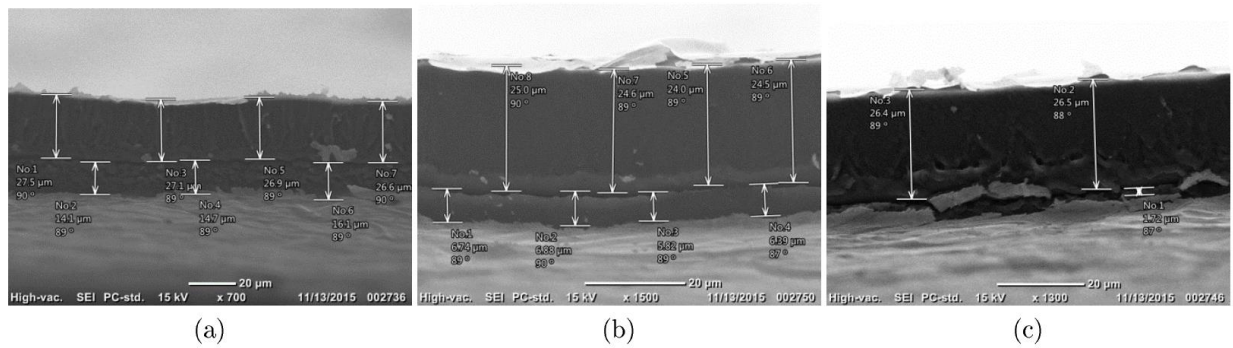


Figure S1: SEM images of specimen Nafion/1s-PEDOT:PSS/Au, from middle point to edge ((a) - (c)) of PEDOT:PSS layer.

For the bilayer laminate with much larger length respect to its width and thickness, the elastic modulus of each layer can be deduced as described by Liu *et al.* previously [S1]. Figure S2 illustrates a bilayer laminate with the length much larger than the other dimensions. The elastic modulus of the entire structure Y^e is dependent on the elastic modulus of each layer Y^a and Y^b as:

$$Y^e = aY^a + bY^b \quad (1)$$

where a and b are the volume fractions of the corresponding layer in the laminate structure [S1].

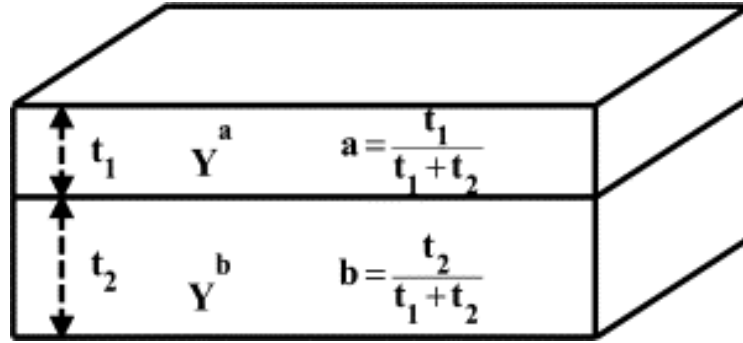


Figure S 2: Schematic of a bilayer laminate for the characterization of the elastic modulus of individual layer [S1].

The thickness of the each layer is read from the SEM images; an average value from the middle point to the edge of the PEDOT:PSS layer was taken for the average thickness. Three tensile tests were conducted to take the average value. The elastic modulus of each component measured, deduced or read from other literatures is listed in Table S1, with the corresponding Poisson's ratio listed in the next column.

Table S 1: The thickness of each layer in IEAP actuator and its physical properties [S2-S5].

Sample	Layer	Thickness (μm)	Elastic Modulus (MPa)	Poisson's Ratio
Nafion/1s-PEDOT:PSS	overall	40.2	20.7	
	Nafion	28.6	27.3	0.487 ^{S2,S3}
	PEDOT:PSS	11.6	4.3	0.33 ^{S4}
Nafion/1s-PEDOT:PSS/Au	gold leaf	0.05	20,000 ^{S1}	0.42 ^{S5}

5.7.2. Simulation of electromechanical response by FEM

FEM is performed to model the electromechanical response of IEAP actuators with different patterns. The mechanical deformation is modeled by ABAQUS finite element code. Due to the pretty small width of the IEAP actuator (1 mm), the normal stress and the shear stresses directed perpendicular to the plane in which the bending occurs are assumed to be zero. As a result, the 3-D configuration of IEAP actuator can be reasonably approximated as a 2-D plane stress

configuration in the preprocessing module, with a 4-node bilinear plane stress quadrilateral (CPS4R) element for the analysis. Moreover, SEM images reveal a non-uniform distribution of PEDOT:PSS layer, whose highest concentration is in the center, and gradually tapers off along the edge. A trapezoid-like geometry is used to represent the PEDOT:PSS pattern. Material's property and geometry of each main component are read from SEM images and Table S1. Tie constraint is employed to model the surface contact with gold electrode as master surface and Nafion with PEDOT:PSS pattern as slave surface, with the assumption that no relative displacement happened due to the hot-pressed bonding. The boundary condition of ENCASTRE ($U1 = U2 = U3 = UR1 = UR2 = UR3 = 0$) is adopted at one end of the model to represent the mechanically fixed end of the actuator.

The actuation response of IEAP actuators with ions from EMI-Tf is caused by the accumulation and depletion of excess charges at the electrodes under an applied voltage, which is equivalent to a thermal bimorph in mechanism. Nafion membrane is divided into four layers along the thickness evenly. The layer connected to cathode and anode are referred to as Nafion/cat and Nafion/ani, respectively. These two layers are used to simulate the expansion and contraction due to ions accumulation and depletion at different electrodes. The other two layers located in the middle are named by Nafion/neu, to simulate the ions depletion during the actuation process. A consistent isotropic thermal coefficient α_L is applied to each main component, and temperature field is used to control the deformation of each layer. In ABAQUS the definition of the isotropic thermal coefficient α_L is the ratio of change in length (ΔL) to the total starting length (L) and change in temperature (ΔT), with the expression as $\Delta L/L = \alpha_L \times \Delta T$. The change in area of the 2D plane cross-section due to thermal expansion is $\Delta A = hl \times (1 + \alpha_L \times \Delta T)^2 - hl \approx 2hl.\alpha_L \times \Delta T$ if we exclude the higher orders due to the pretty small value of ΔL . As a result, the change in area (ΔA)

caused by thermal expansion/contraction is linear to the change in temperature (ΔT). Same approximation is also applicable to the change in volume (ΔV).

Define N as the total amount of cations drifted in the cationic response of actuation. Following paragraphs introduce the detailed procedures and their theoretical support.

1. Actuator 1S

- Cationic response: N cations are drifted from Nafion/neu and Nafion/ani layers homogeneously, and accumulated in PEDOT:PSS layer (attached to cathode) and Nafion/cat layer with volume ratio of 2:1.
- Anionic response: N anions/anionic clusters are drifted and stored in Nafion/ani layer from Nafion/cat and Nafion/neu layers homogeneously. The cations stored in PEDOT:PSS layer (attached to cathode) in previous cationic response won't move out during the anionic response.

The procedures adopted in actuator 1S are based on the observation of a non-ignorable expansion from PEDOT:PSS layer when it only exists on the convex side of Nafion. Meanwhile, IEAP actuator with bare Nafion also displays a noticeable bending, indicating ions accumulation at the outer layers of Nafion and depletion at the inner layers at the same time[S1,S6]. In addition, PEDOT:PSS layer does not contain any ions at the very beginning, thus it won't show any contraction during the simulation.

2. Actuator 2SA

- Cationic response: N cations are drifted from Nafion/neu and Nafion/ani layers homogeneously, and accumulated in PEDOT:PSS layer (attached to cathode) and Nafion/cat layer with volume ratio of 2:1.

- Anionic response: N anions/anionic clusters are drifted from Nafion/neu and Nafion/cat homogeneously. Then, (i) part of the anions/anionic clusters are stored in PEDOT:PSS layer (attached to anode) with the same volume density of the cations in PEDOT:PSS layer (attached to cathode) in the previous cationic response, and (ii) remaining anions/anionic clusters are accumulated in Nafion/ani layer.

The procedures adopted in the simulation of actuator 2SA are based on the same reason with part 1.

3. Actuator 2SS

Actuator 2SS differs remarkably from actuator 1S and 2SA. There are five segments along the length, with 3 segments made of Nafion/2s-PEDOT:PSS and 2 segments made of BNafion. Due to their significant difference in electrochemical and electromechanical responses, a segment-wise procedure is employed as below:

- Cationic response: in each segment made of BNafion, n ($= N/5$) cations are drifted from Nafion/neu and Nafion/ani layers homogeneously, and accumulated in Nafion/cat layer. In each segment made of Nafion/2s-PEDOT:PSS, $n/8$ cations are drifted from Nafion/neu and Nafion/ani layers homogeneously, then accumulated in PEDOT:PSS layer and Nafion/cat layer with volume ratio of 2:1.
- Anionic response: in each segment of BNafion, n anions/anionic clusters are drifted and stored in Nafion/ani layer from Nafion/cat and Nafion/neu layers homogeneously. In each segment made of Nafion/2s-PEDOT:PSS, $n=8$ anions/anionic clusters are drifted from Nafion/neu and Nafion/cat homogeneously.

Then, (i) part of the anions/anionic clusters are drifted and stored in PEDOT:PSS layer(attached to anode) with the same volume density of the cations stored in PEDOT:PSS layer (attached to cathode) in the previous cationic response, and (ii) remaining anions/anionic clusters are accumulated in Nafion/ani layer.

The procedures adopted in actuator 2SS are based on the observation from the equivalent circuit modeling. Specimen Nafion/2s-PEDOT:PSS reveals a much smaller EDL capacitance (0.12 μF) at the electrode surface when compared to the specimen BNafion (2.86 μF). As a result, BNafion and Nafion/2s-PEDOT:PSS are treated differently for a best match of the experimental results.

From the equivalent circuit modeling, the ratio of EDL capacitance of specimen Nafion/2s-PEDOT:PSS and specimen BNafion is $0.12/2.86 = 0.04$, while from the simulation procedures above, this ratio becomes $1/8 = 0.125$, in order to fully match the experimental results. It suggests the complexity to quantify the ions/ion clusters motion during the actuation. However, all the procedures made above is consistent with our previous electrochemical and electromechanical responses, and fully respect to the conclusions in earlier works [S1,S6-S8].

5.7.3. Supporting Information References

- (S1) Liu, S.; Montazami, R.; Liu, Y.; Jain, V.; Lin, M.; Zhou, X.; Heflin, J. R.; Zhang, Q. "Influence of the conductor network composites on the electromechanical performance of ionic polymer conductor network composite actuators". *Sensors and Actuators A:Physical* 2010, 157, 267_275.
- (S2) Wei, H.-C.; Su, G.-D. J. "Design and fabrication of a large-stroke deformable mirror using a gear-shape ionic-conductive polymer metal composite". *Sensors* 2012, 12, 11100_11112.
- (S3) Li, J. Y.; Nemat-Nasser, S. "Micromechanical analysis of ionic clustering in Nafion per-fluorinated membrane". *Mechanics of materials* 2000, 32, 303_314.

- (S4) Greco, F.; Zucca, A.; Taccola, S.; Menciassi, A.; Fujie, T.; Haniuda, H.; Takeoka, S.; Dario, P.; Mattoli, V. "Ultra-thin conductive free-standing PEDOT/PSS nanofilms". *Soft Matter* 2011, 7, 10642_10650.
- (S5) http://www.engineeringtoolbox.com/metals-poissons-ratio-d_1268.html .
- (S6) Montazami, R.; Liu, S.; Liu, Y.; Wang, D.; Zhang, Q.; Heflin, J. R. "Thickness dependence of curvature, strain, and response time in ionic electroactive polymer actuators fabricated via layer-by-layer assembly". *Journal of Applied Physics* 2011, 109, 104301.
- (S7) Liu, Y.; Liu, S.; Lin, J.; Wang, D.; Jain, V.; Montazami, R.; Heflin, J. R.; Li, J.; Madsen, L.; Zhang, Q. "Ion transport and storage of ionic liquids in ionic polymer conductor network composites". *Applied Physics Letters* 2010, 96, 223503.
- (S8) Liu, Y.; Zhao, R.; Gha_ari, M.; Lin, J.; Liu, S.; Cebeci, H.; de Villoria, R. G.; Montazami, R.; Wang, D.; Wardle, B. L. "Equivalent circuit modeling of ionomer and ionic polymer conductive network composite actuators containing ionic liquids". *Sensors and Actuators A: Physical* 2012, 181, 70_76.

CHAPTER 6. INFLUENCE OF TEMPERATURE ON THE ELECTROMECHANICAL PROPERTIES OF IONIC LIQUID-DOPED IONIC POLYMER-METAL COMPOSITE ACTUATORS

Published in the journal of Polymers¹

Abdallah Almomani^{2,3}, Wangyujue Hong^{2,4}, Wei Hong^{2,3,4}, Reza Montazami^{2,4,5}

Abstract

Ionic polymer-metal composite (IPMC) actuators have considerable potential for a wide range of applications. Although IPMC actuators are widely studied for their electromechanical properties, most studies have been conducted at the ambient conditions. The electromechanical performance of IPMC actuators at higher temperature is still far from understood. In this study, the effect of temperature on the electromechanical behavior (the rate of deformation and curvature) and electrochemical behavior (current flow) of ionic liquid doped IPMC actuators are examined and reported. Both electromechanical and electrochemical studies were conducted in air at temperatures ranging from 25 °C to 90 °C. Electromechanically, the actuators showed lower cationic curvature with increasing temperature up to 70 °C and a slower rate of deformation with increasing temperature up to 50 °C. A faster rate of deformation was recorded at temperatures higher than 50 °C, with a maximum rate at 60 °C. The anionic response showed a lower rate of deformation and a higher anionic curvature with increasing temperatures up to 50 °C with an abrupt increase in the rate

¹ This is an open access journal, and the publisher "Multidisciplinary Digital Publishing Institute", allows the authors to re-use the material without obtaining permission.

² Primary researchers and authors. Graduate student, graduate student, academic advisor, and academic advisor, respectively.

³ Department of Aerospace Engineering, Iowa State University.

⁴ Department of Mechanical Engineering, Iowa State University.

⁵ Author of correspondence.

of deformation and decrease of curvature at 60 °C. In both cationic and anionic responses, actuators started to lose functionality and show unpredictable performance for temperatures greater than 60 °C, with considerable fluctuations at 70 °C. Electrochemically, the current flow across the actuators was increased gradually with increasing temperature up to 80 °C during the charging and discharging cycles. A sudden increase in current flow was recorded at 90 °C indicating a shorted circuit and actuator failure.

6.1. Introduction

Ionic polymer-metal composites (IPMCs) are polymer-based soft composites that can be designed as soft actuators and sensors. IPMC actuators have several unique properties, including low density, large bending strain, low noise, high resilience, and low operation voltage; which make their application more practical compare to many of their metal- or ceramic-based counterparts. IPMC actuators have been widely studied, experimentally, and theoretically, as artificial muscles for biomedical applications, biomimetic micro-robotics, and harsh-environment tools such as space exploration micro-grippers [1–8].

Upon fabrication, IPMCs are impregnated by optimum content [9] of ion-rich electrolyte, most often ionic liquids (ILs), as the source for mobilized ions. The operation principle of IPMC actuators is ultimately based on the accumulation of mobilized ions at the opposite electrodes in response to an externally-induced electric field. The difference between the volumes of cations and anions results in a volume imbalance and, therefore, mechanical stress, at the electrodes which, in turn, results in deformation of the IPMC structure toward the side with smaller volume. The motion of ions toward or away from each electrode is due to attractive or repulsive forces between the electrically-charged electrode and the ions, and can be reversed upon modulating the polarity of the electric field. The deformation depends on the

net difference of the volumes at the electrodes. If the drift velocity of the cations and anions are significantly different, a two-step deformation is observed in which the actuator is initially bent toward one side, then toward the other side. Conventionally, the bending caused by cations (toward the anode) is called cationic bending and denoted by positive sign when that resulted by anions (toward the cathode) is called anionic and denoted by negative sign [10,11]. This change in the direction of motion is different from back-relaxation phenomenon [12–14]. A scheme showing the principle of actuation is presented in Figure 6-1.

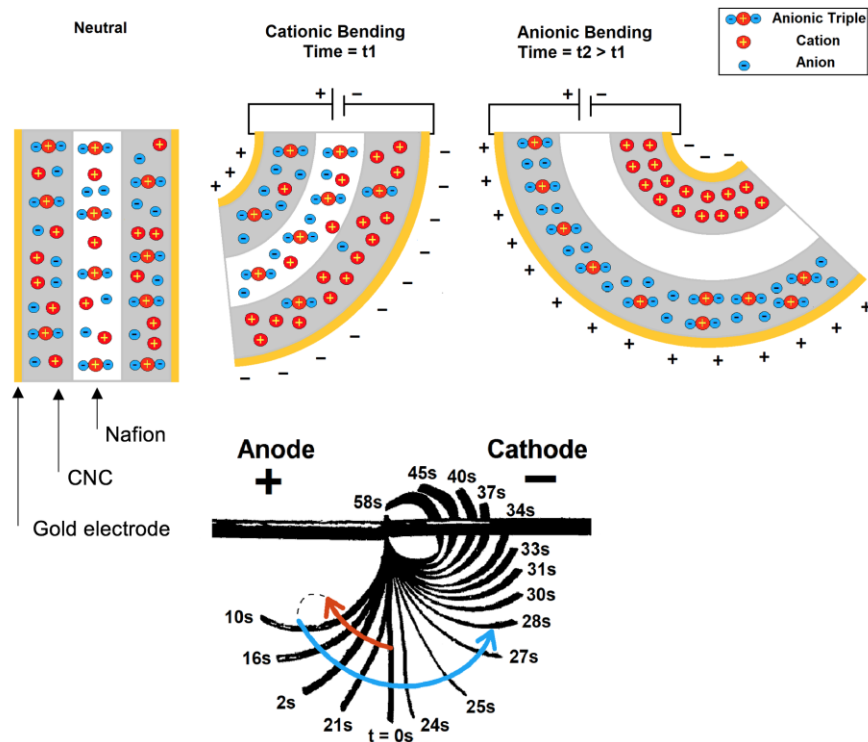


Figure 6-1: Idealistic schematic of cationic and anionic bending mechanism (top, not to scale) and overlaid sequential images of cationic (red arrow) bending followed by anionic (blue arrow) bending (bottom)

Many factors influence dynamics of ion mobility in IPMCs including mean free path of ions which is a factor of membrane thickness as well as membrane's chemical and physical

structures [11,15,16], characteristics of ions (van der Waals volume) [11], and temperature. While characteristics of the membrane and ions are intrinsic to IPMCs and fixed, temperature is considered an external factor that can be changed for the same actuator during operation. Therefore, understanding the effect of temperature on IPMC actuators is critical in the prediction of their electromechanical behavior under different environmental conditions.

Several studies have investigated the performance of IPMC actuators as a function of temperature. Shahinpoor et al. report that IPMC actuators can function at subzero temperatures, down to $-140\text{ }^{\circ}\text{C}$ [3]. On two independent studies, Brunetto et al. and Ganley et al. describe the sensing properties and modeling of the IPMCs for a range of temperatures above the ambient temperature and humidity [17,18]. Cha et al. and Farinholt et al. considered the effect of temperature on the IPMCs' impedance [19,20]. Benziger et al. [21] measured the elastic modulus of Nafion membrane at different temperatures and humidity and observed that under dry conditions, the elastic modulus of Nafion decreased gradually with increasing temperature (up to $60\text{ }^{\circ}\text{C}$), with a steep decrease at $70\text{ }^{\circ}\text{C}$. This behavior was mainly related to the structural changes of Nafion at high temperatures. Nafion consists of a large tetrafluoroethylene (Teflon) backbone with short perfluorovinyl ether side chains terminated with sulfonate (SO_3^-) end groups. In its acidic form, Nafion exists with protons (H^+) in close vicinity of its sulfonate end groups. The most widely-accepted model for the Nafion structure was presented by Hsu and Gierke in 1982 [22]. In that model, Nafion has a cluster network structure with nano-channels that allow ion transport through the membrane. The cluster-network model suggests that Nafion contains very small (few nanometers across) hollow inverted-micelle spheres connected with nanochannels and supported by the Teflon backbone cross-links. This configuration minimizes electrostatic repulsion between the ionic groups, and the cross-links

stiffen the Nafion membrane. Benziger et al. suggested that the change in mechanical properties and the steep decrease in the elastic modulus at high temperatures (>60 °C) are caused by a microstructural change in Nafion—the inverted micelles and nano-channels start to collapse due to the increase of entropy; which causes a decline in mechanical properties.

Sodaye et al. [23,24] studied the scattering parameter (S-parameter) and lifetime of dry acidic Nafion as a function of temperature and found that a larger S-value is related to a larger free volume within the Nafion structure. It was reported that, generally, the free volume increases noticeably with increasing temperature, indicating an expansion of the spherical clusters and nano-channels inside Nafion up to a threshold temperature, ~ 63 °C, where the free volume decreases. This decline in free volume at higher temperature is in agreement with findings reported by Benziger and colleagues, and can imply the collapse of some of the inner structures of Nafion. Such physical changes to the Nafion structure due to temperature variations, and other environmental factors such as humidity and moisture content are expected to influence its ionic and ion transport properties. Moreover, Nafion was reported to have a broad glass transition temperature within approximately 55 – 130 °C [25–27]. At the glass transition temperature, Nafion becomes more rubbery and that may also affect the structure of the membrane and the transport properties of the nano-channels in the Nafion structure and agrees with the results of Sodaye et al. and Benziger et al.

In one study, Hou et al. [28] explored the interionic associations among IL constituent ions with respect to the hydration level and reported that the electrostatic forces may result in the formation of double, triple, and quadruple ion clusters of anions and cations. When the Nafion was dry, triple anionic clusters prevailed due to the strong electrostatic forces between

the charged species. Increasing water content reduced the electrostatic forces and resulted in ionic disassociation.

In this study, rate and magnitude of electromechanical response of IL-doped IPMC actuators are characterized as a function of temperature. In particular, cationic and anionic motions are independently investigated, and the outcomes are integrated into a unifying model and conclusion. The dynamics of ion-cluster formation and deformation are studied utilizing electromechanical and electrochemical behavior of IPMCs in a wide range of temperatures.

6.2. Materials and Methods

6.2.1. Materials

A Nafion (sulfonated tetrafluoroethylene-based fluoropolymer-copolymer) ionomeric membrane of 25 μm thickness (NR-211, IonPower, New castle, DE, USA) was used as received. Poly(allylamine hydrochloride) (PAH) (Sigma-Aldrich, St. Louis, MO, USA) was procured at a concentration of 10 mM and used as polycation. Functionalized gold nanoparticles (AuNPs) of $\sim 3\text{nm}$ diameter, Zeta potential of ca. -40 mV , and a concentration of 20 ppm (Purest Colloids Inc, Westampton, NJ, USA) were used as anionic materials. 1-ethyl-3-methylimidazolium trifluoromethanesulfonate (EMI-Tf (molecular formula, $\text{C}_7\text{H}_{11}\text{F}_3\text{N}_2\text{O}_3\text{S}$)) (Sigma-Aldrich, St. Louis, MO, USA) was used as received. Twenty-four carat gold leaf electrodes of 50 nm thickness (L.A. Gold Leaf Wholesaler Inc., Azusa, CA, USA) were used as the outer electrodes.

6.2.2. Sample Preparation

To fabricate the actuators, the layer-by-layer (LbL) technique [15,29] was used to deposit 20 bilayers of PAH/AuNPs and form the conductive network composites (CNCs) on both surfaces of Nafion films. The Nafion film was mounted on a glass frame using double-

sided tape and an automated robot (StratoSequence 6, NanoStrata Inc., Tallahassee, FL, USA) programmed for five-minute immersions in each ionic solution followed by three one-minute rinses in DI water was used to fabricate the bilayers. After forming the CNCs, the membranes were dried in air, and cut from the glass frame to obtain free-standing IPMCs. The IPMCs were then soaked for about six hours in EMI-TF ionic liquid at 80 °C, to obtain ~30% ionic liquid intake. Ionic liquid intake (IL%) was measured as a percent ratio of weight increase to the initial weight of the membrane, using Equation (6-1):

$$IL(\%) = \frac{W_f - W_i}{W_f} \times 100\% \quad (6-1)$$

where W_i and W_f are the membrane's weights before and after IL intake, respectively.

Upon impregnation with IL, gold leaf electrodes were hot-pressed onto both sides of the membrane, at 95 °C and under ~100 KN of force, for 40 s using a 25 T hydraulic hot press (MTI Corporation, Richmond, CA, USA) [10,30]. The actuators were then cut into $1 \times 10 \text{ mm}^2$ samples for testing.

6.2.3. Electromechanical characterization

Electromechanical characterizations were conducted in an in-house fabricated temperature controlled chamber where a type T (-CO +CP) (Omega Engineering Inc., Norwalk, CT, USA) thermocouple paired with a thermocouple meter (Omega DP41-TC-MDS, Omega Engineering Inc., Norwalk, CT, USA) were used to measure the temperature of the chamber. The desired temperatures were obtained by manually controlling and adjusting a resistive heater. Three different actuators from the same fabricated lot were tested at each testing temperature. Before each test, enough time was allowed to obtain a uniform and stable temperature across the chamber. Actuators were mounted with a clearance of 5 cm of the heater

on an in-house fabricated micro-probe station inside the chamber, and subjected to a +4 V step potential across the thickness using a function generator (Tektronix AFG 3022B, Tektronix Inc., Beaverton, OR, USA). All temperatures were within ± 2 °C of the desired temperature during operation. The actuators were tested at room temperature (25 °C) and temperatures from 30 °C to 70 °C by 10-degree increments. The electromechanical response was monitored and recorded at 30 frames per second using a CCD camera. Image frames were then analyzed to obtain the actuator's radius of curvature as a function of time $r(t)$. Time-dependent curvature $k(t)$, where $k(t) = r(t)^{-1}$, was then calculated and analyzed for different temperatures

6.2.4. Electrochemical characterization

A VersaSTAT-4 potentiostat (Princeton Applied Research, Oak Ridge, TN, USA) was used to apply a ± 4 V step potential and measure the current flow over 60-second intervals across a 1×1 cm² Nafion membrane with 30% ionic liquid intake at room temperature (25 °C) and temperatures from 30 °C to 90 °C by 10-degree increments. The membranes were enclosed between two copper electrodes on both sides and the current density and time were then recorded for analysis.

The same device was also used to apply a 10 mV potential at frequencies ranging from 100 kHz to 0.1 Hz and to measure the samples' electrical impedance. An equivalent RC electrical circuit with a Warburg element was previously proposed by several studies to represent the electrochemical performance across ionic liquid swollen Nafion membranes [9], from which the resistances (R_m) for membranes at different temperatures can be extracted from the Nyquist plot at high frequencies (*i.e.*, 100 kHz), where the electrochemical system exhibits almost pure resistance behavior. The ionic conductivity was then calculated for the samples at different temperatures using Equation (6-2):

$$\sigma = \frac{t}{R_m A} \quad (6-2)$$

where σ is the ionic conductivity, t is the thickness of the membrane, R_m is the resistance deduced from the Nyquist plots at high frequencies, and A is the surface area of the membrane [31]. After that, the Arrhenius equation in its linear form Equation (6-3) was used to fit the experimental at different temperatures:

$$\ln(\sigma) = -\frac{E_a}{R} \left(\frac{1}{T}\right) + \ln(\sigma_0) \quad (6-3)$$

where σ is the ionic conductivity, σ_0 is the maximum ionic conductivity, E_a is the activation energy, R is the gas constant, and T is the temperature.

6.3. Results

6.3.1. Electromechanical Response

6.3.1.1. Cationic Curvature.

The cationic curvature as a function of time at 25 °C and for temperatures from 30 °C to 70 °C by 10-degree increments is shown in Figure 6-2. In this figure, the curvature is considered to be cationic as cations are dominating the bending process (*i.e.*, the bending is toward the anode, as seen in Figure 6-1). After applying a step voltage, the cationic curvature increased to a maximum value and then decreased to zero as time progressed. The decrease in curvature resulted from the accumulation of bigger anionic clusters at the anode [10]. Both maximum cationic curvature and the cationic actuation time (the total time for the actuator to return to the neutral position) were affected as the system temperature increased, as shown in Figure 6-2. The maximum cationic curvature decreased for each temperature increment from 25 °C to 70 °C, as shown in Figure 6-3a. Meanwhile, the cationic actuation time (from the

beginning of the motion back to the idle position) first increased to a maximum at 50 °C, with a sudden decrease at 60 °C, as shown in Figure 6-3b. No detectable bending occurred at temperatures higher than 70 °C.

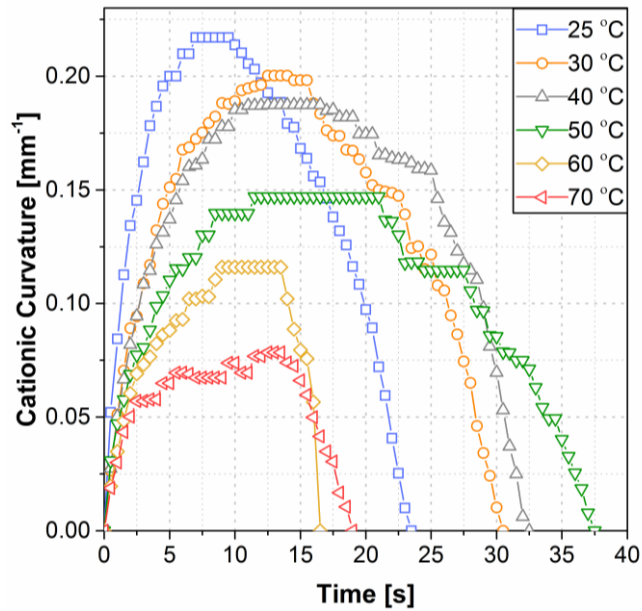


Figure 6-2: The cationic curvature at different temperatures.

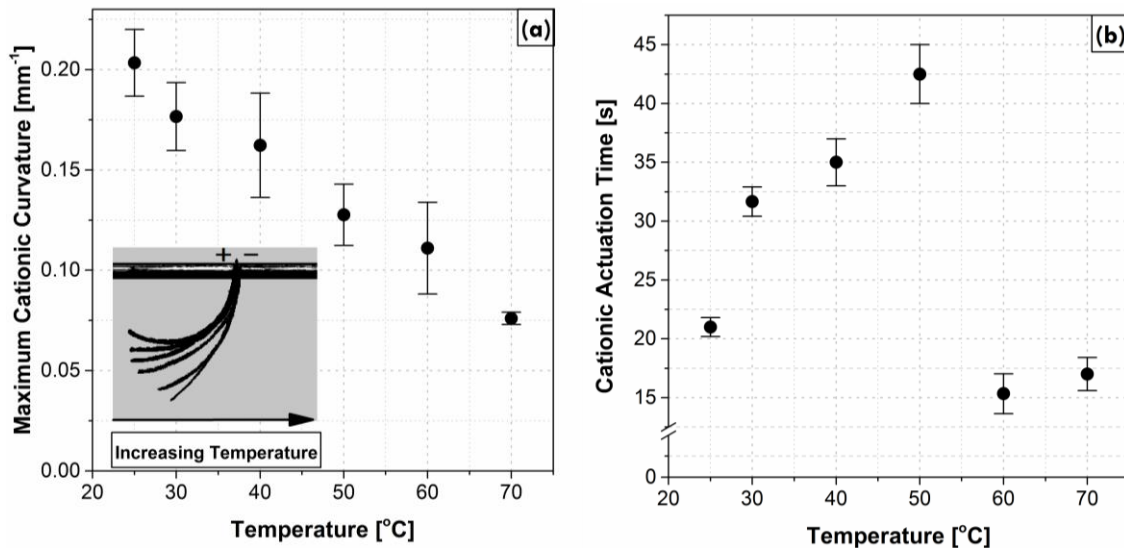


Figure 6-3. (a) The maximum cationic curvature, (b) The cationic actuation time, at different temperatures.

6.3.1.2. Anionic Curvature.

Anionic curvature increased to a steady-state maximum value at each tested temperature from 25 °C through 70 °C. The anionic curvature as a function of time exhibited smooth deformation for temperatures ranging from 25 °C to 50 °C (see Figure 6-4 for a representative example). However, the actuator deformation fluctuated noticeably past 50 °C and up to 70 °C. Anionic curvatures for 25 °C (smooth) and 70 °C (fluctuating) are shown in Figure 6-4. The two curves were shifted to the zero time to be compared side-by-side, see Figure 6-6 for the full actuation cycle data. The maximum anionic curvatures for actuators tested at 25 °C and for temperatures from 30 °C to 70 °C by an increment of 10 °C are shown in Figure 6-5. The maximum anionic curvature increased to a peak value as the temperature increased up to 50 °C and dropped abruptly after that. At temperatures above 70 °C, actuators only showed unpredictable oscillation at the idle position with no clear cationic or anionic curvatures.

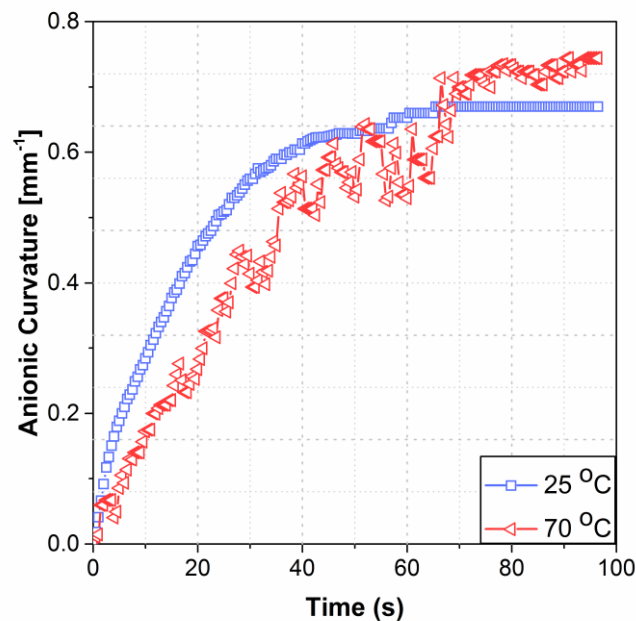


Figure 6-4. The anionic curvature at 25 °C and 70 °C, both shifted to time = zero for comparison.

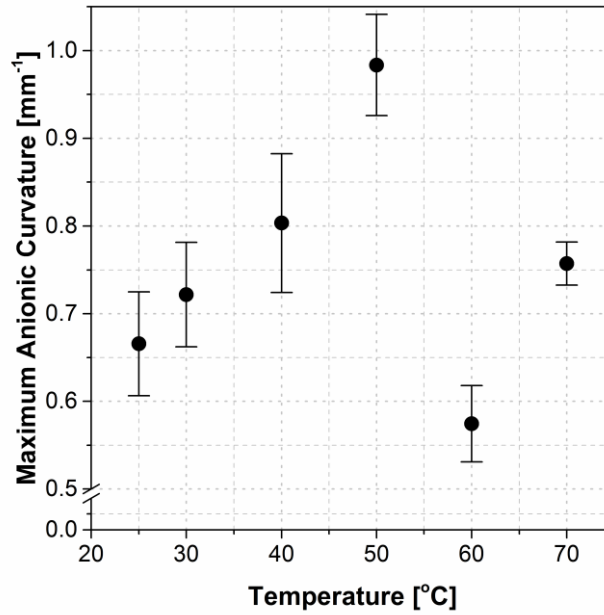


Figure 6-5: The maximum anionic curvature at different temperatures.

6.3.1.3. The time constant for anionic and cationic curvatures.

A two-part first-order system model was used to fit the rate of deformation data for both cationic and anionic motions. In this model, both cations and anions are mobilized once the voltage is applied. Cationic and anionic curvatures were considered to have positive and negative values, respectively, to distinguish their opposing directions of motion. The model was produced using Equation (6-4) with a negative sign for the anionic motion [15,32]:

$$k(t) = k_{cat} \left(1 - \exp\left(\frac{-t}{\tau_{cat}}\right) \right) - k_{an} \left(1 - \exp\left(\frac{-t}{\tau_{an}}\right) \right) \quad (6-4)$$

where $k(t)$ is the net curvature as a function of time, k_{cat} and k_{an} are the cationic and anionic coefficients denoting the maximum value of each, t is the time, and τ_{cat} and τ_{an} are the cationic and anionic time constants, respectively. Experimental data fitted with analytical curves for 25 °C and 70 °C are shown in Figure 6-6.

The time constants at different temperatures are shown in Figure 6-7. The actuators had a lower rate of deformation (both τ_{cat} and τ_{an} increased) with increasing temperatures up to 50 °C. A sudden drop in τ_{cat} and τ_{an} values were observed at 60 °C. At 70 °C the rate of deformation was small, yet associated with considerable fluctuations in motion.

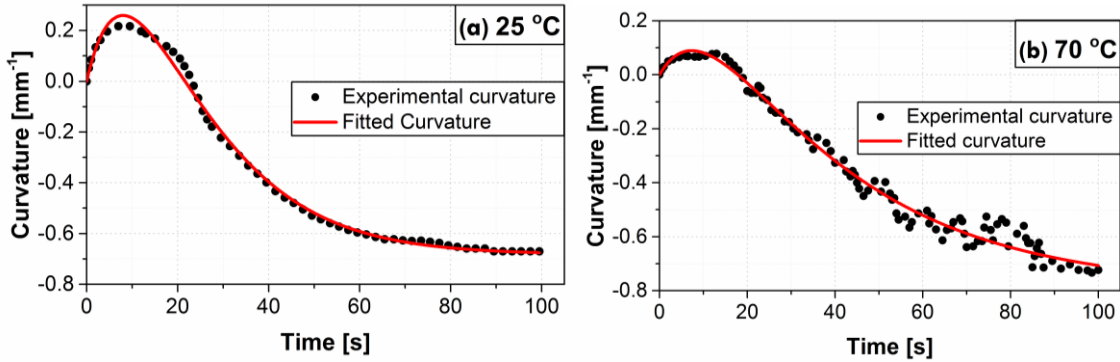


Figure 6-6 Experimental and fitted time dependent curvature at (a) at 25 °C, and (b) 70 °C.

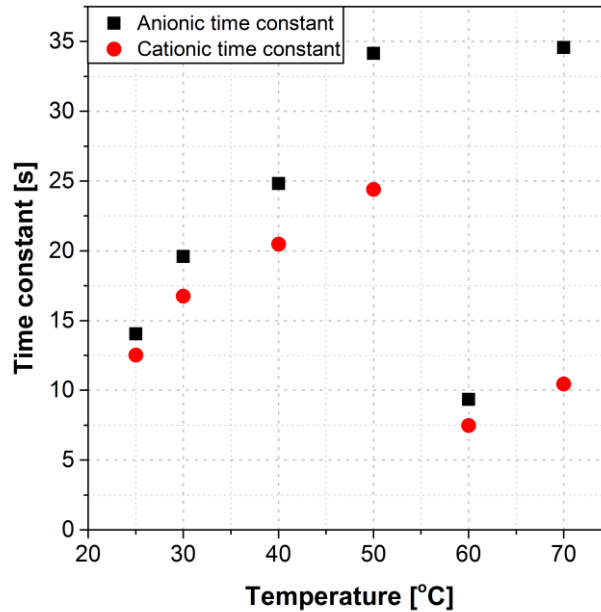


Figure 6-7. The time constant of cationic and anionic curvatures at different temperatures.

6.3.2. Electrochemical characterization

Presented in Figure 6-8 is the time dependent current flow measured at different temperatures. Despite the lack of electromechanical response at temperatures higher than 70 °C, electrochemical behavior of the actuators followed a constant pattern up to 80 °C, and exhibited a jump along with a relatively flat (time independent) high current flow at 90 °C indicating physical and/or chemical degradation of the actuator. The system then completely failed after about 60 seconds at 90 °C when the current flow dropped to zero.

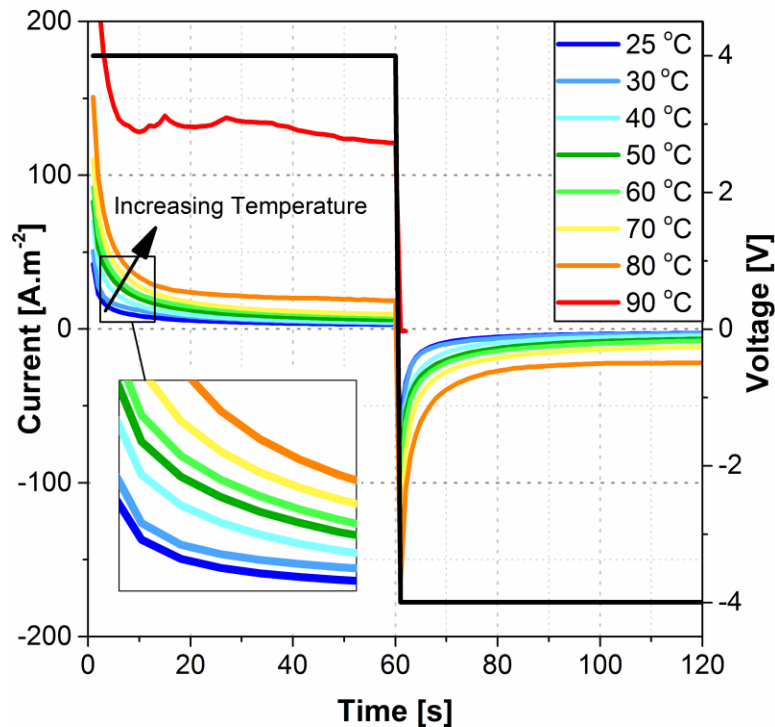


Figure 6-8. The current flow after applying 4 V across a $1 \times 1 \text{ cm}^2$ Nafion membrane with 30% EMI-TF ionic liquid at different temperatures. The leftmost gray line is the current flow at room temperature; each colored line above it shows an increase in temperature from 30 °C to 90 °C.

Figure 6-9 shows the ionic conductivity across the membranes calculated at different temperatures. The results showed an enhanced conductivity at higher temperatures. Moreover, a different conductivity behavior was noticed for the temperature range between 25 °C and 50

°C than the temperature range between 55 °C and 70 °C after fitting the conductivity data with the Arrhenius equation (Equation (6-3)).

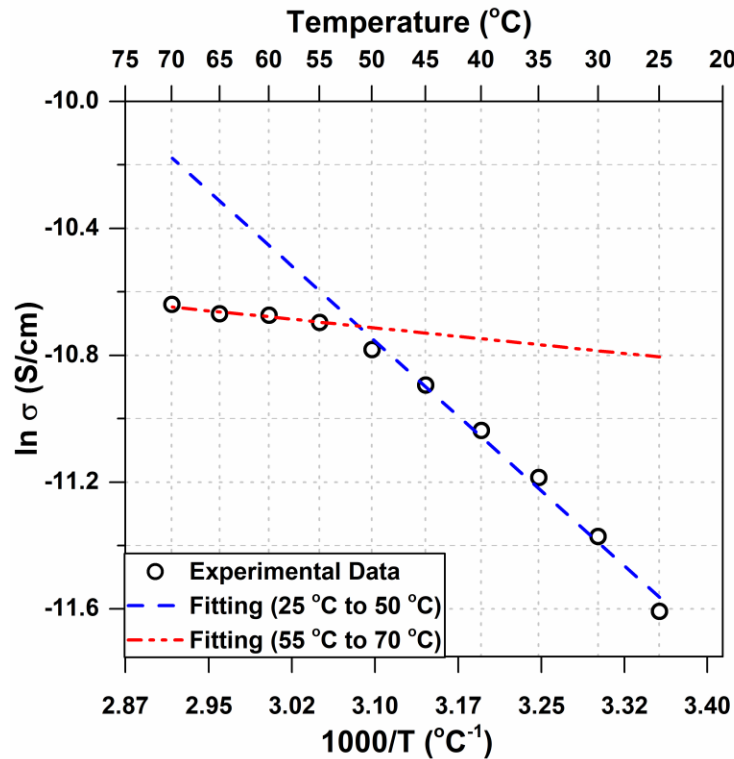


Figure 6-9: Arrhenius conductivity fitting for temperatures from 25 °C to 70 °C.

6.4. Discussion

Experimental data confirmed two distinct deformation patterns for cationic and anionic curvatures, suggesting that each is differently affected by temperature. The magnitude of the cationic curvature exhibited an inversely proportional dependence on temperature as the temperature was increased from 25 °C to 70 °C (Figure 6-3a); while this correlation for anionic curvature was a direct correlation up to 50 °C followed by a sharp drop at 60 °C and increase at 70 °C (Figure 6-5). The irregular behavior of the anionic curvature was also observed for time constants of both cationic and anionic curvatures (Figure 6-7).

It is speculated that the irregular behavior of the IPMCs at higher temperatures is due to two main factors: 1) changes in Nafion's nano-structure, and 2) changes in IL composition and transportation through Nafion.

Changes in Nafion's nano-structure has been subject to a number of studies, as described in the introduction section, and while it partially explains temperature dependent behavior of IPMC actuators, it fails to explain the distinct behaviors of cationic and anionic curvatures. It is speculated that changes in IL composition and transportation at different temperatures have a strong contributing factor to such distinct behaviors and can be used to explain the temperature-dependent behavior of IPMC actuators.

Deformation of IPMC actuators is a result of ion mobility, in case of this study EMI^+ and Tf^- . Previous studies have indicated presence of Tf^- - EMI^+ - Tf^- anionic clusters in EMI-Tf ionic liquid; which are considerably more massive than EMI^+ cations. Increasing the number of anionic clusters will enhance anionic curvature, considering the more significant difference in van der Waals volume of the cluster compared to that of EMI^+ , and the fact that for each cluster one cation is contributing to anionic curvature rather than, naturally, cationic curvature. However, the drifting velocity of such ionic clusters is lower due to the increased mass for the net one elementary charge. The drifting velocity V_d is reversibly related to the ion mass as shown in Equation (6-5) [33]:

$$V_d = 2\sqrt{\frac{KT}{3m}} \quad (6-5)$$

where K is the Boltzmann constant, T is absolute temperature, and m is the mass of the ion.

The magnitude of the maximum cationic curvature (Figure 6-3a), and the cationic and anionic rates of deformation (Figure 6-7), are both consequent to the net difference in magnitudes of cations and anions (including anionic clusters) drifting velocities that are vectors pointing at opposite directions or the amount of the moving ions. A larger net difference in velocities or a lower amount of moving anions/anionic clusters results in a higher maximum cationic curvature, as well as higher cationic and ionic rates of deformation, and vice versa. The magnitude of the maximum anionic curvature (Figure 6-5), on the other hand, solely depends on the net volume difference of the accumulated ions at the two electrodes which, in turn, depends on the abundance of anionic clusters accumulated at the anode.

The maximum cationic curvature decreases with increasing temperature from 25 °C through 70 °C. This indicates a lower net difference between the cations and anions/anionic clusters drifting velocities or a higher number of anions/anionic clusters are being drifted and canceling the cationic motion. Figure 6-7 shows higher time constants for both cationic and anionic motions with increasing temperature. The higher time constant may conclude a slower drifting velocity of the charged species and lower current density. Instead, the current flow across the Nafion membranes increases with increasing temperature as shown in Figure 6-8. As cations are smaller in size and less massive than the anions/anionic clusters, they assumed to move freely at all temperatures. Thus, the number of moving cations is assumed to be the same or differ slightly at elevated temperatures. On the other hand, some of the larger and more massive anionic clusters will be trapped inside the Nafion's nano-channels at low temperatures. Increasing temperature will expand Nafion's nano-channels and increase the kinetic energy of the clusters, which increases the number of the moving anions/anionic clusters with a lower drifting velocity will explain the lower maximum cationic curvature and lower rate of

deformations with increasing temperature up to 50 °C. To illustrate this, the current flow across the membrane can be modeled by Equation (6-6):

$$I \propto -C_0 \exp\left(\frac{-E_a}{RT}\right) \left[1 - \exp\left(\frac{-t}{\tau(T)}\right)\right] + C_1 \quad (6-6)$$

where I is the current flow across the membrane, C_0 is a constant related to the concentration of the IL, E_a is the activation energy, R is the gas constant, T is the temperature, t is time, $\tau(T)$ is the time constant as a function of temperature, and C_1 is a constant to represent the steady state current flow. The equation shows that a higher current could be achieved with increasing temperature for the same initial IL concentration even for a higher time constant. Moreover, protons (H^+) have a significant effect on the current flow. Protons are significantly smaller compared to EMI^+ and Tf^- ions, making it easier for them to drift across the Nafion membrane. Due to their size, increasing the protons' kinetic energy will result in a greater current flow. This is true even at higher temperatures that break the inner nano-structure of Nafion. At 90 °C, the high current flow indicates a short circuit and actuator failure.

Anionic curvature increases with increasing temperature up to 50 °C followed by a sudden decrease in curvature which is concurrent with an increase in the rate of deformation (decreasing time constant) occurred at 60 °C. The increase in anionic curvature can be explained by the larger number of anionic clusters accumulated at the anode due to the increased temperature. In addition to the ions' greater kinetic energy, ion transport through Nafion is also expected to be facilitated by the expansion of the nano-structure of Nafion due to the increasing temperatures up to 50 °C, before a physical change in both the IL composition and the Nafion nano-structure at temperatures above 50 °C occur.

At 60 °C, there was an increase in both cationic and anionic rates of deformations and a steep drop in the anionic curvature. If ions become smaller (ion clusters dispersion into single ions), lower curvature and a higher rate of deformation result. It is speculated that at high temperatures (>50 °C), the kinetic energy of some the ions forming the ion clusters will be higher than the potential energy of the clusters. This will cause a dispersal of some of the clusters into single ions and increase the entropy of the system. Thus, at high temperature, ionic dispersal will result in a lower number of the anionic clusters to exist and decrease the net anionic curvature. The high energy and higher number of small single ions will result in a higher ion transport rate and a higher rate of deformation (time constant decreases). Ionic dispersal hypothesis can be supported by the conductivity results at different temperatures shown in Figure 6-9. The slope of the linear fitted line for different temperature ranges represents the activation energy needed for ion transportation. The activation energy is lower for temperatures >50 °C which concludes a smaller ionic species. Smaller ionic species shall result in an even higher conductivity (the conductivity at >50 °C should lie above the single dashed blue line in Figure 6-9). Instead, the conductivity at >50 °C is lower than the previous range trend. This might be due to the change and the breakage of some nano-channels in Nafion structure. Upon dispersion of ion clusters, both cationic and anionic curvatures again follow the same trend as that observed for lower temperatures, *i.e.*, the decreasing rate of deformation as the temperature increases to 70 °C, with a steep decrease for the anionic curvature (Figure 6-7). Benziger et al. demonstrated that, in dry conditions, the elastic modulus shows a steep decrease at temperatures between 70 °C and 100 °C [21]. The sudden decrease in modulus is related to the increase of entropy at high temperatures. This extra entropy randomly disperses the ionic groups in Nafion and breaks some of the inner structures and nano-channels. Breaking

these structures also affects the ions' transport across the membrane. Majsztrik et al. reported the same results in their study about the effects of temperature and hydration on tensile creep viscoelastic response of Nafion [34]. Thus, breaking of some of the inner channels and clusters at higher temperatures can affect and limit the ion transport, and explain both the decrease in the rate of deformation and the decrease in the actuation curvature. The cluster breakage has more of an effect on the anionic rate of deformation, which results from the slower movement of the larger anionic clusters. That explains the greater difference in the rate of deformation at 70 °C (Figure 6-7).

6.5. Conclusion

In summary, this work investigates the effect of temperature on the electromechanical performance of IL-doped IPMC actuators. Cationic and anionic curvatures exhibited two distinct behaviors as a function of increasing temperature. Considering changes in the kinetic energy of ions as a function of temperature, ion mobility using Arrhenius relation, and physical changes of Nafion's nano-structure, it is concluded that the complex electromechanical behaviors of IL-doped IPMC actuators at higher temperatures can be explained by changes in IL structure, *i.e.*, dispersion of ion clusters in the IL and the number of the drifted ions at higher temperatures. It is suggested that the kinetic energy of the mobilized ions is higher than the potential energy of the ionic clusters at higher temperatures, which results in the dispersal of ionic clusters.

Acknowledgments: Reza Montazami would like to thank Sarah Kreutner for her work during the technical editing phase of this study.

Author Contribution: A.A. and R.M. conceived and designed the experiments; A.A. performed the experiments, analyzed, and interpreted the data; Wa.H and We.H. contributed to analysis and interpretation of the data; A.A. and R.M wrote the paper.

Conflicts of Interest: The authors declare no conflict of interest.

6.6. References

- [1] R. Tiwari and E. Garcia, "The state of understanding of ionic polymer metal composite architecture: a review," *Smart Materials and Structures*, vol. 20, no. 8, p. 083001, 2011.
- [2] M. Shahinpoor, "Ionic polymer–conductor composites as biomimetic sensors, robotic actuators and artificial muscles—a review," *Electrochimica Acta*, vol. 48, no. 14, pp. 2343-2353, 2003.
- [3] M. Shahinpoor, Y. Bar-Cohen, J. Simpson, and J. Smith, "Ionic polymer-metal composites (IPMCs) as biomimetic sensors, actuators and artificial muscles-a review," *Smart materials and structures*, vol. 7, no. 6, p. R15, 1998.
- [4] C. Jo, D. Pugal, I.-K. Oh, K. J. Kim, and K. Asaka, "Recent advances in ionic polymer–metal composite actuators and their modeling and applications," *Progress in Polymer Science*, vol. 38, no. 7, pp. 1037-1066, 2013.
- [5] K. Asaka and H. Okuzaki, *Soft Actuators: Materials, Modeling, Applications, and Future Perspectives*. Japan: Springer, 2014, p. 507.
- [6] W.-S. Chu et al., "Review of biomimetic underwater robots using smart actuators," *International Journal of Precision Engineering and Manufacturing*, vol. 13, no. 7, pp. 1281-1292, 2012.
- [7] A. A. Amiri Moghadam, W. Hong, A. Kouzani, A. Kaynak, R. Zamani, and R. Montazami, "Nonlinear dynamic modeling of ionic polymer conductive network composite actuators using rigid finite element method," *Sensors and Actuators A: Physical*, vol. 217, no. 0, pp. 168-182, 2014.
- [8] C. Meis, R. Montazami, and N. Hashemi, "Ionic electroactive polymer actuators as active microfluidic mixers," *Analytical Methods*, 10.1039/C5AY01061F vol. 7, no. 24, pp. 10217-10223, 2015.
- [9] W. Hong, A. Almomani, and R. Montazami, "Influence of ionic liquid concentration on the electromechanical performance of ionic electroactive polymer actuators," *Organic Electronics*, vol. 15, no. 11, pp. 2982-2987, 2014.

- [10] R. Montazami, D. Wang, and J. R. Heflin, "Influence of conductive network composite structure on the electromechanical performance of ionic electroactive polymer actuators," *International Journal of Smart and Nano Materials*, vol. 3, no. 3, pp. 204-213, 2012.
- [11] W. Hong, C. Meis, J. R. Heflin, and R. Montazami, "Evidence of counterion migration in ionic polymer actuators via investigation of electromechanical performance," *Sensors and Actuators B: Chemical*, vol. 205, no. 0, pp. 371-376, 2014.
- [12] M. J. Fleming, K. J. Kim, and K. K. Leang, "Mitigating IPMC back relaxation through feedforward and feedback control of patterned electrodes," *Smart Materials and Structures*, vol. 21, no. 8, p. 085002, 2012.
- [13] E. Shoji and D. Hirayama, "Effects of humidity on the performance of ionic polymer–metal composite actuators: experimental study of the back-relaxation of actuators," *The Journal of Physical Chemistry B*, vol. 111, no. 41, pp. 11915-11920, 2007.
- [14] V. Vunder, A. Punning, and A. Aabloo, "Mechanical interpretation of back-relaxation of ionic electroactive polymer actuators," *Smart Materials and Structures*, vol. 21, no. 11, p. 115023, 2012.
- [15] R. Montazami, S. Liu, Y. Liu, D. Wang, Q. Zhang, and J. R. Heflin, "Thickness dependence of curvature, strain, and response time in ionic electroactive polymer actuators fabricated via layer-by-layer assembly," *Journal of Applied Physics*, vol. 109, no. 10, p. 104301, 2011.
- [16] C. Meis, N. Hashemi, and R. Montazami, "Investigation of spray-coated silver-microparticle electrodes for ionic electroactive polymer actuators," *Journal of Applied Physics*, vol. 115, no. 13, p. 134302, 2014.
- [17] P. Brunetto, L. Fortuna, P. Giannone, S. Graziani, and S. Strazzeri, "Characterization of the temperature and humidity influence on ionic polymer–metal composites as sensors," *Instrumentation and Measurement, IEEE Transactions on*, vol. 60, no. 8, pp. 2951-2959, 2011.
- [18] T. Ganley, D. L. Hung, G. Zhu, and X. Tan, "Modeling and inverse compensation of temperature-dependent ionic polymer–metal composite sensor dynamics," *Mechatronics, IEEE/ASME Transactions on*, vol. 16, no. 1, pp. 80-89, 2011.
- [19] Y. Cha, H. Kim, and M. Porfiri, "Influence of temperature on the impedance of ionic polymer metal composites," *Materials Letters*, vol. 133, pp. 179-182, 2014.
- [20] K. M. Farinholt and D. J. Leo, "Modeling the electrical impedance response of ionic polymer transducers," *Journal of Applied Physics*, vol. 104, no. 1, p. 014512, 2008.
- [21] J. Benziger, A. Bocarsly, M. J. Cheah, P. Majsztrik, B. Satterfield, and Q. Zhao, "Mechanical and transport properties of nafion: effects of temperature and water activity," in *Fuel Cells and Hydrogen Storage: Springer*, 2011, pp. 85-113.

- [22] W. Y. Hsu and T. D. Gierke, "Ion transport and clustering in Nafion perfluorinated membranes," *Journal of Membrane Science*, vol. 13, no. 3, pp. 307-326, 1983.
- [23] H. Sodaye, P. Pujari, A. Goswami, and S. Manohar, "Temperature dependent positron annihilation studies in Nafion-117 polymer," *Radiation Physics and Chemistry*, vol. 58, no. 5, pp. 567-570, 2000.
- [24] Y. Jean, P. Mallon, and D. Schrader, *Principles and applications of positron and positronium chemistry*. World Scientific, 2003.
- [25] Q. Shen, S. Trabia, T. Stalbaum, V. Palmre, K. Kim, and I.-K. Oh, "A multiple-shape memory polymer-metal composite actuator capable of programmable control, creating complex 3D motion of bending, twisting, and oscillation," *Scientific reports*, vol. 6, 2016.
- [26] T. Xie, K. A. Page, and S. A. Eastman, "Strain - Based Temperature Memory Effect for Nafion and Its Molecular Origins," *Advanced Functional Materials*, vol. 21, no. 11, pp. 2057-2066, 2011.
- [27] T. Xie, "Tunable polymer multi-shape memory effect," *Nature*, vol. 464, no. 7286, pp. 267-270, 2010.
- [28] J. Hou, Z. Zhang, and L. A. Madsen, "Cation/anion associations in ionic liquids modulated by hydration and ionic medium," *The Journal of Physical Chemistry B*, vol. 115, no. 16, pp. 4576-4582, 2011.
- [29] S. Liu et al., "Layer-by-layer self-assembled conductor network composites in ionic polymer metal composite actuators with high strain response," *Applied Physics Letters*, vol. 95, no. 2, p. 023505, 2009.
- [30] S. Liu et al., "Influence of the conductor network composites on the electromechanical performance of ionic polymer conductor network composite actuators," *Sensors and Actuators A: Physical*, vol. 157, no. 2, pp. 267-275, 2010.
- [31] Matthew D. Bennetta, , Donald J. Leo, G. L. Wilkes, F. L. Beyer, and T. W. Pechar, "A model of charge transport and electromechanical transduction in ionic liquid-swollen Nafion membranes," vol. 47, no. 19, pp. 6782-6796, 7 September 2006 2006.
- [32] Y. Liu et al., "Ion transport and storage of ionic liquids in ionic polymer conductor network composites," *Applied Physics Letters*, vol. 96, no. 22, p. 223503, 2010.
- [33] R. Montazami, "Smart Polymer Electromechanical Actuators for Soft Microrobotic Applications," Virginia Polytechnic Institute and State University, 2011.
- [34] P. W. Majsztrik, A. B. Bocarsly, and J. B. Benziger, "Viscoelastic response of Nafion. Effects of temperature and hydration on tensile creep," *Macromolecules*, vol. 41, no. 24, pp. 9849-9862, 2008.

CHAPTER 7. ENGINEERING IONIC CONDUCTIVITY OF IONOMERIC MEMBRANES: INFLUENCE OF VAN DER WAALS VOLUME OF COUNTERIONS AND TEMPERATURE

To be submitted

Abdallah Almomani^{1,2}, Luis Granadillo^{1,3}, Wei Hong^{1,2,4}, Reza Montazami^{1,4}

Abstract

Ionomeric membranes are essential constituents of many ionic devices including fuel cells, lithium-ion polymer batteries, and ionomeric polymer transducers. Understanding the dynamics of ionic conductivity of ionomeric membranes is significant in better understanding and optimizing ionic devices. In this work, effects of temperature and Van der Waals volume of Nafion counterions on ionic conductivity of Nafion ionomeric membrane are studied. Ionic conductivity of lithium (Li^+), potassium (K^+), and 1-Ethyl-3-methylimidazolium (EMI^+) ion-exchanged Nafion membranes at temperatures varying from 25-70 °C was investigated and a direct correlation between ionic conductivity and both temperature and Van der Waals volume of counter ions was observed. Ionic conductivity as a function of temperature (for all three counterions) exhibited two distinct slopes below and above ~50 °C which is an indication of changes in activation energy, and confirms previously claims of ionic decomposition of EMI-Tf ionic liquid around ~50 °C.

¹ Primary researchers and authors. Graduate student, undergraduate student, academic advisor, and academic advisor, respectively.

² Department of Aerospace Engineering, Iowa State University.

³ Department of Materials Science and Engineering, Iowa State University.

⁴ Department of Mechanical Engineering, Iowa State University.

7.1. Introduction

Ionomers (ion permeable polymers) have been subjected to numerous studies over the last several years. The significance of these studies has increased as ionomers have become essential in ionic devices, primarily those with energy generation and storage applications such as sensors and actuators, fuel cells, lithium-ion polymer batteries, and artificial muscles [1-7]. The functionality of devices that use ionomers mainly depends on the ion mobility (diffusion and/or drifting of ions) through ionomeric membrane. Ion mobility through membrane is dependent on many factors, including the chemical structure of the ionomer, the driving force (e.g. electric field), source and type of ions (aqueous electrolyte, ionic liquid, etc.), as well as the ambient conditions (e.g. humidity and temperature). Owing to its thermal and chemical stability and high ion permeability, Nafion has been one of the most desirable ion permeable membranes; thus, its ion transport properties have been subjected to several studies [8-11].

Nafion consists of long tetrafluoroethylene (Teflon) backbone structure with short perfluorovinyl ether side chains terminated with sulfonate (SO_3^-) ionic groups. The sulfonate ionic groups are accompanied by proton (H^+) counterions. Numerous fuelcell studies have confirmed diffusion-derived proton permeability of Nafion. Channelized nanostructure along with presence of ionic groups and counterions are known to be responsible for proton permeability of Nafion. Previous studies by others and us have confirmed that the proton counterions can be substituted by other cations through conventional ion exchange processes [12, 13]. It is also shown by others and us that drift-driven cation permeability of Nafion can be achieved, resulting in superior electromechanical attributes [7, 14-17]. In one study, Hong *et al.* [7] investigated the correlations between electromechanical response and Van der Waals (VdW) volume of Nafion counterions in ionic electroactive polymer actuators; and observed

an increased cationic response with increasing VdW volume of counterion. In another study, Bennett and colleagues studied the ion permeability of Nafion membranes containing counterions of different VdW volumes and impregnated with 1-ethyl-3-methylimidazolium trifluoromethanesulfonate (EMI-Tf) ionic liquid [18]. Correlations among ion permeability, VdW volume of counterions, and ionic liquid uptake were studied and a direct correlation between ion permeability and VdW volume was observed for a constant ionic liquid uptake.

In addition to ionic composition, ion permeability of Nafion also depends on environmental conditions such as temperature. On two independent studies, Uosaki *et al.* and Cappadonia *et al.* studied the ionic conductivity of Nafion at low temperatures, ranging from subzero to room temperature [19, 20]. Matos *et al.* studied the ionic conductivity of Nafion at higher temperatures, from room temperature up to 180 °C [21]. All studies were conducted using pristine (proton counterion) Nafion and confirmed a direct proportionality between ion permeability and temperature. In our previous studies on effects of temperature on electromechanical response of ionic electroactive polymer actuators [22] two distinct behaviors were observed for two temperature ranges: 1) 25 °C - 50 °C and 2) 60 °C - 70 °C. The distinct behaviors were speculated to be a result of variations in ionic liquid composition and nanostructure of Nafion at higher temperatures as Nafion has a broad glass transition temperature that starts at about 55 °C [23-25].

There exists a knowledge gap in explaining the combined effect of temperature and VdW volume of counterions on the ion permeability of Nafion. In this work, we have investigated temperature dependence ion permeability of Nafion membranes containing counterions of different VdW volumes using electrochemical and analytical means.

7.2. Materials and Methods

7.2.1. Materials

Nafion (sulfonated tetrafluoroethylene based fluoropolymer-copolymer) of 25 μm thickness (NR-211, IonPower, DE-USA) was used as the ionomer membrane. 1-ethyl-3-methylimidazolium trifluoromethanesulfonate (EMI-Tf molecular formula, $\text{C}_7\text{H}_{11}\text{F}_3\text{N}_2\text{O}_3\text{S}$) (Sigma-Aldrich, MO-USA) ionic liquid was used as electrolyte and as received. Lithium chloride (LiCl, Sigma-Aldrich, MO-USA), potassium chloride (KCl, Sigma-Aldrich, MO-USA), and 1-Ethyl-3-methylimidazolium chloride ($\text{C}_6\text{H}_{11}\text{ClN}_2$ (EMICl), Sigma-Aldrich, MO-USA) salts were used as sources of the counterions that were to be exchanged with protons in Nafion membranes.

7.2.2. Sample Preparation

The preparation of samples started with exchanging the protons in Nafion with one of the counterions to be tested. The procedure for the counterion exchange is explained in detail previously [7]. Briefly, Nafion membrane in the protonated form were pretreated by boiling in 1.0 M sulfuric acid for 120 minutes, followed by boiling in deionized (DI) water for 120 minutes. The membrane was then exchanged from the proton form to one of the three neutralized forms by soaking in 0.5 M aqueous salt solutions for two days at 80 °C, followed by eight days at 60 °C. The three forms of ion exchanged membranes studied are lithium, potassium, and 1-ethyl-3-methylimidazolium (EMI). The membranes were then rinsed thoroughly and soaked in DI water for 3 hours to remove any excess salt. Membranes were then dehydrated in a vacuum oven (110 °C, -100 kPa) for 3 days. Dehydrated membranes were then impregnated by soaking in EMI-Tf for 48 hours at 80 °C and then cut into $1 \times 1 \text{ cm}^2$ samples for testing.

7.2.3. Experimental Procedure

Membranes were placed between two $1 \times 1 \text{ cm}^2$ copper electrodes that were glued to two separate glass substrates. Hot glue was then used to seal the structures before submerging it into a temperature-controlled water bath. A hot plate (Corning $5 \times 7 \text{ in}^2$ PC-420D, Corning, NY-USA) with temperature feedback control was used to achieve the desired temperature in the water bath and a VersaSTAT-4 potentiostat (Princeton Applied Research, IL-USA) was used to apply a 10 mV potential at frequencies ranging from 100 kHz to 0.1 Hz and to monitor electrical impedance.

7.3. Results and Discussion

Ionic conductivity, $\sigma(T)$, of ion-exchanged Nafion membranes as a function of temperature was calculated. Specimens were characterized for their electrochemical properties as a function of frequency. Presented in Figure 7-1 are Nyquist plots of different specimens and temperatures. The Nyquist plots were used to obtain resistance, R_T , at different temperatures at high frequency, and the ion conductivity was calculated from Equation (7-1),

$$\sigma(T) = \frac{t}{R_T A} \quad (7-1)$$

where t is the thickness of the membrane and A is the surface area of the membrane [18].

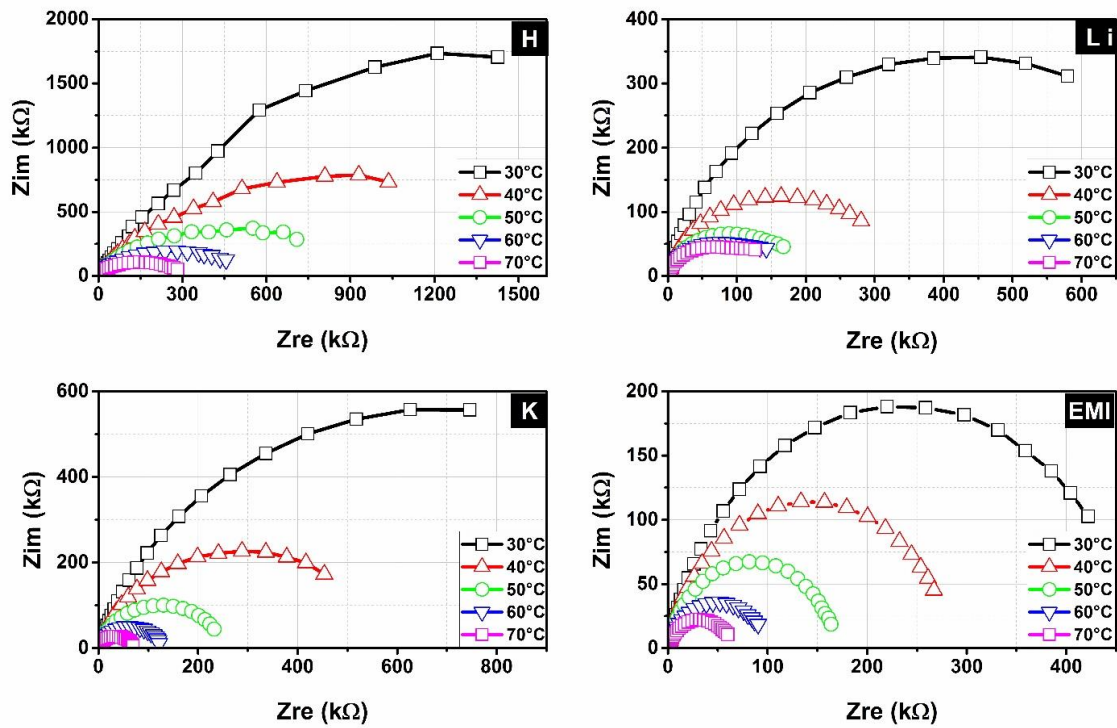


Figure 7-1: Nyquist plots for membranes with different counterions at different temperatures

As presented in Figure 7-2, ionic conductivity exhibited direct correlations with both temperature and the VdW volume of the counterions; it is speculated that the increased ionic conductivity is the consequence of two main structural changes in the ionic system: nanostructure and ionic composition. Each of the structural changes can occur as a result of a number of different cause.

VdW volume of counterions: Nafion consists of a channelized structure with very small and hollow inverted-micelle spheres connected with nanochannels that allow ion diffusion and drift [26]. It is suggested that larger ions, including counterions, may expand the narrow nanochannels between the inverted-micelle spheres, resulting in an increased mobility of ions through the membranes and allowing larger ions to be transported [7]. Additionally, it is experimentally proven that the counterions in (ion-exchanged and pristine) Nafion membrane

are mobilized under an external electric field [7, 18]. Bennett *et al.* have suggested that counterions transport through membranes by “hopping” among free Tf⁻ sites after being displaced by EMI⁺ cations at the Nafion exchange sites. At the same ionic liquid uptake for samples with different counterions, the electrostatic binding energy is lower for counterions with larger VdW volumes, meaning less ionic liquid is required to displace these counterions. This will increase the amount of the free ionic liquid within the membrane and enhances ionic conductivity.

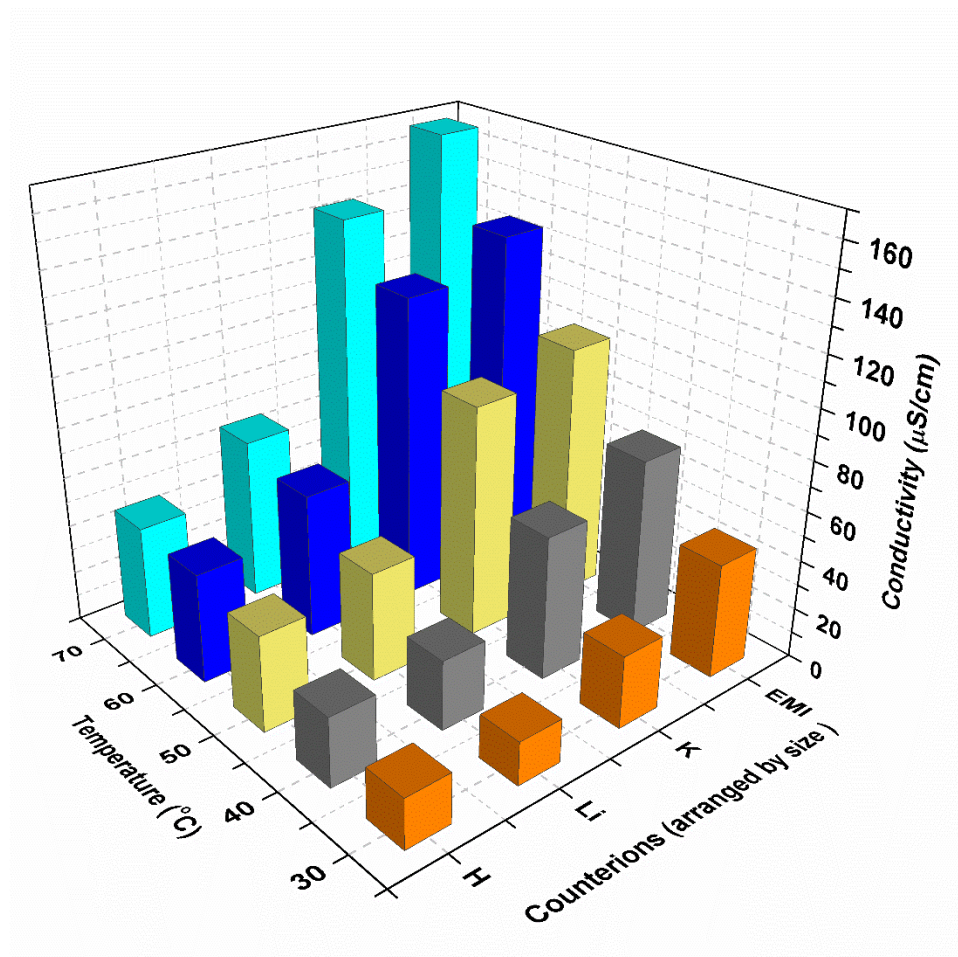


Figure 7-2: Conductivity across Nafion membranes with different counterions at different temperatures.

Temperature: Increasing ionic conductivity with increasing temperature is due to the increase in kinetic energy of the ions as a function of temperature [19-21] and can be explained using Arrhenius equation for ionic conductivity, Equation (7-2):

$$\sigma(T) = \sigma_0 \exp\left(\frac{-E_a}{RT}\right) \quad (7-2)$$

where σ_0 is the maximum ionic conductivity, E_a is the activation energy, R is the gas constant, and T is the temperature. Equation (7-2) can also be rearranged to obtain Equation (7-3),

$$\ln(\sigma(T)) = \frac{-E_a}{R}(T^{-1}) + \ln(\sigma_0) \quad (7-3)$$

which exhibits a linear relationship between T^{-1} and $\ln(\sigma(T))$. In previous studies, however, two distinct ranges of linear fitting (different slopes) were observed for experimental data obtained at low ($< \sim 50$ °C) and high ($> \sim 50$ °C) temperature ranges. The different slopes signify a different activation energies E_a within each temperature range since E_a represents the slope of the linear Arrhenius relation, as demonstrated in Equation (3). Presented in Figure 3 are experimental data fitted with the linear Arrhenius equation (equation 3). A general trend of higher ionic conductivity for higher temperatures is observed, with different slopes for temperatures below and above 50 °C. The two trends of ionic conductivity are in good agreement with our previous studies on the electromechanical response of ionic electroactive actuators tested within these temperature ranges [22]. The two distinct ionic conductivity slopes can be explained by changes in ionic composition of the ionic liquid as well as changes to the nanostructure of Nafion. Changes in ionic composition is mainly related to the dispersal of large ionic complexes to smaller ionic species at elevated temperature (*i.e.* ~ 60 °C), which require a lower activation energy to be transported through the membranes, as well as the changes in the nanostructure on Nafion that occurs at about the same temperature. After the

conductivity data was fitted with the Arrhenius equation, the fitted lines showed a smaller slope for the temperatures between 60 °C and 70 °C compared to the temperatures ranging from 30 °C to 50 °C, indicating a lower required activation energy at elevated temperatures, which is characteristic of smaller ions. Moreover, smaller mobilized ions should result in an even higher conductivity than the previous trend (the conductivity at 60 °C and 70 °C should lie above the single dashed blue lines in figure 3); however, a conductivity lower than the low-temperature trend was observed. This is expected to be a consequence of the change and breakage of nanochannels in the membrane due to the broad glass transition temperature of Nafion that starts at ~55 °C[23-25], and affects the ion transport through the membranes.

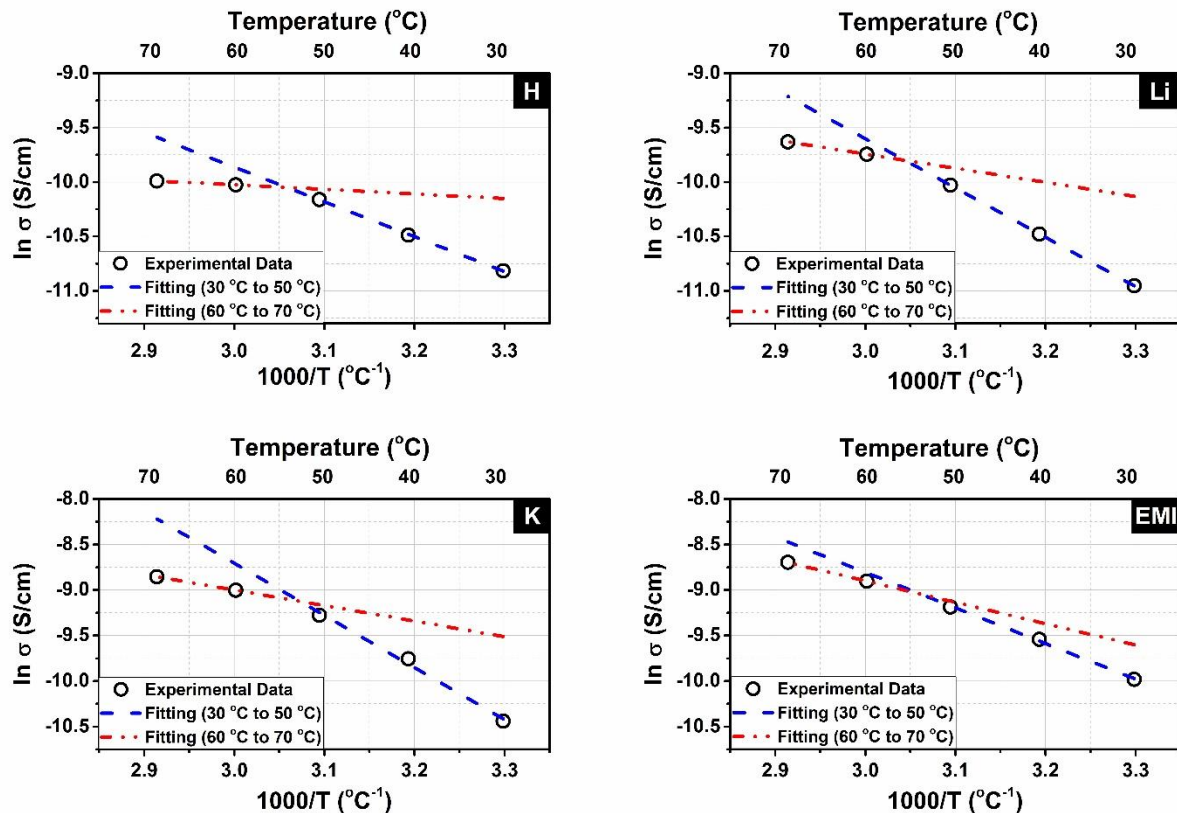


Figure 7-3: Arrhenius plots of ionic conductivity for Nafion membranes at different temperatures and for different counterions.

7.4. Conclusion

Ionic conductivity of Nafion as a function of temperature and Van der Waals volume of counter ions is studied. A direct relation was observed between increasing ionic conductivity and both increasing temperature and increasing Van der Waals volume of counter ions. At higher temperatures, the increased kinetic energy enhances the ionic conductivity. Counterions with larger Van der Waals volume are speculated to expand the narrow nanochannels within the nanostructure of Nafion which is expected to enhance ion mobility; and thus, ionic conductivity. The ionic conductivity data was fitted with the Arrhenius equation and showed two different trends at two different temperature ranges. This observation can verify previously claimed dispersion of ionic complexes to smaller ions or smaller ionic complexes which requires a lower activation energy at elevated temperatures.

Acknowledgements: This work was supported in part by funding from the Iowa State University Foundation.

7.5. References

- [1] A. Della Santa, D. De Rossi, and A. Mazzoldi, "Characterization and modelling of a conducting polymer muscle-like linear actuator," *Smart Materials and Structures*, vol. 6, no. 1, p. 23, 1997.
- [2] T. Wallmersperger, B. J. Akle, D. J. Leo, and B. Kröplin, "Electrochemical response in ionic polymer transducers: an experimental and theoretical study," *Composites Science and Technology*, vol. 68, no. 5, pp. 1173-1180, 2008.
- [3] I. Must, U. Johanson, F. Kaasik, I. Pöldsalu, A. Punning, and A. Aabloo, "Charging a supercapacitor-like laminate with ambient moisture: from a humidity sensor to an energy harvester," *Physical Chemistry Chemical Physics*, vol. 15, no. 24, pp. 9605-9614, 2013.
- [4] W. Hong, A. Almomani, and R. Montazami, "Electrochemical and morphological studies of ionic polymer metal composites as stress sensors," *Measurement*, vol. 95, pp. 128-134, 2017.
- [5] A. Jablonski, P. J. Kulesza, and A. Lewera, "Oxygen permeation through Nafion 117 membrane and its impact on efficiency of polymer membrane ethanol fuel cell," *Journal of Power Sources*, vol. 196, no. 10, pp. 4714-4718, 2011.

- [6] J. Yang, S. Ghobadian, P. J. Goodrich, R. Montazami, and N. Hashemi, "Miniaturized biological and electrochemical fuel cells: challenges and applications," *Physical Chemistry Chemical Physics*, vol. 15, no. 34, pp. 14147-14161, 2013.
- [7] W. Hong, C. Meis, J. R. Heflin, and R. Montazami, "Evidence of counterion migration in ionic polymer actuators via investigation of electromechanical performance," *Sensors and Actuators B: Chemical*, vol. 205, no. 0, pp. 371-376, 2014.
- [8] D. R. Morris and X. Sun, "Water - sorption and transport properties of Nafion 117 H," *Journal of Applied Polymer Science*, vol. 50, no. 8, pp. 1445-1452, 1993.
- [9] T. Okada, S. Møller-Holst, O. Gorseth, and S. Kjelstrup, "Transport and equilibrium properties of Nafion® membranes with H⁺ and Na⁺ ions," *Journal of Electroanalytical Chemistry*, vol. 442, no. 1, pp. 137-145, 1998.
- [10] T. Okada, G. Xie, O. Gorseth, S. Kjelstrup, N. Nakamura, and T. Arimura, "Ion and water transport characteristics of Nafion membranes as electrolytes," *Electrochimica Acta*, doi: DOI: 10.1016/S0013-4686(98)00132-7 vol. 43, no. 24, pp. 3741-3747, 1998.
- [11] S. Tan and D. Belanger, "Characterization and transport properties of Nafion/polyaniline composite membranes," *The Journal of Physical Chemistry B*, vol. 109, no. 49, pp. 23480-23490, 2005.
- [12] M. D. Bennett, "Electromechanical transduction in ionic liquid-swollen Nafion membranes," 2005.
- [13] R. Montazami, "Smart Polymer Electromechanical Actuators for Soft Microrobotic Applications," Virginia Polytechnic Institute and State University, 2011.
- [14] B. J. Akle, M. D. Bennett, D. J. Leo, K. B. Wiles, and J. E. McGrath, "Direct assembly process: a novel fabrication technique for large strain ionic polymer transducers," *Journal of Materials Science*, vol. 42, no. 16, pp. 7031-7041, 2007.
- [15] Y. Liu et al., "Equivalent circuit modeling of ionomer and ionic polymer conductive network composite actuators containing ionic liquids," *Sensors and Actuators A: Physical*, vol. 181, pp. 70-76, 2012.
- [16] Y. Liu et al., "Ion transport and storage of ionic liquids in ionic polymer conductor network composites," *Applied Physics Letters*, vol. 96, no. 22, p. 223503, 2010.
- [17] S. Liu et al., "Layer-by-layer self-assembled conductor network composites in ionic polymer metal composite actuators with high strain response," *Applied Physics Letters*, vol. 95, no. 2, p. 023505, 2009.
- [18] Matthew D. Bennetta, , Donald J. Leo, G. L. Wilkes, F. L. Beyer, and T. W. Pechar, "A model of charge transport and electromechanical transduction in ionic liquid-swollen Nafion membranes," vol. 47, no. 19, pp. 6782-6796, 7 September 2006 2006.

- [19] K. Uosaki, K. Okazaki, and H. Kita, "Conductivity of Nafion membranes at low temperatures," *Journal of Electroanalytical Chemistry and Interfacial Electrochemistry*, vol. 287, no. 1, pp. 163-169, 1990.
- [20] M. Cappadonia, J. W. Erning, and U. Stimming, "Proton conduction of Nafion® 117 membrane between 140 K and room temperature," *Journal of Electroanalytical Chemistry*, vol. 376, no. 1-2, pp. 189-193, 1994.
- [21] B. R. Matos, C. A. Goulart, E. I. Santiago, R. Muccillo, and F. C. Fonseca, "Proton conductivity of perfluorosulfonate ionomers at high temperature and high relative humidity," *Applied Physics Letters*, vol. 104, no. 9, p. 091904, 2014.
- [22] A. Almomani, W. Hong, W. Hong, and R. Montazami, "Influence of Temperature on the Electromechanical Properties of Ionic Liquid-Doped Ionic Polymer-Metal Composite Actuators," *Polymers*, vol. 9, no. 8, p. 358, 2017.
- [23] T. Xie, "Tunable polymer multi-shape memory effect," *Nature*, vol. 464, no. 7286, pp. 267-270, 2010.
- [24] T. Xie, K. A. Page, and S. A. Eastman, "Strain - Based Temperature Memory Effect for Nafion and Its Molecular Origins," *Advanced Functional Materials*, vol. 21, no. 11, pp. 2057-2066, 2011.
- [25] Q. Shen, S. Trabia, T. Stalbaum, V. Palmre, K. Kim, and I.-K. Oh, "A multiple-shape memory polymer-metal composite actuator capable of programmable control, creating complex 3D motion of bending, twisting, and oscillation," *Scientific reports*, vol. 6, 2016.
- [26] W. Y. Hsu and T. D. Gierke, "Ion transport and clustering in Nafion perfluorinated membranes," *Journal of Membrane Science*, vol. 13, no. 3, pp. 307-326, 1983.

CHAPTER 8. CONCLUSIONS AND FUTURE WORK

8.1. Conclusions

The goal of this dissertation is to present some studies that directly affect the performance of the ionic electroactive polymer (IEAP) transducers. The studies were performed on actuators and sensors as functions of nanostructure (*i.e.* changing the structure of the CNC), ionic liquid uptake, and temperature. The concluding remarks of each study is summarized in a paragraph below.

In Chapter 3, a study on the effect of ionic liquid concentration on the performance of the IEAP actuators was presented. IEAP actuators consisting of Nafion ionomeric membrane and EMI-Tf ionic liquid were fabricated and tested for different IL concentrations. It was expected to have a better actuation performance by increasing the IL concentration. Although the current flow across the membranes was higher with increasing the concentration, the electromechanical response had different behavior. We found that increasing concentration of ionic liquids in IEAP actuators results in an enhanced electromechanical response up to an optimum IL concentration. After that, increasing the IL concentration will form a secondary layer of ions, and generate undesired strain that partially cancels and reduces the strain generated by the ion layer at the interface. In short, the optimum (not maximum) concentration of ionic liquids should be incorporated in IEAP actuators to achieve a maximum electromechanical response.

In Chapter 4, we reported a significant enhancement of IEAP sensors sensitivity by changing the structure of the CNC by adding small salt molecules during fabrication. The sensitivity of the IEAP sensor was enhanced by at least 3 to 4 folds for sensors with the salt molecules compared to IEAP without the salt molecules. It was found that the salt molecules

will change the thickness, porosity, and conductivity of the CNC layers which reflect the enhancement in the sensing performance. By changing the amount of the added salt molecules, the sensitivity of the stress sensors can be tolerated as desired.

In chapter 5, an intrinsic angular deformation of IEAP actuators was achieved by incorporating conjugated polymer (CP), PEDOT:PSS, patterns in the structure of soft actuators. Angular deformation with sharp angles of 90° and beyond was achieved instead of the conventional circular deformation exhibited by IEAP actuators. Different deformation shapes were achieved in this study depending on the location, size, and number of the CP segments and the direction of motion of the actuators. With different combinations of the orientation, size, shape, number, and location of the CP patterns, more complex shapes and even a 3D deformation could be achieved. A finite element analysis (FEM), in addition to some electrochemical studies, were performed to explain this behavior as described in detail in this chapter.

In chapter 6 and chapter 7, the effect of effect of temperature on the electromechanical and electrochemical performance of IEAP transducers were studied. In chapter 6, the electromechanical performance was studied on actuators operated in air inside a temperature controlled environment. Cationic and anionic curvatures exhibited two distinct behaviors as a function of increasing temperature as presented in detail in this chapter. It is believed that both the change in the internal structure of the Nafion membranes and the ionic liquid structure at different temperatures have a direct effect on the electromechanical performance. In chapter 7, the ionic conductivity of Nafion as a function of temperature and Van der Waals volume of counterions was studied. The ionic conductivity was found to be directly proportional to the increase of the Van der Waal volume of the counterions and to the increase in temperature.

The ionic conductivity data were fitted with the Arrhenius equation and showed two different trends at two different temperature ranges. This observation support and verify the results achieved in chapter 6.

8.2. Future work

In chapter 5, we discussed fabrication and modeling of soft ionic electroactive actuators with tunable non-linear angular deformation. The next step of the future work is to find some applications for such actuators. An example for that is fabrication microgrippers with angular deformation as shown in Figure 8-1. This type of grippers will enhance the gripping capability by using only IEAP actuators without the need of any end attachments.

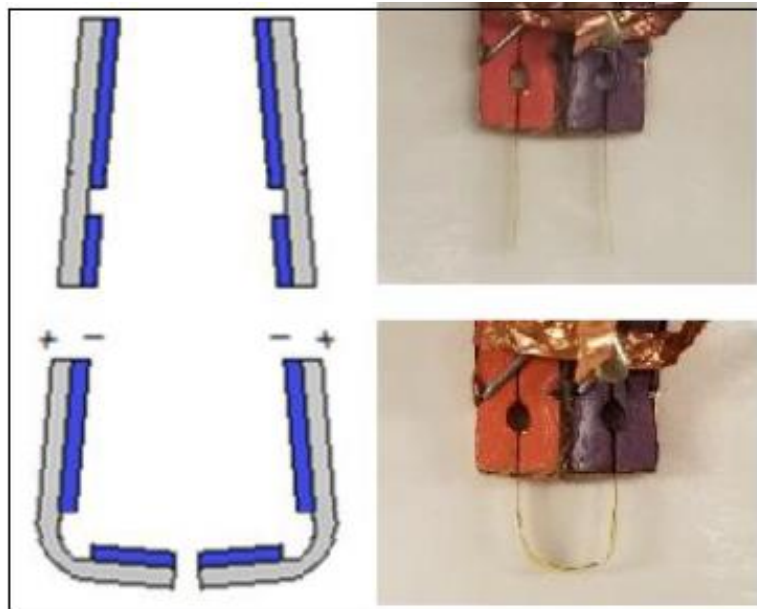


Figure 8-1: Microgrippers fabricated with actuators with angular motion

Another example is to use these actuators to generate more complex structure or achieve 3D motion of the actuators by changing the conductive polymers patterns during fabrication. An actuator that would have a 3D motion is shown in Figure 8-2(a). And a set of actuators that would generate a complex structure (cube) are shown in Figure 8-2(b).

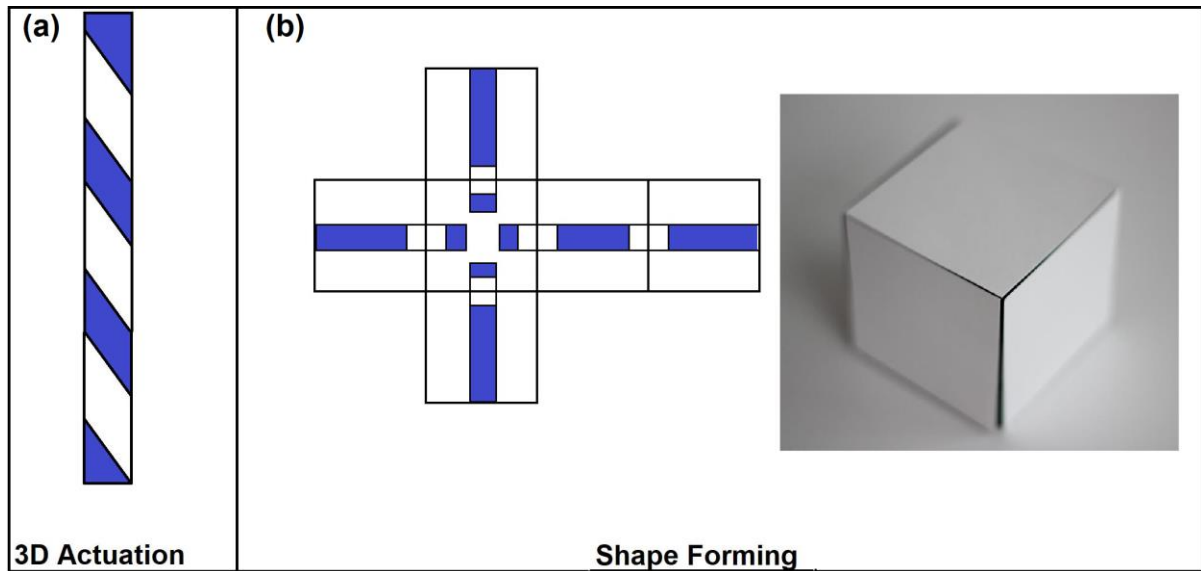


Figure 8-2: (a) Actuators with 3D motion. (b) Complex shape (cube) formation using IEAP actuators with angular motion

As for the sensing part, IEAP sensors could be implemented in many applications such as: touch sensor, artificial skins, keyboards, and touch screens. Figure 8-3 shows some applications where IEAP sensors can be used.

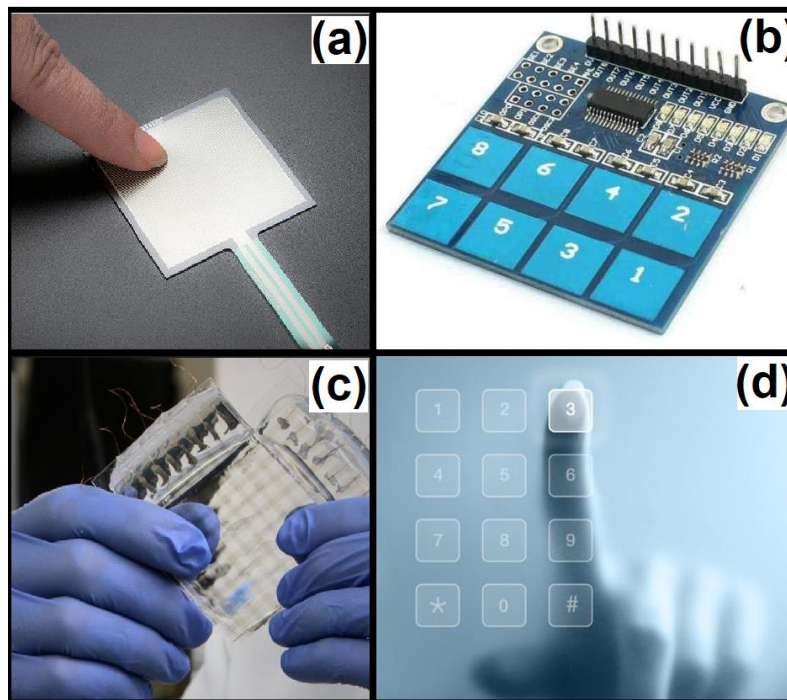


Figure 8-3: Some application of IEAP sensor. (a) touch sensors, (b) keyboards, (c) artificial skin, and (d) touch screen.